Yukawa matrix unification in the Minimal Supersymmetric Standard Model

Mateusz Kamil Iskrzyński

arXiv:1511.08832v1 [hep-ph] 27 Nov 2015

PhD dissertation under the supervision of
prof. dr hab. Mikołaj Krzysztof Misiak
at the Institute of Theoretical Physics, Faculty of Physics, University of Warsaw

Warsaw, August 2015

Abstract

In this dissertation, the Minimal Supersymmetric Standard Model (MSSM) is studied as a low-energy theory stemming from the $SU(5)$ Grand Unified Theory (GUT). The well-known gauge coupling unification in the MSSM is considered to be one of the main virtues of the model. Similarly, Yukawa couplings of the bottom quark and tau lepton become relatively close to each other at the GUT scale $M_{\rm GUT} \simeq 2 \times 10^{16}\,\text{GeV}$. However, it is not the case for the first- and second-generation Yukawa couplings, unless large threshold corrections arise at the scale $\mu_{\rm sp}$ at which the superpartners are being decoupled. Here, we investigate a possibility of satisfying the minimal $SU(5)$ boundary condition $\mathbf{Y}^d = \mathbf{Y}^{eT}$ for the full 3×3 down-quark and lepton Yukawa matrices at the GUT scale within the R-parity conserving MSSM.

We give numerical evidence in favour of the statement:

There exist regions in the parameter space of the R-parity conserving MSSM for which the unification of the down-quark and lepton Yukawa matrices takes place, while the predicted values of flavour, electroweak and other collider observables are consistent with experimental constraints.

Furthermore, we find evidence that the bottom-tau and strange-muon Yukawa unification is possible with a stable MSSM vacuum in the standard form, where only the neutral Higgs fields acquire non-vanishing vacuum expectation values. However, if the equality of the electron and down-quark Yukawa couplings at $M_{\rm GUT}$ is demanded, only such cases remain, for which the standard MSSM vacuum is metastable, though sufficiently long-lived.

We investigate two separate scenarios of the soft supersymmetry breaking terms at $M_{\rm GUT}$. In the first one, it is assumed that the soft terms are non-universal but flavour-diagonal in the super-CKM basis. In such a case, the trilinear Higgs-squark-squark A-terms can generate large threshold corrections to the Yukawa matrix $\mathbf{Y}^d$ at the superpartner decoupling scale $\mu_{\rm sp}$, while no significant new contributions to the Flavour Changing Neutral Current processes are generated. In effect, the $SU(5)$ boundary condition $\mathbf{Y}^d = \mathbf{Y}^{eT}$ at the GUT scale can be satisfied. However, the large trilinear terms make the usual Higgs vacuum metastable (though sufficiently long-lived). We broaden the previous studies of such a scenario by including results from the first LHC phase, notably the measurement of the Higgs particle mass, as well as a quantitative investigation of the relevant flavour observables.

In the second scenario, we consider non-vanishing flavour off-diagonal entries in the soft SUSY-breaking mass matrices. As we aim to alleviate the metastability problem, the diagonal A-terms are assumed to be proportional to the respective Yukawa couplings. We show that a non-trivial flavour structure of the soft SUSY-breaking sector can allow a precise bottom-tau and strange-muon Yukawa coupling unification, while satisfying all phenomenological constraints.

Streszczenie

W niniejszej rozprawie rozważany jest Minimalny Supersymetryczny Model Standardowy (MSSM) jako niskoenergetyczna teoria efektywna wynikająca z Teorii Wielkiej Unifikacji (GUT) opartej o symetrię $SU(5)$. Dobrze znana unifikacja sprzężeń cechowania w MSSM jest uważana za jedną z głównych zalet tego modelu. Podobnie, także stałe Yukawy kwarku bottom i leptonu tau mają zbliżone wartości przy skali GUT, $M_{\rm GUT} \simeq 2 \times 10^{16}\,\text{GeV}$. Nie ma to jednak miejsca w przypadku pierwszej i drugiej generacji, o ile duże poprawki progowe nie wystąpią przy skali odprzęgania superpartnerów $\mu_{\rm sp}$. W niniejszej pracy analizowana jest możliwość spełnienia w ten sposób minimalnych warunków brzegowych $SU(5)$ przy skali GUT $\mathbf{Y}^d = \mathbf{Y}^{eT}$ dla pełnej (3×3) macierzy Yukawy kwarków dolnych i leptonów w ramach MSSM zachowującego R-parzystość.

W pracy zaprezentowane są numeryczne argumenty przemawiające za następującą tezą: *Istnieją obszary przestrzeni parametrów zachowującego R-parzystość MSSM, w których zachodzi unifikacja macierzy Yukawy kwarków dolnych i leptonów, a przewidywane przez model wartości obserwabli zapachowych, elektrosłabych oraz innych kluczowych pomiarów dokonanych w zderzaczach cząstek są zgodne z ograniczeniami doświadczalnymi.*

Pokazujemy również, że unifikacja stałych Yukawy kwarku bottom i leptonu tau oraz kwarku dziwnego i mionu jest możliwa bez naruszenia warunku stabilności standardowej próżni MSSM, w której tylko nienaładowane pola Higgsa przyjmują próżniowe wartości oczekiwane. Jeśli żąda się także równości stałych Yukawy kwarku dolnego i elektronu przy $M_{\rm GUT}$, pozostają tylko przypadki, w których standardowa próżnia MSSM jest metastabilna, ale dostatecznie długo żyjąca.

Rozważamy dwa odrębne scenariusze dla członów miękko łamiących supersymetrię przy skali $M_{\rm GUT}$. W pierwszym z nich zakładamy, że człony miękkie są nieuniwersalne, ale diagonalne w przestrzeni zapachu w bazie super-CKM. W takim wypadku, trójliniowe sprzężenia Higgs-skwark-skwark (człony A) mogą wygenerować duże poprawki progowe do macierzy Yukawy $\mathbf{Y}^d$ przy skali odprzęgania superpartnerów $\mu_{\rm sp}$. Jednocześnie nie pojawiają się żadne nowe znaczące wkłady do procesów z prądami neutralnymi zmieniającymi zapach. W rezultacie, warunek brzegowy $\mathbf{Y}^d = \mathbf{Y}^{eT}$ może być spełniony przy skali GUT. Jednakże, duże człony trójliniowe czynią zwyczajną próżnię Higgsa metastabilną (choć o czasie życia dłuższym niż historia Wszechświata). Niniejsza praca poszerza uprzednie wyniki tego scenariusza poprzez uwzględnienie wyników z pierwszej fazy działania LHC, zwłaszcza pomiaru masy bozonu Higgsa, jak też ilościowo rozważając istotne obserwable zapachowe.

W drugim scenariuszu rozważamy nieznikające pozadiagonalne w zapachu elementy macierzy mas miękko łamiących supersymetrię. W celu uniknięcia problemu metastabilności założone diagonalne człony A są proporcjonalne do odpowiednich sprzężeń Yukawy. Wykazujemy, iż nietrywialna struktura zapachowa członów miękko łamiących superymetrię pozwala na precyzyjną unifikację stałych Yukawy kwarku bottom i leptonu tau oraz kwarku dziwnego i mionu, przy spełnieniu wszystkich ograniczeń fenomenologicznych.

Acknowledgments

First, this work would not have been undertaken, pursued and completed without the supervision of Professor Mikołaj Misiak. His intellect, scientific passion, optimism, best intentions and kindness have often taken as conversational input a sceptical, wavering PhD student and returned a refreshed wanderer ready to focus on the next mountain to climb.

The second part of the work which has led to results that are presented here owes much to Dr. Kamila Kowalska, her proficiency, energy and experience in handling all the technical issues in supersymmetric phenomenology. Her understanding what is feasible, and when to stop researching a problem chiefly contributed to the successful completion of this thesis. I am truly grateful for the spirit-raising experience of our collaboration.

The TTP Institute of the Karlsruhe Institute of Technology will remain in my memory as a perfectly organised and welcoming place, teeming with extremely specialised, energetic research. Professor Ulrich Nierste and Dr. Andreas Crivellin have largely inspired the research projects I have pursued. I am indebted as well to the hospitality of CERN, by far the most motivating physics environment I have been working in, thanks to the invitation and personal kindness of Professor Christophe Grojean. The helpful remarks of Professor Gian Giudice brought the vacuum metastability issue to my attention.

Everything I did owes much to the kind support of my Parents and the rest of the family. It is their early formation that cradled my inquisitive curiosity and ambition. Later, it was dr Elżbieta Zawistowska, the exceptional teacher and the spirit of the XIV Stanisaw Staszic High School in Warsaw, that inspired me to choose the field of physics. I would not have pursued in particle physics if Professor Jan Kalinowski's lecture had not shown us the logic in it.

I would like to thank all the people whose friendship, kindness and love accompanied me in life, in its ups and downs. My sisters and brothers in arms Ola, Michał, Radek, Marcin and especially Maciek – our long evening conversations at Nowolipki street were helpful way beyond Mathematica tips. Those who shared our cramped nest at Hoża street, notably Ola, Wojtek and Lis. The homemade-lunch lovers Bogusia, Jędrek and Arek – our discussions were an important daily break. Rysiek for his uniqueness and our underground seminars. The most reliable friends not only from the high peaks, Klara, Jola, Janek, Karol and Tomek. The whole Epifania Choir, especially our director Wiesaw Jeleń, who left us the memory and testimony of his great open heart, patience and love to music.

I would like to thank the kind people I met during my international exchanges. Otto for his lasting friendship. The whole Karlsruhe community, Ricarda, Guillaume, Jens, Jens, Nikolai. Remembering Yannan, who is not among us anymore. The happy CERN company, especially Christine, Robb, Juan, Mindaugas.

I owe very special gratitude to all those who were close to me during those years, they profoundly changed me and made this time truly genuine, even if it did not last. There would have been no final success if not the love and happiness I enjoyed. Thank you.

Contents

Outline **13**

1 Introduction **16**
1.1 Preliminaries . . . 16
1.1.1 Renormalisation Group Equations . . . 16
1.1.2 Threshold corrections . . . 17
1.2 The Standard Model . . . 18
1.2.1 Field content and Lagrangian density . . . 18
1.2.2 Spontaneous Electroweak Symmetry Breaking and fermion masses . . . 21
1.3 Grand Unified Theories . . . 22
1.3.1 Algebraical considerations . . . 22
1.3.2 Gauge interactions . . . 23
1.3.3 Gauge coupling unification . . . 24
1.3.4 Hierarchy problem . . . 24
1.4 Supersymmetry . . . 25
1.4.1 The SUSY algebra . . . 26
1.4.2 Softening the hierarchy problem . . . 27
1.4.3 The Minimal Supersymmetric Standard Model . . . 28
1.4.4 The MSSM spectrum and field bases . . . 31
1.4.5 Gauge coupling unification . . . 32
1.5 Yukawa coupling unification in the MSSM . . . 34

2 Two MSSM scenarios for the SU(5) Yukawa matrix unification **38**
2.1 Large diagonal A terms . . . 38
2.2 General Flavour Violating MSSM . . . 39
2.3 Threshold corrections in the diagonal soft term case . . . 41
2.4 Threshold corrections with flavour mixing in the soft terms . . . 45

3 Phenomenological constraints **47**
3.1 Flavour Changing Neutral Currents . . . 47
3.1.1 Kaon mixing . . . 48
3.1.2 B-meson mixing . . . 49
3.1.3 Rare B decays . . . 50
3.1.4 Lepton Flavour Violation . . . 52
3.2 Higgs boson mass measurement . . . 53
3.3 LHC SUSY searches . . . 54
3.4 Electroweak vacuum stability . . . 54

3.5 Dark matter 57

4 Numerical Tools **60**
4.1 Spectrum generators 60
4.2 Numerical setup for the large A-term scenario 62
4.3 Numerical tools for the GFV MSSM scenario 62

5 Large diagonal A terms – numerical results **64**
5.1 Regions with the successful **SU**(**5**) Yukawa matrix unification 64
5.2 Flavour observables 65
5.3 Electroweak symmetry breaking 67

6 Numerical results for the GFV_{23} scenario **71**
6.1 Regions with the successful bottom-tau and strange-muon unification 71
6.2 Phenomenology of the GFV_{23} scenario 73
6.2.1 Dark matter 73
6.2.2 Higgs, flavour and electroweak observables 75
6.2.3 LHC direct SUSY searches 77
6.2.4 Electroweak symmetry breaking 79

7 Numerical results of the GFV_{123} scenario **82**
7.1 Regions with the **SU**(**5**) Yukawa matrix unification 82
7.2 Phenomenology of the GFV_{123} scenario 84
7.2.1 Lepton Flavour Violating observables 84
7.2.2 EW vacuum stability 85

8 Conclusions **89**
8.1 Summary 89
8.2 Open questions and discussion 90

List of Figures

1.1 Explanation of threshold corrections. 17
1.2 Diagrams illustrating the hierarchy problem in the non-SUSY $SU(5)$ GUT. . 25
1.3 Diagrams illustrating the SUSY solution to the hierarchy problem. 27
1.4 Renormalisation scale dependence of the SM and MSSM gauge couplings. . . 32
1.5 Renormalisation scale dependence of the MSSM gauge couplings. 33
1.6 RG-running of Y_s and Y_μ in the MSSM with an adjusted lower-end boundary. 36

2.1 Diagrams describing the gluino-mediated threshold corrections to the Yukawa couplings. 41
2.2 A diagram contributing to the higgsino-mediated threshold corrections to the Yukawa couplings. 42
2.3 Y_b/Y_τ at $M_{\rm GUT}$ as a function of A^{de}_{33} and m_0. 43
2.4 Y_s/Y_μ at $M_{\rm GUT}$ as a function of A^{de}_{22} and m_0. 44
2.5 Y_d/Y_e at $M_{\rm GUT}$ as a function of A^{de}_{11} and m_0. 45
2.6 Diagrams contributing to the gluino-mediated threshold correction with flavour mixing. 46

3.1 MSSM Feynman diagrams contributing to $\bar{K}^0 K^0$ mixing 48
3.2 Examples of SM diagrams contributing to $\overline{\mathcal{B}}(B_s \to \mu^+\mu^-)$. 50
3.3 SM LO Feynman diagrams contributing to $\mathcal{B}(\bar{B} \to X_s\gamma)$ 51
3.4 Sample MSSM diagrams contributing to $\mathcal{B}(\bar{B} \to X_s\gamma)$ 52
3.5 Sample SM and MSSM diagrams generating the $\mu^+ \to e^+\gamma$ decay. 53
3.6 CMS SUSY searches summary plot for the 8 TeV data. 55
3.7 ATLAS SUSY searches summary plot for the 8 TeV data. 56
3.8 Evidence of dark matter - galaxy rotation curves and gravitational lensing. . 58

4.1 Iterative procedure of solving RGE problem in MSSM. 61

5.1 Points consistent with SU(5) Yukawa matrix unification in the $\tan\beta\times(A^{de}_{11}/M_{1/2})$ and $\tan\beta \times (A^{de}_{22}/M_{1/2})$ planes. 68
5.2 Points consistent with SU(5) Yukawa matrix unification in the $\tan\beta\times(A^{de}_{33}/M_{1/2})$ and $\tan\beta \times M_{1/2}$ planes. 69
5.3 Dependence of $\delta\mathcal{B}_\gamma$ on A^{de}_{33} and $\tan\beta$. 70
5.4 Dependence of $\delta\overline{\mathcal{B}}_{s\mu}$ on A^{de}_{33} and $\tan\beta$. 70

6.1 GFV_{23} points in the planes ($M_{1/2}$, A^d_{33}), (m_{H_d}/m_{H_u}, $\tan\beta$), and (m^{dl}_{23}/m^{dl}_{33}, m^{dl}_{22}/m^{dl}_{33}) 74

6.2 Relative distributions of points gathered by the GFV_{23} scan in $\tan\beta$, and a scatter plot showing these points in the plane (m_{22}^{dl},μ). 75
6.3 Scatter plot of the GFV_{23} points in the planes (m_A, μ), ($m_{\tilde{\chi}_1^0}$, σ_p^{SI}) and ($\tan\beta$, $M_{1/2}$) 76
6.4 Properties of points that successfully fit DM relic density. 77
6.5 Scatter plot of the GFV_{23} points in the planes (m_h, M_{SUSY}), ($\mathcal{B}\left(\overline{B} \to X_s\gamma\right)$, $\mathcal{B}(B_s \to \mu^+\mu^-)$) and ($\epsilon_K$, $\Delta M_{B_d}/\Delta M_{B_s}$) 78
6.6 GFV_{23} points in the planes ($\mathcal{B}(\mu^+ \to e^+\gamma)$, $\mathcal{B}(\mu^+ \to e^+e^+e^-)$), and ($\mathcal{B}(\tau^+ \to \mu^+\gamma)$, $\mathcal{B}(\tau^+ \to \mu^+\mu^+\mu^-)$) 79
6.7 Characteristic spectra. 80
6.8 GFV_{23} points in the planes ($m_{\tilde{d}_1}$, $m_{\tilde{\chi}_1^0}$), and ($m_{\tilde{d}_1}$, $m_{\tilde{g}}$) 81
6.9 Histograms of points gathered by the GFV_{23} scan as a function of $A_{33}^d/(Y_{33}^d\widetilde{m}_3)$. 81

7.1 Scatter plot of the GFV_{123} points in the planes (m_{13}^{dl}/m_{33}^{dl}, m_{12}^{dl}/m_{33}^{dl}) and (m_{23}^{dl}/m_{33}^{dl}, m_{13}^{dl}/m_{33}^{dl}) 84
7.2 Scatter plost of the GFV_{123} points in the planes (A_{12}^{de}/A_{33}^{de}, A_{21}^{de}/A_{33}^{de}), (A_{13}^{de}/A_{33}^{de}, A_{31}^{de}/A_{33}^{de}) and (A_{23}^{de}/A_{33}^{de}, A_{32}^{de}/A_{33}^{de}) 85
7.3 GFV_{123} points in the planes ($M_{1/2}$, A_{33}^d), (m_{H_d}/m_{H_u}, $\tan\beta$), and (m_{11}^{dl}/m_{22}^{dl}, m_{11}^{dl}/m_{33}^{dl}) 86
7.4 $\mathcal{B}(\mu^+ \to e^+\gamma)$ calculated for points from GFV_{123} scan. 87
7.5 EW vacuum CCB (a) and UFB (b) stability bounds on the elements $A_{12/21}^d$ and $A_{12/21}^e$. 88

List of Tables

1.1 Field content of the Standard Model. 19
1.2 MSSM matter fields. 28

4.1 Standard Model parameters used in numerical calculations for the large diagonal A-term scenario. 62
4.2 Standard Model parameters used in numerical calculations for GFV scenario. 63

5.1 Examples of points with a successful Yukawa unification in the large diagonal A terms scenario. 65
5.2 Values of the threshold corrections and other characteristics of the points. . . 65
5.3 Masses of selected sfermions (in GeV). 66
5.4 Masses of the gluino, neutralinos, charginos, pseudoscalar A_0 and the value of μ parameter (in GeV). 66
5.5 Values of the ratios $A^d_{ii}/\widetilde{m}_i$ at the scale M_{SUSY}. 67

6.1 Experimental constraints applied in the analysis. 72
6.2 Ranges of the input SUSY parameters used in the final GFV_{23} scan. 73

7.1 Ranges of the input SUSY parameters used in the initial GFV_{123} scan. . . . 83
7.2 Ranges of the input SUSY parameters in the final scan for the GFV_{123} scenario. 87

Outline

In the years when the research resulting in this thesis was performed, a major breakthrough in particle physics took place. In 2012, the experiments ATLAS and CMS at the Large Hadron Collider (LHC)[1] at CERN announced the discovery of a particle whose properties overlap with those of the Standard Model (SM) Higgs boson. Thus, all the particles postulated by the SM have already been observed, and, at the time of writing, all its parameters are known with an arguably good precision. On the other hand, despite decades of dedicated studies, no clear contradiction between the SM predictions and experimental data has been observed, provided the SM is supplemented with dimension-five operators that generate the neutrino masses. Also, the Dark Matter (DM) in the Universe is not explained within the SM, which can be resolved by adding an extra (super)weakly interacting particle. Admittedly, there are a few earth-based measurements in which tensions with the SM predictions occur, but they either seem to be debatable or at least statistically allowed given the large number of observables considered. At present, there is no principle that would clearly show a direction for phenomenology beyond the SM. In this work, we make a step on a path that follows a very traditional, popular, and still uncontested direction, namely unification of all the known gauge interactions within what might be its simplest realisation possible.

Supersymmetric Grand Unified Theories (SUSY GUTs) have been the topic of numerous studies since the original formulation of the $SU(5)$ model [1]. A successful unification of the gauge couplings at $M_{\rm GUT} \simeq 2 \times 10^{16}\,\text{GeV}$ in the Minimal Supersymmetric Standard Model (MSSM) is a phenomenological triumph of this programme. GUT symmetries are decisively helpful, as they provide boundary conditions at the high energy scale. In effect, the dimensionality of the huge MSSM parameter space gets reduced.

A not yet completely solved quantitative issue of SUSY GUTs is a consistent treatment of their Yukawa sector. In typical MSSM scenarios, an equality of the down-quark and lepton Yukawa matrices at $M_{\rm GUT}$ would contradict the measured masses of the first- and second-generation fermions. To reconcile those two constraints without introducing non-minimal Higgs sectors above $M_{\rm GUT}$, one needs to consider large threshold corrections either at $M_{\rm GUT}$, or at the superpartner decoupling scale $\mu_{\rm sp}$. In this work, we focus on adjusting the threshold corrections at the matching scale $\mu_{\rm sp}$ between the SM and the MSSM, while assuming that those at $M_{\rm GUT}$ are small. We analyse two MSSM scenarios, an essential difference between which lies in the role of flavour. The first one assumes the soft supersymmetry breaking terms (soft terms) to be flavour-diagonal in the super-CKM basis, and can be nicknamed "large diagonal A-term scenario". The second one makes use of the soft-term flavour-off-diagonal entries, which implies considering the General Flavour Violating (GFV) MSSM. We first analyzed the large A-term scenario, and the obtained results served as a motivation for our second attempt to resolve the Yukawa matrix unification problem.

[1] Definitions of all the abbreviations used in this work are collected in the List of Acronyms on page 92.

Our analysis of the first scenario updates that of Ref. [2] with a broader range of $\tan\beta$ (reaching 40) and a universal scalar mass m_0. We have taken into account new experimental data, and performed a quantitative study of flavour observables. Results from the LHC experiments at 7 and 8 TeV have constrained the superpartner masses both via direct searches and by fixing the lightest Higgs boson mass. This calls for an up-to-date analysis of the Yukawa unification. We confirm that the $SU(5)$ Yukawa coupling unification of all the three families is phenomenologically viable, and attainable for a wide range of $\tan\beta$. However, its price in this case is that the standard MSSM vacuum (in which only the neutral Higgs fields acquire non-vanishing Vacuum Expectation Values (VEVs)) becomes a metastable one. Fortunately, it remains sufficiently long-lived, i.e. its estimated lifetime is significantly longer than the present age of the Universe. The outcome of this research was published in Ref. [3].

The second framework assumes that the diagonal entries of the trilinear terms have the same hierarchy as the Yukawa couplings. However, non-zero off-diagonal entries in the sfermion mass matrices and trilinear terms are allowed.

First, we restrict ourselves to the cases of bottom-tau and strange-muon Yukawa couplings. In the strange-muon case, the necessary threshold corrections are the largest and most troublesome. We begin with introducing flavour violation into the GUT-scale soft terms solely via the $(m^2_{\tilde{d}})_{23}$ and $(m^2_{\tilde{l}})_{23}$ elements of the down-type squark and lepton-doublet soft mass matrices, respectively. The role of $(m^2_{\tilde{d}})_{23}$ is to "transmit" the large threshold correction that affects the bottom quark Yukawa coupling to the strange quark one. We call this scenario GFV_{23}, as only the second and third generations are involved.

We perform a full phenomenological analysis of this scenario, taking into account such observables as the mass and decay rates of the lightest Higgs boson, electroweak (EW) precision tests, flavour observables, relic density of the neutralino DM, limits on the spin-independent proton-neutralino scattering cross-section, as well as the 8 TeV LHC exclusion bounds from the direct SUSY searches. We find that the $SU(5)$ Yukawa unification condition for the third and second generations is consistent at 3σ with all the considered experimental constraints, and it does *not* imply metastability of the standard MSSM vacuum, contrary to the large diagonal A-term scenario.

The phenomenological features of the GFV_{23} scenario make it an alternative to models that assume Minimal Flavour Violation (MFV). A crucial role in the successful Yukawa coupling unification in the GFV case is played by the chirality-preserving mixing term $(m^2_{\tilde{d}})_{23}$ between the second and third generations of down-type squarks. This particular mixing is less constrained by the Flavour Changing Neutral Current (FCNC) processes, as compared to other off-diagonal entries in the soft terms. Moreover, low values of $\tan\beta$ and heaviness of the squarks make supersymmetric contributions to the flavour observables relatively small in the considered scenario.

In the GFV MSSM, one may also attempt to unify the electron and down-quark Yukawa couplings. However, it requires relatively large values of the flavour-violating soft terms that involve the first generation. We analyse this framework as the so-called GFV_{123} scenario. Investigating the Lepton Flavour Violating (LFV) observables, we find that for the points with a full $SU(5)$ Yukawa matrix unification, the predicted values of $\mathcal{B}(\mu^+ \to e^+\gamma)$ and $\mathcal{B}(\mu^+ \to e^+e^+e^-)$ exceed the experimental 90% C.L. upper limits.

Our analysis of the GFV scenarios has been published[2] in Ref. [4], prepared in collabo-

[2] See the current (v2) arXiv version of the article where both the GFV_{23} and GFV_{123} scenarios are described. The journal version is restricted to the GFV_{123} case, while the LFV constraint, indicated near Eq. (3.2) there, is discussed further in the "note added in the proof".

ration with dr K. Kowalska. She was the main contributor to the derivation of constraints from dark matter, as well as from the direct SUSY searches at the LHC.

In our discussion of the $SU(5)$ unification of the Yukawa couplings, we restrict ourselves solely to the minimal case in which one demands equality of the lepton and down-quark Yukawa matrices at the GUT scale. We treat the up-quark Yukawa matrix as unrelated, and use a basis in which the SM quark flavour mixing originates from this matrix only. Moreover, we assume that the neutrino masses and mixings originate from decoupling of superheavy right-handed neutrinos whose Majorana mass matrix has an arbitrary flavour structure. Thus, no constraints from the neutrino experiments affect our analysis.

The thesis is organised as follows. In Chapter 1, the theoretical background and reasoning introducing the problem of Yukawa unification in the MSSM is described. In Chapter 2, the two scenarios for the soft terms are defined, and an illustrative analysis of supersymmetric threshold corrections to the Yukawa couplings is performed. Chapter 3 introduces the phenomenological constraints imposed on the model. In Chapter 4, numerical tools employed in the analysis are described. Chapter 5 scrutinises the results obtained in the first scenario – with large diagonal A-terms. Chapter 6 shows the outcome of our investigation of the GFV_{23} scenario, namely the successful bottom-tau and strange-muon Yukawa coupling unification. Then, Chapter 7 describes how the GFV_{123} scenario is capable of the full $SU(5)$ Yukawa matrix unification, but comes short of satisfying the LFV constraints. We conclude in Chapter 8.

CHAPTER 1

Introduction

The problems addressed in this work can be described by a perturbative Quantum Field Theory (QFT). Throughout the whole introduction, we aim at recalling the definitions that are necessary for a qualitative understanding of the presented results, rather than at introducing quantitative techniques of the perturbative QFT from the outset. These are covered in an extensive collection of textbooks, see e.g. Refs. [5–8].

1.1 Preliminaries

Before introducing the models we deal with in this work, let us briefly review a few of the basic concepts that matter for our purpose. In particular, one should mention the idea of *effective theories* that is crucial for the phenomenology of fundamental interactions. It provides a language for describing the same phenomena in terms of several QFTs defined at different scales, and rules for correlating their parameters.

We shall deal with the simplest version of an effective QFT that originates from heavy particle decoupling. In the framework of perturbative QFT, it is based on the following observation. If a model contains particles with masses heavier than the center-of-mass energy of a given process, all the diagrams influencing the process can contain those heavy fields only as intermediate states. They can never appear at the external legs. Therefore, in an effective theory to which the considered model can be reduced, those heavy fields are not explicitly present as degrees of freedom. They only modify interactions between the remaining particles.

For example, the SM can be viewed as an effective field theory derived from a model containing additional particles. This, in turn, can also be an effective theory that has a more fundamental source. In this way, our description of the fundamental interactions can consist of layers of theories, unravelling when higher energies are reached. In this dissertation, we will consider the SM as originating from the MSSM at the scale $\mu_{\rm sp}$, further described by a supersymmetric GUT, valid above $M_{\rm GUT}$.

1.1.1 Renormalisation Group Equations

Values of the renormalised constants of a given effective QFT are determined at specified energy scales. Each scale corresponds to the energy scale of the process which is used for the considered parameter determination. Once the parameters are fixed, we often need to use

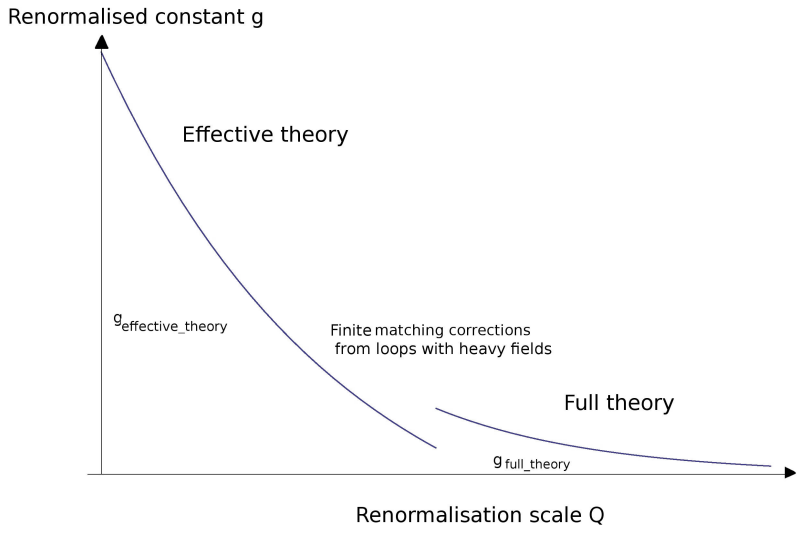

Figure 1.1: An illustration of the matching for a parameter g between the full and effective theories. The discontinuity is given by the threshold correction (see the text).

them in processes that take place at very different energy scales. This requires modifying the renormalisation scheme for the parameters to avoid introducing spurious perturbative uncertainties. Throughout the present thesis, unless explicitly specified, we shall assume that our parameters are renormalised in the modified Minimal Subtraction ($\overline{MS}$) scheme at various renormalisation scales Q. Values of the renormalised (running) couplings $c_i(Q)$ at any scale Q can be determined by solving the Renormalisation Group Equations (RGEs) of a form

$$Q\frac{d}{dQ}\begin{pmatrix} c_1(Q) \\ c_2(Q) \\ ... \end{pmatrix} = f(c_1(Q), c_2(Q), ...). \tag{1.1}$$

The function f can be calculated order-by-order in perturbation theory from the $\overline{MS}$ renormalisation constants of the considered QFT. The RGEs are systems of ordinary differential equations. As they might be coupled and non-linear, they are often unsolvable analytically. In such cases, testing a high-energy theory with the help of low-energy observables requires scanning the high-energy theory parameter space, and numerically solving the RGEs point-by-point in this space.

1.1.2 Threshold corrections

Having renormalised a given effective QFT, and having solved its RGEs, we know the values of its renormalisation-scale-dependent couplings at all scales. However, when one works with several layers of effective theories, a new question arises: how to translate parameters of one theory to the parameters of another? In other words, what are the relations between renormalised couplings of two different effective theories that describe the same physical system? We illustrate this in Fig. 1.1, where g stands for a particular parameter that is present both theories (e.g., the QCD gauge coupling in the MSSM and SM). In the plot, the two theories are nicknamed "full theory" and "effective theory", but they can actually both be effective. In each of them, the coupling g depends on the renormalisation scale Q. The

dependence is different, because the spectra of the two theories are different. We want to use the full (effective) theory above (below) a certain scale that we shall call $\mu_{\rm sp}$, to maintain the analogy with the case of passing from the MSSM to the SM. The scale $\mu_{\rm sp}$ is called the matching scale. The relation between the couplings at this scale takes the form

$$g_{\text{effective theory}}(\mu_{\rm sp}) = g_{\text{full theory}}(\mu_{\rm sp}) + \Delta g(\mu_{\rm sp}), \tag{1.2}$$

where $\Delta g(\mu_{\rm sp})$ is called the *threshold correction*. It is responsible for the discontinuity in the curve presented in Fig. 1.1. Its presence means that the "same" renormalised coupling g means different things in both models. The consistency requirement from which the actual values of threshold corrections are derived is that both theories must give the same predictions for physical processes involving only light particles (i.e. the low-energy theory degrees of freedom). Instead of matching the physical amplitudes, it is often more convenient to match several light-particle Green's functions with arbitrary off-shell momenta. If, in addition, an expansion in these momenta is applied prior to the loop momentum integration, evaluation of the threshold corrections becomes particularly simple. In such a case, they are given by finite parts of the loop diagrams involving heavy fields on the full theory side, as indicated in Fig. 1.1.

1.2 The Standard Model

In this section we introduce the foundation of our present understanding of particle physics - the Standard Model. It is an experimentally unchallenged starting point of any high energy speculations.

1.2.1 Field content and Lagrangian density

The Standard Model (SM) is a renormalisable gauge theory, based on three Lie groups $U(1)$, $SU(2)$ and $SU(3)$. Starting from the successful unified theory of electroweak interactions by Sheldon Glashow [9], it was conceived independently by Steven Weinberg and Abdus Salam [10]. They applied the mechanism worked out in Refs. [11–14], further referred to as the *Higgs mechanism*, to resolve the electroweak theory problems with unitarity and weak boson masses. The SM contains the following fields.[1]

Gauge fields:

- gluons: G^A_μ,
- W bosons: W^I_μ,
- B boson: B_μ,

Matter fermion fields:

- left-handed leptons: $l^p_i = \begin{pmatrix} \nu^p \\ e^p_L \end{pmatrix}_i$,

[1] The indices $i = 1, 2$ and $a = 1, 2, 3$ – weak isospin and colour – correspond to the fundamental representations of $SU(2)$ and $SU(3)$, respectively, $I = 1, 2, 3$ and $A = 1, \ldots, 8$ – to their adjoint representations, whereas $p = 1, 2, 3$ enumerates the fermion generations called flavours.

field	representation		hypercharge
	$SU(3)$	$SU(2)$	$U(1)_Y$
G_μ	**8**	1	0
W_μ	1	**3**	0
B_μ	1	1	0
q	**3**	**2**	$\frac{1}{6}$
u_R	**3**	1	$\frac{2}{3}$
d_R	**3**	1	$-\frac{1}{3}$
l	1	**2**	$-\frac{1}{2}$
e_R	1	1	-1
φ	1	**2**	$\frac{1}{2}$

Table 1.1: Field content of the Standard Model.

- right-handed leptons: e_R^p ,
- left-handed quarks: $q_i^{ap} = \begin{pmatrix} u_L^{ap} \\ d_L^{ap} \end{pmatrix}_i$,
- right-handed quarks: u_R^{ap}, d_R^{ap},

Higgs scalar fields:

- The Higgs doublet: φ_i.

Using

$$\varepsilon = \begin{pmatrix} 0 & 1 \\ -1 & 0 \end{pmatrix}$$

we also define $\tilde{\varphi} = \varepsilon\varphi^*$, which implies that $\tilde{\varphi}^\dagger = -\varphi^T\varepsilon$.

To concisely define the SM Lagrangian density in terms of its fields, we need to introduce a few more objects. A covariant derivative of the left-handed quark field has the following form:

$$D_\mu q = \left(\partial_\mu + ig_s G_\mu^A T^A + igW_\mu^I S^I + ig' Y_q\right) q, \tag{1.3}$$

or, with explicit isospin and colour indices

$$(D_\mu q)_j^a = \left(\partial_\mu + ig' Y_q\right) q_j^a + ig_s G_\mu^A T_{ab}^A q_j^b + igW_\mu^I S_{jk}^I q_k^a. \tag{1.4}$$

Here, T^A and S^I are the fundamental representation generators of, respectively, the SU(2) and SU(3) groups, while $Y_q = \frac{1}{6}$ denotes the hypercharge of the field q. Covariant derivatives of other matter, gauge and Higgs fields are defined in an analogous manner, following the field assignment to various representations of $SU(2)$ and $SU(3)$, as given in Tab. 1.1. Generators of singlet representations are equal to zero.

The field-strength tensors of the SM gauge fields are given by

- $SU(3)$
$$G^A_{\mu\nu} = \partial_\mu G^A_\nu - \partial_\nu G^A_\mu - g_s f^{ABC} G^B_\mu G^C_\nu, \tag{1.5}$$
- $SU(2)$
$$W^I_{\mu\nu} = \partial_\mu W^I_\nu - \partial_\nu W^I_\mu - g\varepsilon^{IJK} W^J_\mu W^K_\nu, \tag{1.6}$$
- $U(1)_Y$
$$B_{\mu\nu} = \partial_\mu B_\nu - \partial_\nu B_\mu. \tag{1.7}$$

In the following, we will suppress the isospin, colour and flavour indices, as contractions of them will always be straightforward, e.g.,

$$(\bar{q}\,\mathbf{Y^{u\star}} u_R)\tilde{\varphi} \quad \equiv \quad \bar{q}_i^{ap}\,\mathbf{Y}^{\mathbf{u}\star}_{pp'}\,u_R^{ap'}\,\tilde{\varphi}_i.$$

With the above-listed objects at hand, the Lagrangian density of the Standard Model can be written as follows:[2]

$$\begin{aligned}\mathcal{L}_{\rm SM} = &-\tfrac{1}{4}G^A_{\mu\nu}G^{A\mu\nu} - \tfrac{1}{4}W^I_{\mu\nu}W^{I\mu\nu} - \tfrac{1}{4}B_{\mu\nu}B^{\mu\nu}\\ &+ (D_\mu\varphi)^\dagger(D^\mu\varphi) + m^2\varphi^\dagger\varphi - \tfrac{1}{2}\lambda(\varphi^\dagger\varphi)^2\\ &+ i\left[\bar{l}\,\not{D} l + \bar{e}_R\,\not{D} e_R + \bar{q}\,\not{D} q + \bar{u}_R\,\not{D} u_R + \bar{d}_R\,\not{D} d_R\right]\\ &- \left[(\bar{l}\mathbf{Y^{e\star}}e_R)\varphi + (\bar{q}\mathbf{Y^{u\star}}u_R)\tilde{\varphi} + (\bar{q}\mathbf{Y^{d\star}}d_R)\varphi + \text{h.c.}\right].\end{aligned} \tag{1.8}$$

To describe the observed neutrino masses and mixings without introducing new degrees of freedom, the SM needs to be thought about as an effective theory, the so-called Standard Model Effective Field Theory (SMEFT). Its Lagrangian density has the following general form:

$$\mathcal{L}_{\rm SMEFT} \;=\; \mathcal{L}_{\rm SM} \;+\; \frac{1}{\Lambda}\sum_k C_k^{(5)}Q_k^{(5)} \;+\; \frac{1}{\Lambda^2}\sum_k C_k^{(6)}Q_k^{(6)} \;+\; \dots\,, \tag{1.9}$$

where $Q_k^{(n)}$ stand for dimension-n operators built out of the SM fields, $C_k^{(n)}$ are the corresponding coupling constants (Wilson coefficients), and Λ is a certain scale that defines the validity region of our effective theory. All the phenomenological predictions are given as series in powers of $1/\Lambda$, with masses and kinematical invariants standing in the numerators. Thus, the quantities in the numerators must be much smaller than Λ.

Imposing the SM gauge symmetry on $Q_n^{(5)}$ leaves out just a single operator [15], up to a Hermitian conjugation and flavour assignments. It reads

$$Q^{pr}_{\nu\nu} = \varepsilon_{jk}\varepsilon_{mn}\varphi_j\varphi_m(l^p_k)^T C l^r_n \;\equiv\; (\tilde{\varphi}^\dagger l^p)^T C(\tilde{\varphi}^\dagger l^r), \tag{1.10}$$

where C is the charge conjugation matrix. After the Electroweak Symmetry Breaking (EWSB), such operators generate the neutrino masses and mixings. Since the neutrino masses are very small, it is conceivable that the scale Λ standing in front of $Q^{pr}_{\nu\nu}$ in Eq. (1.9) is very large, many orders of magnitude above the electroweak scale. If this is the case, the neutrinos can be treated as massless for our purpose. We are going to assume this is the case, and ignore the presence of $Q^{pr}_{\nu\nu}$ in what follows.

As far as the Dark Matter is concerned, we shall not introduce any candidate for it in the SM but rather assume that it will come with the MSSM degrees of freedom, above the $\mu_{\rm sp}$ matching scale.

[2] We take the Yukawa coupling matrices complex conjugated here to make the notation consistent with the standard MSSM expression (1.32) for the superpotential.

1.2.2 Spontaneous Electroweak Symmetry Breaking and fermion masses

In the Standard Model with unbroken gauge symmetry, all the gauge bosons are massless. On the other hand, we know that in Nature, to the contrary, they are among the heaviest known elementary particles. Giving masses to the gauge bosons was the purpose for introducing the Higgs field into the SM Lagrangian, and then invoking the Higgs mechanism. It is a spontaneous breaking of the $SU(2) \times U(1)_Y$ symmetry to the residual electromagnetic gauge symmetry $U(1)_{em}$. The Higgs field φ (being a complex-valued $SU(2)$ doublet) acquires a vacuum expectation value (VEV). Without loss of generality (by using the gauge symmetries), one can write the VEV as

$$\langle 0|\varphi|0\rangle = \frac{1}{\sqrt{2}}\begin{pmatrix}0\\ v\end{pmatrix}. \tag{1.11}$$

Substituting the above VEV into $\mathcal{L}_{\rm SM}$, one finds the tree-level masses of the W and Z bosons, namely $M_W = \frac{1}{2}vg$ and $M_Z = \frac{1}{2}v\sqrt{g^2+g'^2}$. The measured values of these masses and gauge couplings imply that $v \approx 246$ GeV.

In fact, not only do the W and Z bosons acquire masses from their interactions with the Higgs doublet φ. Also the fermion mass terms originate from their Yukawa interactions with φ:

$$\mathcal{L}_{\rm f.\,mass} \;=\; -\frac{v}{\sqrt{2}}\left[\bar{u}_L \mathbf{Y^{u\star}} u_R + \bar{d}_L \mathbf{Y^{d\star}} d_R + \bar{e}_L \mathbf{Y^{e\star}} e_R + \text{h.c.}\right]. \tag{1.12}$$

The physical Higgs field h^0 is a real scalar field that parameterises the departure of φ from the VEV. In the so-called unitary gauge, we have

$$\varphi = \frac{1}{\sqrt{2}}\begin{pmatrix}0\\ v+h^0\end{pmatrix}. \tag{1.13}$$

The fermion mass sector is the main focus of the analysis performed in this work. The basis in which we have defined the SM in Eq. (1.8) is known as the *weak-eigenstate basis* or the *interaction basis*. The Yukawa couplings, being matrices in flavour space, are not diagonal in that basis. Their singular value decomposition leads to the *fermion mass-eigenstate basis* $\left\{\hat{u}_L, \hat{u}_R, \hat{d}_L, \hat{d}_R, \hat{e}_L, \hat{e}_R\right\}$, in which the mass matrices $\mathbf{m}^u, \mathbf{m}^d, \mathbf{m}^e$ are real and diagonal:

$$\bar{u}_L \mathbf{Y^{u\star}} u_R \tfrac{v}{\sqrt{2}} + \text{h.c.} \;=\; \bar{\hat{u}}_L (V_{uL}^\dagger \mathbf{Y^{u\star}} V_{uR}) \hat{u}_R \tfrac{v}{\sqrt{2}} + \text{h.c.} \;=\; \bar{\hat{u}}_L \mathbf{m}^u \hat{u}_R \;+\; \text{h.c.}\,, \tag{1.14}$$

$$\bar{d}_L \mathbf{Y^{d\star}} d_R \tfrac{v}{\sqrt{2}} + \text{h.c.} \;=\; \bar{\hat{d}}_L (V_{dL}^\dagger \mathbf{Y^{d\star}} V_{dR}) \hat{d}_R \tfrac{v}{\sqrt{2}} + \text{h.c.} \;=\; \bar{\hat{d}}_L \mathbf{m}^d \hat{d}_R \;+\; \text{h.c.}\,, \tag{1.15}$$

$$\bar{e}_L \mathbf{Y^{e\star}} e_R \tfrac{v}{\sqrt{2}} + \text{h.c.} \;=\; \bar{\hat{e}}_L (V_{eL}^\dagger \mathbf{Y^{e\star}} V_{eR}) \hat{e}_R \tfrac{v}{\sqrt{2}} + \text{h.c.} \;=\; \bar{\hat{e}}_L \mathbf{m}^e \hat{e}_R \;+\; \text{h.c.}\,. \tag{1.16}$$

Passing to the mass-eigenstate basis undergoes via the following unitary redefinitions of the fields in the flavour space:

$$u_L = V_{uL}\hat{u}_L\,, \quad u_R = V_{uR}\hat{u}_R\,, \quad d_L = V_{dL}\hat{d}_L\,, \quad d_R = V_{dR}\hat{d}_R\,, \quad e_L = V_{eL}\hat{e}_L\,, \quad e_R = V_{eR}\hat{e}_R\,. \tag{1.17}$$

Such a transformation is neither a symmetry of $\mathcal{L}_{\rm SM}$, nor it can be compensated by a redefinition of its parameters. This fact is a consequence of that different flavour transformations

are applied separately to particular components of the $SU(2)$ doublets. However, apart from the Yukawa terms, the only other part of the Lagrangian density that gets affected by the considered basis change are the interactions of quarks with charged W bosons

$$W^{\pm} = \tfrac{1}{\sqrt{2}}(W^1 \mp iW^2). \tag{1.18}$$

Rewriting them in the mass-eigenstate basis, we get

$$\mathcal{L}_{\mathrm{SM}} \ni -g\bar{u}_L\gamma^\mu d_L W^+_\mu + \mathrm{h.c.} = -g\overline{\hat{u}}_L(V^\dagger_{uL}V_{dL})\gamma^\mu \hat{d}_L W^+_\mu + \mathrm{h.c.}\ . \tag{1.19}$$

Here,

$$(V^\dagger_{uL}V_{dL}) \equiv V_{CKM} \tag{1.20}$$

stands for the Cabibbo-Kobayashi-Maskawa [16, 17] matrix (CKM matrix). This matrix is the only source of flavour- and CP-violation in the SM, once the fields are expressed in the mass-eigenstate basis.

It is important to stress that the flavour- and CP-violation are basis-dependent concepts. Before we pass to the mass-eigenstate basis, we are not even able to define the discrete CP symmetry that is being tested in experiments.[3] Flavour in the interaction basis is violated by the Yukawa couplings but conserved by the gauge interactions. On the other hand, in the mass-eigenstate basis, the Yukawa interactions with h^0 conserve flavour, but the gauge interactions do not.

Although all the SM constituents correspond to distinct experimentally established particles, its underlying structure remains complicated. We have three independent gauge groups and three generations, each involving five different matter representations. Thus, there seems to remain some space for a further simplification of our description of fundamental interactions.

1.3 Grand Unified Theories

In this section, the grand unification idea is motivated, and the $SU(5)$ GUT, the simplest model realising this idea, is introduced. Gauge coupling unification is discussed as the historical quantitative argument for the GUTs. In the last part, we observe how the hierarchy problem arises in the considered framework.

1.3.1 Algebraical considerations

The involved algebraical structure of the SM symmetry group $SU(3) \times SU(2) \times U(1)$ and its representations have motivated efforts to find a simpler gauge symmetry group. It would get spontaneously broken to the SM group, by analogy to the breaking of the SM group to $SU(3) \times U(1)_{em}$. This idea becomes even more natural at present, once the SM Higgs mechanism has already been experimentally confirmed by the discovery of the Higgs boson at the LHC.

[3] The transformation $\psi \to C\bar{\psi}^T$ applied to each fermionic field does not commute with the linear transformations (1.17) that involve *complex* unitary matrices.

The smallest simple Lie group that can embed the SM group is $SU(5)$.[4] It was also the first one proposed for the role of a GUT group [18]. The lowest-dimensional irreducible representations of $SU(5)$ are two complex 5-dimensional ones ($\mathbf{5}$, $\bar{\mathbf{5}}$), and two complex 10-dimensional ones ($\mathbf{10}$, $\overline{\mathbf{10}}$). The crucial issue that governs the assignments of matter fields to their $SU(5)$ representations are the branching rules that describe how a $SU(5)$ representation is decomposed into a direct sum of the $SU(3) \times SU(2) \times U(1)$ representations. Below, we specify the representations by their dimensions in the cases of $SU(3)$ and $SU(2)$, and by the corresponding $U(1)$ generator eigenvalue.

To discuss the representation embedding, it is convenient to deal with fermions of fixed chirality. By convention, one chooses the left-handed ones. The fermionic $SU(2)$ doublets of the SM are taken as they stand, while the SU(2) singlets are described in terms of charge-conjugates of the original right-handed fields. Thus, we deal with a set of five left-handed fermionic representations of the SM group, namely q, u^c_R, d^c_R, l, e^c_R. It appears that those fields can be embedded into the $\bar{5}$ and 10 representations of $SU(5)$ as follows:

$$\begin{aligned} \underbrace{(\bar{\mathbf{3}}, \mathbf{1}, \tfrac{1}{3})}_{d^c_R} \oplus \underbrace{(\mathbf{1}, \mathbf{2}, -\tfrac{1}{2})}_{l} &= \underbrace{\bar{\mathbf{5}}}_{\Psi_{\bar{5}}}, \\ \underbrace{(\mathbf{3}, \mathbf{2}, \tfrac{1}{6})}_{q} \oplus \underbrace{(\bar{\mathbf{3}}, \mathbf{1}, -\tfrac{2}{3})}_{u^c_R} \oplus \underbrace{(\mathbf{1}, \mathbf{1}, 1)}_{e^c_R} &= \underbrace{\mathbf{10}}_{\Psi_{10}}, \end{aligned} \tag{1.21}$$

where we have used the conventional SM normalisation for the hypercharges Y. The proper GUT normalisation $Y_1 = \sqrt{\frac{3}{5}}Y$ is needed to ensure a uniform normalisation condition for all the $SU(5)$ generators: $\mathrm{Tr}(a^i_{SU(5)} a^j_{SU(5)}) = \frac{1}{2}\delta^{ij}$. It is achieved by rescaling the coupling constant g'. The choice of $\bar{\mathbf{5}}$ and $\mathbf{10}$ is necessary to fit the SM hypercharges. Remarkably, it also guarantees that the considered GUT gauge symmetry is anomaly-free.

In fact, it is easy to understand why the embedding of down-quarks and leptons into a single $\bar{\mathbf{5}}$ representation means that their respective hypercharges must follow the proportion of $-2:3$. The reason lies in the dimensions of the corresponding representations of $SU(3)$ and $SU(2)$ – the $SU(5)$ generator corresponding to $U(1)_Y$ must be traceless. A similar argument holds in the case of $\mathbf{10}$. In this way, the $SU(5)$ model solves the puzzle of charge quantization in the SM, explaining why they are commensurable at all, and it does so without resort to anomalies.

1.3.2 Gauge interactions

In addition to the matter fields $\Psi_{\bar{5}}$ and Ψ_{10}, the $SU(5)$ GUT includes the gauge fields Σ, belonging to the adjoint 24-dimensional representation. Under the action of the $SU(3) \times SU(2) \times U(1)$ subgroup, the gauge bosons decompose as:

$$\underbrace{(\mathbf{8}, \mathbf{1}, 0)}_{G} + \underbrace{(\mathbf{1}, \mathbf{3}, 0)}_{W} + \underbrace{(\mathbf{1}, \mathbf{1}, 0)}_{B} + \underbrace{(\mathbf{3}, \mathbf{2}, -\tfrac{5}{6})}_{X} + \underbrace{(\bar{\mathbf{3}}, \mathbf{2}, \tfrac{5}{6})}_{X^*} = \underbrace{\mathbf{24}}_{\Sigma} \tag{1.22}$$

The gauge multiplet contains all the SM gauge fields – gluons G, electroweak bosons W and B, as well as additional gauge fields X that carry both the $SU(2)$ and $SU(3)$ indices.

[4] Both are rank-4 groups.

The latter fields, if present in Nature, would mediate the yet-unobserved proton decay. The current lower bounds on the proton lifetime [19] imply that the masses of the X bosons must be very large (often called *superheavy*). These masses are by construction of the same order as M_{GUT}, i.e. the scale at which the GUT gauge symmetry is broken to the SM one. Thus, experimental bounds on the proton lifetime provide important constraints on M_{GUT} (see below).

The scalar sector has to serve a twofold purpose. The SM Higgs mechanism of weak-scale mass generation is realised by a field belonging to the fundamental representation $H_{\mathbf{5}}$. Other scalar fields, e.g., $\Phi_{\mathbf{24}}$ are responsible for breaking the $SU(5)$ symmetry to $SU(3) \times SU(2) \times U(1)$. Particular scalar sectors of the non-supersymmetric GUTs have been discussed in detail in Ref. [20].

In the following, we shall review two features of the model: the gauge coupling unification and the *hierarchy problem*. To formulate them, let us write explicitly the kinetic terms for the matter and $H_{\mathbf{5}}$ Higgs fields. They read

$$\mathcal{L}_{SU(5)} \ni i\overline{\Psi}_{\bar{5}} \not{D} \Psi_{\bar{5}} + i\overline{\Psi}_{10} \not{D} \Psi_{10} + (D_\mu H_5)^\dagger (D^\mu H_5), \tag{1.23}$$

with the covariant derivatives acting in the following way

$$\begin{aligned} (D_\mu H_5)^a &= \partial_\mu H_5^a + i g_5 (\Sigma_\mu)^a{}_b H_5^b, \\ (D_\mu \Psi_{\bar{5}})^a &= \partial_\mu \Psi_{\bar{5}}^a + i g_5 (-\Sigma_\mu^\star)^a{}_b \Psi_{\bar{5}}^b, \\ (D_\mu \Psi_{10})^{ab} &= \partial_\mu (\Psi_{10})^{ab} + i g_5 (\Sigma_\mu)^a{}_c (\Psi_{10})^{cb} + i g_5 (\Sigma_\mu)^b{}_d (\Psi_{10})^{ad}. \end{aligned} \tag{1.24}$$

1.3.3 Gauge coupling unification

The simplicity of the $SU(5)$ GUT, apparent in Eq. (1.24), relies on existence of only a single gauge coupling g_5. The strong and electroweak interactions are unified at the scale $M_{\mathrm{GUT}} \gg M_Z$. However, they must attain their significantly hierarchical coupling strengths at the low scales. At the time the model was conceived, the quantitative unification of gauge couplings based on the SM RGEs worked quite well within experimental errors of the 1970's. All the three properly normalised gauge couplings appeared to meet at a scale $M_{\mathrm{GUT}}^{1970s} \sim 10^{14 \div 15}\,\mathrm{GeV}$. The current knowledge is described further in the text.

The big hierarchy between the scales M_Z and M_{GUT} leaves a natural question of what happens at the intermediate scales. An assumption that no new particles exist at intermediate scales might be motivated by the successful gauge coupling unification. The unification could be spoiled by possible new physics that does not fit into the GUT framework.

1.3.4 Hierarchy problem

One of the features of Eqs. (1.23) and (1.24) is an interaction between the SM Higgs doublet φ (a part of the H_5 multiplet) and the superheavy gauge bosons X. The corresponding one-loop radiative corrections to the Higgs propagator are given by the diagrams in Fig. 1.2. They generate threshold corrections of the order of M_{GUT}^2 in the GUT-SM matching condition for the Higgs mass parameter m in the SM Lagrangian (1.8):

$$m^2 = m_{\mathrm{GUT}}^2 + \mathcal{O}(M_{\mathrm{GUT}}^2), \tag{1.25}$$

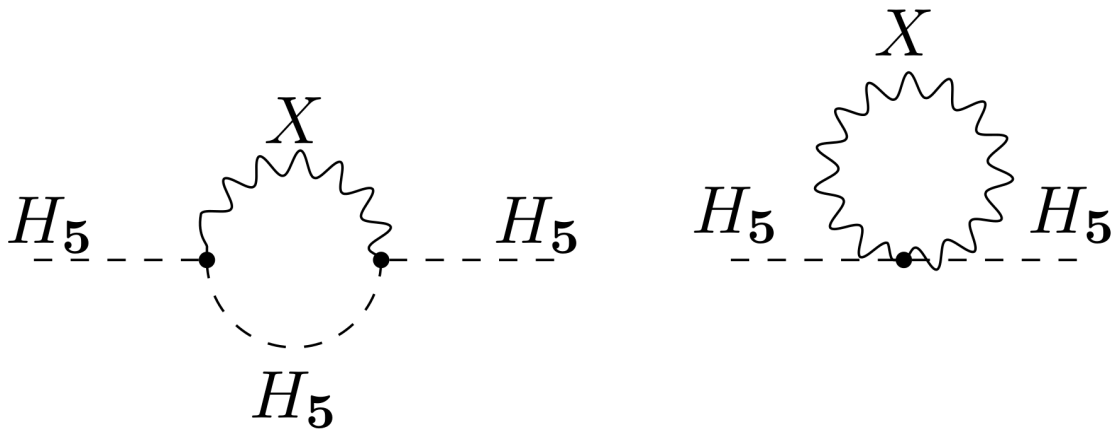

Figure 1.2: One-loop self-energy diagrams for the Higgs multiplet $H_{\mathbf{5}}$ that involve the gauge bosons X. They renormalise the scalar mass squared by contributions the order of M^2_{GUT}.

where m^2_{GUT} is the corresponding mass parameter in the GUT Lagrangian. The value of m of the order of $\mathcal{O}(100\,\mathrm{GeV})$ could only be a result of an "accidental" cancellation of contributions that are greater by many orders of magnitude. Such a fine-tuning problem occurs in all the "particle desert" scenarios that assume the SM at the weak scale, a GUT at the high scale, and nothing in between. It is often referred to as the *hierarchy problem*.

There are two main phenomenological routes of addressing the hierarchy problem, where the "particle desert" assumption is relaxed above a certain scale μ_0. They rely either on compositeness of the Higgs boson or on supersymmetry.[5] Both of them lead to the Higgs mass parameter being naturally of the order of $\mathcal{O}\left(\mu_0^2\right)$ instead of $\mathcal{O}(M^2_{\mathrm{GUT}})$. The first strategy treats the Higgs doublet as a bound state analogous to QCD mesons with a confinement scale $\mu_0 \sim 1\,\mathrm{TeV}$. Supersymmetric extensions of the SM are introduced in the next section. Interestingly, the physical Higgs mass is an observable where both scenarios yield different predictions. Supersymmetry generically predicts a smaller mass, whereas the composite Higgs models – a bigger one. The LHC measurement has posed a challenge for both frameworks, yet not excluding definitely any of them. A vast literature on this subject is reviewed, e.g., in Refs. [21–23].

1.4 Supersymmetry

In this section, supersymmetry (SUSY) is introduced as a framework in which both the hierarchy problem can be solved, and a precise gauge coupling unification can be achieved. First, it is defined as an algebraical concept. Next, the absence of quadratic radiative corrections to the Higgs boson mass is discussed. Subsequently, the Minimal Supersymmetric Standard Model (MSSM) is described, including the gauge coupling unification issue. At this point, the stage for considering the Yukawa coupling unification is set. For a detailed introduction to supersymmetry, see, e.g., Refs. [24, 25].

[5] In the case of supersymmetry, μ_0 is given by the superpartner decoupling scale μ_{sp}.

1.4.1 The SUSY algebra

As we have already noted, the SM has significant shortcomings if treated as a direct foundation for Grand Unified Theories. One of the possible directions for extending the model is to ask whether new principles of symmetry could be introduced simultaneously with extending the particle spectrum.

The complete symmetry of the SM as a relativistic QFT is given by its gauge group $SU(3) \times SU(2) \times U(1)$, and the Poincaré group $\mathcal{P}$ of the spacetime symmetries. The latter is generated by P_μ and $M_{\mu\nu}$ (with $\mu, \nu = 0, 1, 2, 3$) obeying the following commutation rules:

$$\begin{aligned} [P_\mu, P_\nu] &= 0, \\ [M_{\mu\nu}, P_\rho] &= -i(\eta_{\mu\rho} P_\nu - \eta_{\nu\rho} P_\mu), \\ [M_{\mu\nu}, M_{\rho\xi}] &= i(\eta_{\nu\rho} M_{\mu\xi} - \eta_{\nu\xi} M_{\mu\rho} - \eta_{\mu\rho} M_{\nu\xi} + \eta_{\mu\xi} M_{\nu\rho}). \end{aligned} \tag{1.26}$$

Coleman and Mandula showed in Ref. [26] that for any local relativistic QFT in four dimensions, generators T_s of any Lie group that describes an internal symmetry must commute with the Poincaré algebra ones

$$[P_\mu, T_s] = 0 = [M_{\mu\nu}, T_s]. \tag{1.27}$$

This is equivalent to saying that fields of different spin must transform independently under internal symmetries that are described by Lie groups. It seemed therefore, that the only way of changing the symmetries governing the model was to introduce different gauge groups, or different global symmetries, either continuous or discrete ones.

However, it turns out that there exist possible symmetries which are not described by Lie groups, and which nontrivially extend the Poincaré transformations. It was shown a few years later by Golfand and Likhtman [27], as well as by Wess and Zumino [28]. The mathematical framework governing such symmetries is based on Lie superalgebras, which differ from Lie algebras by being defined through both commutation and anticommutation relations among their elements.

As first derived in Ref. [29], a supersymmetric algebra contains the above-mentioned Poincaré generators P_μ and $M_{\mu\nu}$, together with a set of anticommuting supersymmetry generators in the $(\frac{1}{2}, 0)$ and $(0, \frac{1}{2})$ representations of the Lorentz group. The latter are denoted by Q_α and $\bar{Q}_{\dot{\beta}}$ with $\alpha, \dot{\beta} = 1, 2$ enumerating their spinorial indices. They are Hermitian conjugates of each other. In general, there could be more generations of Q's, but their number, called N, is restricted to 1 in most of the phenomenological applications.

The algebra of $N = 1$ supersymmetry has the following structure in addition to Eq. (1.26)

$$\begin{aligned} \{Q_\alpha, \bar{Q}_{\dot{\beta}}\} &= 2(\sigma^\mu)_{\alpha\dot{\beta}} P_\mu, \\ \{Q_\alpha, Q_\beta\} &= 0 = \{\bar{Q}_{\dot{\alpha}}, \bar{Q}_{\dot{\beta}}\}, \\ [Q_\alpha, P_\mu] &= 0 = [\bar{Q}_{\dot{\alpha}}, P_\mu], \\ [Q_\alpha, M_{\mu\nu}] &= -\frac{1}{2}(\sigma_{\mu\nu})_\alpha{}^\beta \, Q_\beta, \\ [\bar{Q}_{\dot{\alpha}}, M_{\mu\nu}] &= \frac{1}{2}(\bar{\sigma}_{\mu\nu})^{\dot{\beta}}{}_{\dot{\alpha}} \, \bar{Q}_{\dot{\beta}}. \end{aligned} \tag{1.28}$$

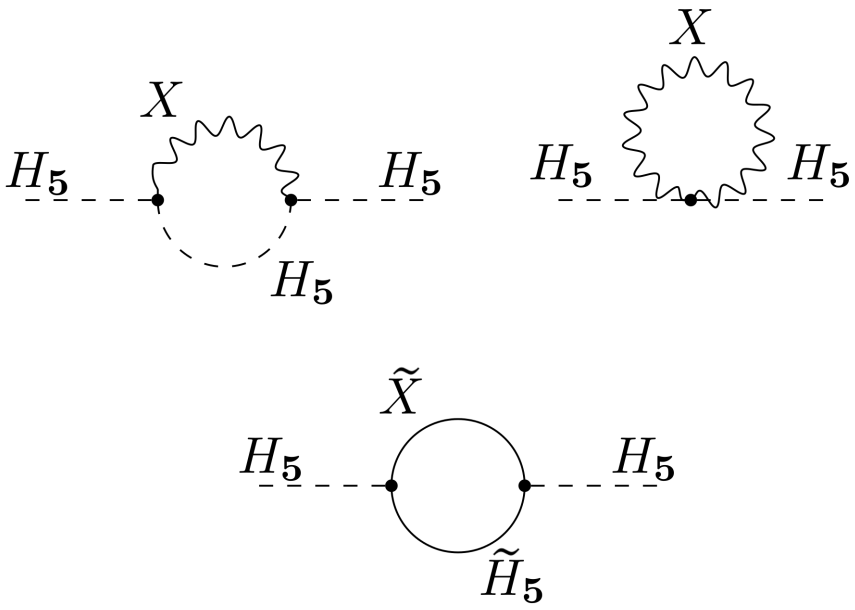

Figure 1.3: One-loop self-energy diagrams for the Higgs multiplet $H_{\mathbf{5}}$ that involve the gauge bosons X and their superpartners – the gauginos $\tilde{X}$.

The latter two commutation rules above are consistent with the fact that Q and $\bar{Q}$ transform respectively as the $(\frac{1}{2}, 0)$ and $(0, \frac{1}{2})$ Weyl spinors under the spacetime transformations. In the $N = 1$ case, the SUSY generators commute with other internal symmetry generators, including the gauge group ones.

1.4.2 Softening the hierarchy problem

Supersymmetry imposes relations between fermionic and bosonic states. The action of Q or $\bar{Q}$ changes the spin of a state by $\pm\frac{1}{2}$, while preserving its energy and momentum, as follows from Eq. (1.28). Physical fields of different spin that are related by supersymmetry transformations are called *superpartners*. The same coupling constants parameterise interactions of both superpartners with other fields, which allows for cancellations among otherwise unrelated Feynman diagrams. This fact turns out to give a solution to the hierarchy problem, which is among the main phenomenological arguments in favour of SUSY. In a supersymmetric GUT, radiative corrections to the Higgs boson mass coming from loops with superheavy gauge bosons X from Fig. 1.2 are accompanied by the ones involving their superpartners, as illustrated in Fig. 1.3. Contributions of the order of $\mathcal{O}(M_{\mathrm{GUT}}^2)$ from these three diagrams to the Higgs boson mass squared cancel in an exact manner thanks to supersymmetric relations between the gauge boson and gaugino couplings, and to equality of their masses in the unbroken SUSY limit.

Similar cancellations occur also in higher-loop diagrams, which follows from the so-called non-renormalisation theorem [30] that holds for any SUSY model. The theorem states that certain terms in the Lagrangian[6] do not get renormalised, i.e., all the relevant Feynman diagrams cancel out. In our context it means that loop corrections can affect only the

[6] specifically, the terms that originate from differentiating the superpotential - see below.

Superfields	Left-handed fermions	Complex scalars
$Q = \begin{pmatrix} U_L \\ D_L \end{pmatrix}$	$q = \begin{pmatrix} u_L \\ d_L \end{pmatrix}$	$\tilde{q} = \begin{pmatrix} \tilde{u}_L \\ \tilde{d}_L \end{pmatrix}$
U_R^c	u_R^c	$\tilde{u}_R^c$
D_R^c	d_R^c	$\tilde{d}_R^c$
$L = \begin{pmatrix} N \\ E_L \end{pmatrix}$	$l = \begin{pmatrix} \nu \\ e_L \end{pmatrix}$	$\tilde{l} = \begin{pmatrix} \tilde{\nu} \\ \tilde{e}_L \end{pmatrix}$
E_R^c	e_R^c	$\tilde{e}_R^c$
$H_d = \begin{pmatrix} H_d^0 \\ H_d^- \end{pmatrix}$	$\tilde{h}_d = \begin{pmatrix} \tilde{h}_d^0 \\ \tilde{h}_d^- \end{pmatrix}$	$h_d = \begin{pmatrix} h_d^0 \\ h_d^- \end{pmatrix}$
$H_u = \begin{pmatrix} H_u^+ \\ H_u^0 \end{pmatrix}$	$\tilde{h}_u = \begin{pmatrix} \tilde{h}_u^+ \\ \tilde{h}_u^0 \end{pmatrix}$	$h_u = \begin{pmatrix} h_u^+ \\ h_u^0 \end{pmatrix}$

Table 1.2: The MSSM matter field content. For brevity, the colour and flavour indices have been omitted, as they are identical to those in Sec. 1.2.1. To introduce the necessary notation, the isospin structure has been made explicit.

gauge-kinetic terms in the Lagrangian, but not the mass terms or Yukawa interactions. An immediate consequence is the absence of quadratic ultraviolet divergences because the scalar mass terms are the only ones for which quadratic divergences would be allowed by power counting.[7]

The non-renormalisation theorem implies that in a SUSY GUT, contrary to Eq. (1.25), the Higgs mass squared does not receive any threshold corrections scaling as M_{GUT}^2. This statement holds to all orders in perturbation theory.

1.4.3 The Minimal Supersymmetric Standard Model

As we have seen, supersymmetry possesses certain phenomenological advantages. Let us now describe a theory that acts as a supersymmetric extension of the SM. It is known as the Minimal Supersymmetric Standard Model (MSSM).

In the MSSM, we find each of the SM fields from Tab. 1.1 embedded in a *superfield* that contains also another physical field – its scalar or fermionic partner.[8] In this way, one extends the field content to get partners of quarks, leptons and Higgs scalars, called *squarks*, *sleptons* and *higgsinos*, respectively. The SM vector gauge fields have their corresponding spin-$\frac{1}{2}$ partners, called *gauginos*:

- gluinos: $\tilde{g}_\mu^A \qquad (A = 1, \ldots, 8)$,

[7] We are not considering quantum corrections to the vacuum energy here, and we assume absence pure singlets, i.e. fields being in singlet representations of all the symmetries.

[8] We restrict to describing the MSSM explicitly in terms of the physical component fields.

- winos: $\tilde{W}^I_\mu \qquad (I = 1, \ldots, 3)$,
- bino: $\tilde{B}_\mu$.

To write a symbol for each superpartner, a tilde is added over the corresponding SM symbol. A summary of the MSSM matter field content is given in Tab. 1.2. The squarks and sleptons will commonly be called *sfermions*. Let us note the appearance of two distinct Higgs doublets H_d and H_u. It is necessary due to holomorphy constraints on the SUSY interactions, which forces us to replace φ and $\tilde{\varphi}$ in the Yukawa terms by two independent fields. Moreover, making the gauge symmetries free of chiral anomalies requires having two higgsino fields with opposite hypercharges. The H_d and H_u hypercharges are equal to $-\frac{1}{2}$ and $\frac{1}{2}$, respectively.

A generic formula for the supersymmetric part of the MSSM Lagrangian density is a sum of kinetic terms $\mathcal{L}_{kin}$, interactions $\mathcal{L}_f$ involving fermions, and a scalar potential term $(-V_\phi)$

$$\mathcal{L}^{\text{SUSY}}_{\text{MSSM}} = \mathcal{L}_{kin} + \mathcal{L}_f - V_\phi. \tag{1.29}$$

The kinetic terms are given by

$$\mathcal{L}_{kin} \;=\; \sum_k (D_\mu \phi_k)^\dagger (D^\mu \phi_k) \;+\; i \sum_j \bar{\psi}_j \not{D} \psi_j \;+\; \mathcal{L}^{gauge}_{kin}, \tag{1.30}$$

where the indices i and j enumerate all the MSSM scalars and left-handed fermions (including the gauginos), respectively. The last term stands for the gauge boson kinetic terms which are identical to those in the SM

$$\mathcal{L}^{gauge}_{kin} = -\tfrac{1}{4} G^A_{\mu\nu} G^{A\mu\nu} - \tfrac{1}{4} W^I_{\mu\nu} W^{I\mu\nu} - \tfrac{1}{4} B_{\mu\nu} B^{\mu\nu}. \tag{1.31}$$

For specifying the remaining parts of the Lagrangian, it is convenient to introduce a functional W called the *superpotential*. It defines the non-gauge interactions between the MSSM superfields as

$$W_{\text{MSSM}} = Q \mathbf{Y^u} U^c_R H_u + Q \mathbf{Y^d} D^c_R H_d + L \mathbf{Y^e} E^c_R H_d + \mu H_d H_u, \tag{1.32}$$

where μ is a dimensionful parameter. For all practical purposes within the MSSM phenomenology, it is enough to view the superpotential just as a step in an algorithm of defining the Lagrangian density. The $\mathcal{L}_f$ terms have the following form:

$$\mathcal{L}_f = -\tfrac{1}{2} \sum_{i,j} \psi_i^T C \psi_j \left(\frac{\partial^2 W}{\partial \Phi_i \partial \Phi_j} \right)_{\Phi \to \phi} - \sqrt{2} \sum_{i,G,a} g_G \phi_i^\dagger T^a_G (\lambda^a_G)^T C \psi_i \quad + \quad \text{h.c.}\,, \tag{1.33}$$

where $\Phi \to \phi$ means replacing the superfield by its scalar component. The indices i, j run over all the (scalar, fermion) multiplets. In the second term, λ^a_G denotes a gaugino corresponding to the group G, with a being its adjoint representation index.

The scalar potential V_ϕ can be split into parts usually called D- and F-terms,

$$V_\phi \;=\; \sum_i |F_i|^2 + \tfrac{1}{2} \sum_{G,a} g^2_G D^a_G D^a_G \tag{1.34}$$

with

$$F_i = \left(\frac{\partial W}{\partial \Phi_i} \right)_{\Phi \to \phi} \qquad \text{and} \qquad D^a_G = \sum_i (\phi_i^\dagger T^a_G \phi_i). \tag{1.35}$$

If $\mathcal{L}^{\text{SUSY}}_{\text{MSSM}}$ defined as above was the complete Lagrangian density, the superpartners would have the same mass as the corresponding SM fields. This would contradict the experimental fact that no superpartner has been observed so far. One needs to include additional mass and interaction terms that explicitly break SUSY but, at the same time, do not violate the key property of non-renormalisation of the superpotential terms (and thus cancellation of the ultraviolet quadratic divergences). It can be done by adding the following bi- and trilinear terms:

$$\begin{aligned}\mathcal{L}^{\text{soft}}_{\text{MSSM}} = &-\tfrac{1}{2}[m_{\tilde{g}}(\tilde{G}^a)^T C\tilde{G}^a + m_{\tilde{W}}(\tilde{W}^I)^T C\tilde{W}^I + m_{\tilde{B}}\tilde{B}^T C\tilde{B} + h.c.] - m^2_{h_d} h_d^\dagger h_d - m^2_{h_u} h_u^\dagger h_u \\ &- \tilde{q}^\dagger(\mathbf{M}^2_{\tilde{q}})\tilde{q} - (\tilde{u}^c_R)^\dagger(\mathbf{M}^2_{\tilde{u}})(\tilde{u}^c_R) - (\tilde{d}^c_R)^\dagger(\mathbf{M}^2_{\tilde{d}})(\tilde{d}^c_R) - \tilde{l}^\dagger(\mathbf{M}^2_{\tilde{l}})\tilde{l} - (\tilde{e}^c_R)^\dagger(\mathbf{M}^2_{\tilde{e}})(\tilde{e}^c_R) \\ &+ \tilde{q}\mathbf{A^u}\tilde{u}^c_R h_u + \tilde{q}\mathbf{A^d}\tilde{d}^c_R h_d + \tilde{l}\mathbf{A^e}\tilde{e}^c_R h_d + B\mu h_d h_u \quad + \quad \text{h.c.}\,,\end{aligned} \tag{1.36}$$

where the sfermion masses $\mathbf{M}^2_{\tilde{f}}$ and the trilinear Higgs-sfermion-sfermion couplings $\mathbf{A}^f$ are matrices in the flavour space. Thus, the complete Lagrangian density reads

$$\mathcal{L}_{\text{MSSM}} = \mathcal{L}^{\text{SUSY}}_{\text{MSSM}} + \mathcal{L}^{\text{soft}}_{\text{MSSM}}. \tag{1.37}$$

The SUSY-breaking terms introduced in $\mathcal{L}^{\text{soft}}_{\text{MSSM}}$ are all proportional to parameters of positive dimension in the units of mass. Thus, by power counting, they cannot introduce quadratic ultraviolet divergences. For this reason, the considered SUSY breaking is called *soft*. The soft-SUSY-breaking terms in $\mathcal{L}^{\text{soft}}_{\text{MSSM}}$ are called *soft terms*, and the corresponding parameters – *soft parameters*.

All the soft parameters are assumed to be of the order of $\mu_{\text{sp}} \sim \mathcal{O}(1\,\text{TeV})$ which is much lower than M_{GUT}. Thus, they do not reintroduce the hierarchy problem in the (SUSY GUT)-MSSM matching conditions despite breaking SUSY explicitly. One may ask whether keeping the soft terms much smaller than M_{GUT} is natural in any sense. In 1979, Gerardus 't Hooft defined the concept of *naturalness*, used as a way of selecting theories among those equally plausible from the experimental point of view. According to him, a theory can be called natural, if "at an energy scale Q, a physical parameter or a set of physical parameters $c_i(Q)$ is allowed to be very small only if the replacement $c_i(Q) \to 0$ would increase the symmetry of the system" [31]. In our case, setting the soft terms to zero increases the symmetry, so the considered solution to the hierarchy problem is natural in the sense of 't Hooft's criterion.

The complete MSSM Lagrangian (1.37) is closed under renormalisation. However, contrary to the SM case, it does not contain all the terms that are allowed for the given field content by the gauge symmetries and renormalisability alone. In the SM, there is a non-anomalous global $U(1)$ symmetry that comes as accidental, i.e., it is not imposed in the theory definition but still turns out to be a global symmetry of the Lagrangian. This symmetry is generated by $B - L$, where B is the baryon number and L is the lepton number. For all the quarks (leptons) in Tab. 1.1, we have $B = \frac{1}{3}$ and $L = 0$ ($B = 0$ and $L = 1$). Thus, for the multiplets in Tab. 1.2, we have $B - L = \{\frac{1}{3}, -\frac{1}{3}, -\frac{1}{3}, -1, 1, 0, 0\}$. In the MSSM, if we did not impose the global $B - L$ symmetry in the theory definition, we could write the following additional terms in the superpotential:

$$W_{\not{B-L}} = aU^c_R D^c_R D^c_R + bQLD^c_R + cLLE^c_R + dLH_u, \tag{1.38}$$

where the appropriate (unique) colour and isospin contractions are understood, while the (arbitrary) flavour structure is encoded in the coefficients a, b, c, d.

Since violation of B and/or L is strongly constrained by experimental data (including the nucleon lifetime bounds), one usually assumes that the above terms are absent. It can be achieved by either imposing the very $B-L$ global symmetry or some discrete symmetry. The simplest example of a sufficient discrete symmetry is the so-called *matter parity* under which all the matter superfields change sign, while the Higgs ones do not. Another example is the *R-parity* defined for each component field by $(-1)^{3B+L+2S}$, with B, L and S being the baryon, lepton number and spin, respectively. The R-parity seems to be the least straightforward but is nevertheless the most popular for forbidding the unwanted superpotential terms. In the following, we shall always assume that the MSSM we consider is R-parity conserving.

It is easy to observe in Tab. 1.2, that all the SM particles are R-even, while their superpartners (called *sparticles*) are R-odd. This means that all physical processes have to involve even numbers of the superpartners, and the Lightest Supersymmetric Particle (LSP) is stable. The LSP is thus a natural candidate for a Dark Matter (DM) particle. Moreover, the R-parity conserving MSSM is able to successfully explain the observed DM relic density.

As far as the soft terms are concerned, the gauge symmetries, R-parity and the requirement that all the coupling constants are dimensionful are still not sufficient to restrict $\mathcal{L}^{\text{soft}}_{\text{MSSM}}$ to the form given in Eq. (1.36). In principle, one might add to $\mathcal{L}^{\text{soft}}_{\text{MSSM}}$ all the terms with dimensionful couplings that are present in $\mathcal{L}^{\text{SUSY}}_{\text{MSSM}}$, but ignoring the SUSY-induced correlations between the couplings, namely the fact that the triple-scalar terms in $\mathcal{L}^{\text{SUSY}}_{\text{MSSM}}$ are uniquely determined by the Yukawa matrices and the higgsino mass μ. Such non-holomorphic triple-scalar soft terms would not introduce quadratic ultraviolet divergences, as the MSSM contains no pure singlets. However, loop corrections from them would renormalise the extra soft contribution to the higgsino mass term, so the total higgsino mass would no longer be protected by the SUSY non-renormalisation theorem. Although the presence of such extra soft terms is conceivable (see, e.g., Refs. [32–34]), they are not necessary, as the theory closes under renormalisation without them. In fact, they are not included in most of the MSSM analyses in the literature. In the present work we shall assume their absence, too, taking the soft Lagrangian as it stands in Eq. (1.36).

1.4.4 The MSSM spectrum and field bases

Similarly to the SM case, one needs to pass from the interaction basis to the mass eigenstate basis after the EWSB takes place. We assume that the MSSM parameters are such that only the two Higgs doublets acquire non-vanishing VEVs. Then we use the $SU(2)$ gauge symmetry to simplify the scalar potential. Finally, we find that in the minimum the two VEVs can be written as

$$\langle 0|h_u|0\rangle = \frac{1}{\sqrt{2}}\begin{pmatrix} v_u \\ 0 \end{pmatrix}, \qquad \langle 0|h_d|0\rangle = \frac{1}{\sqrt{2}}\begin{pmatrix} 0 \\ v_d \end{pmatrix}. \tag{1.39}$$

They spontaneously break the electroweak symmetry $SU(2)\times U(1)_Y$ down to $U(1)_{em}$. Once we define $v = \sqrt{v_d^2 + v_u^2}$, the gauge boson masses are given by the same expressions as in the SM in terms of v and the gauge couplings. A useful parameter is the ratio of the two VEVs:

$$\tan\beta = \frac{v_u}{v_d}. \tag{1.40}$$

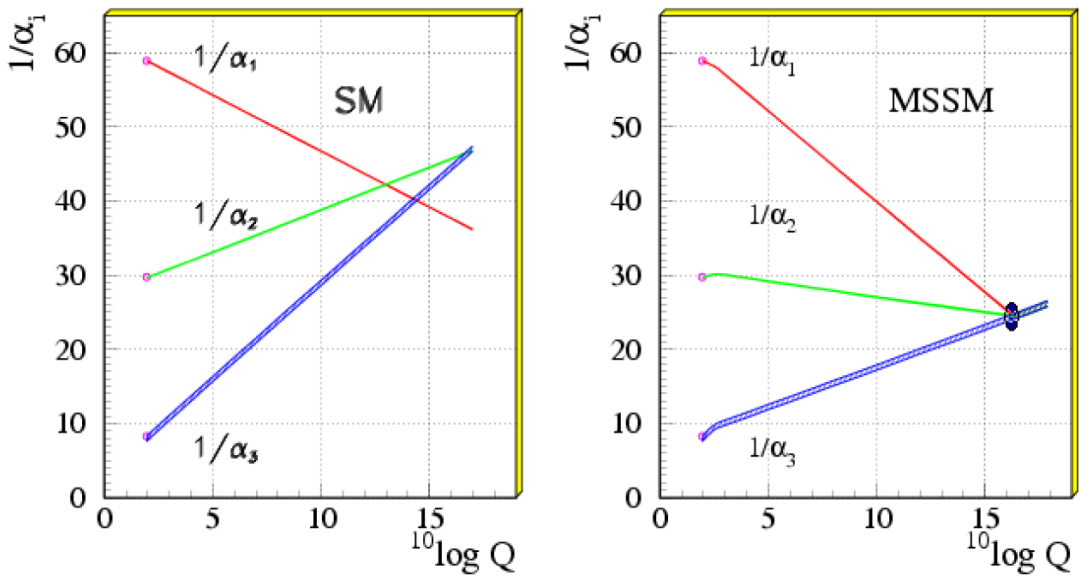

Figure 1.4: Illustration of the gauge coupling unification in the SM (left) and MSSM (right), adopted from Fig. 16.1 of Ref. [19].

Most of the MSSM mass eigenstates are mixtures of some of the interaction eigenstate fields. The electrically neutral gauginos (the bino $\tilde{B}$ and the neutral wino $\tilde{W}_3$) mix with the neutral higgsinos $\tilde{h}_d^0$ and $\tilde{h}_u^0$ to form four *neutralinos* $\chi_i^0, i = 1, \ldots, 4$. Those are especially relevant for phenomenology, as they provide the best candidate for a dark matter particle. Analogously, the charged winos $\tilde{W}_{1,2}$ mix with the charged higgsinos $\tilde{h}_u^+$ and $\tilde{h}_d^-$ to form Dirac fermions called *charginos* $\chi_j^\pm, j = 1, 2$. The chiral matter fermions combine to the Dirac ones in the same way as in the SM, except for that $\tan\beta$ affects relations between their Yukawa couplings and masses. The CKM matrix arises after the Yukawa matrix diagonalization, again in the same way as in the SM. The sfermion mass matrices require, in general, an additional diagonalization, which gives three distinct complex-scalar mass eigenstates for the sneutrinos, six for sleptons, and six for each type of squarks (up- and down-type). As compared to the SM, the number of particles with (potentially) different masses is more than tripled, and the number of free parameters increases roughly by a factor of 6.

As far as the choice of the flavour basis is concerned, one of the most popular bases to express the MSSM fields is the *super-CKM* basis. It is defined as a basis in which the Q, U and D superfields are assumed to have been rotated from the interaction basis, in order to diagonalise the fermion masses, exactly as in the SM. It means that the super-CKM basis Yukawa matrices are diagonal, whereas the soft terms have been rotated in the same way as the fermions from their interaction basis. A detailed description of the transformation between those two bases for all the soft terms can be found in Ref. [35].

1.4.5 Gauge coupling unification

When the GUTs were postulated, the uncertainty in estimation of the strong interaction coupling $\alpha_s \equiv \alpha_3$ and the ratio α_1/α_2 were so large that all the three couplings seemed to attain the same value at the scale $M_{\mathrm{GUT}}^{1970s} \sim 10^{14\div15}$ GeV. Later however, as the measurements

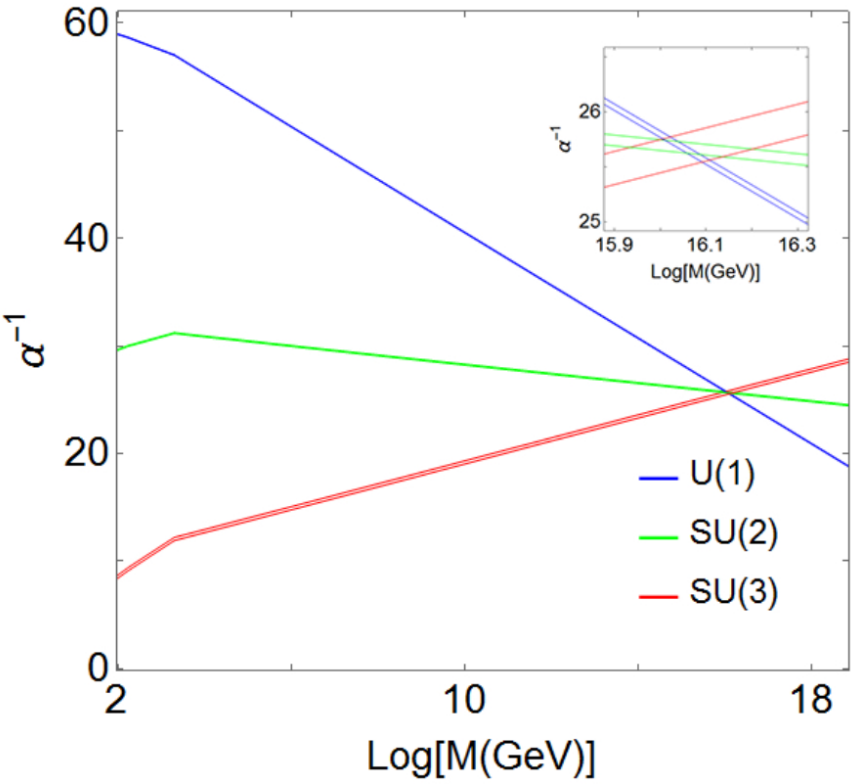

Figure 1.5: Illustration of the gauge coupling unification in the MSSM, adopted from Fig. 1 of Ref. [36]. The plot has been obtained using 2-loop RGEs, and for the sparticle masses around 2 TeV (see the text).

and lattice calculations became more accurate, it turned out that at this scale they miss each other by around twelve standard deviations [19]. This is illustrated in the left plot of Fig. 1.4 where the inverse gauge couplings are plotted as functions of the renormalisation scale.

In the MSSM, the RGEs governing the gauge coupling evolution are different. At the one-loop level, they depend on nothing but the particle spectrum and the gauge couplings themselves. The evolution of the three couplings in the MSSM is illustrated in the right plot of Fig. 1.4, and, more precisely, in Fig. 1.5 that is adopted from Ref. [36]. The inset in the latter figure shows a focus of the crossing point at $M_{\rm GUT} \sim 10^{16}\,{\rm GeV}$. The bands correspond to the experimental 3σ ranges. Although the applied two-loop RGEs depend only on the gauge and Yukawa couplings, the precise outlook of the crossing point at $M_{\rm GUT}$ depends on the remaining MSSM parameters that affect the threshold corrections at $\mu_{\rm sp}$. In the considered example, the gauge couplings cross at a single point with an accuracy better than the experimental 1σ.

However, with the current high-precision experimental determination of the gauge couplings,[9] measuring the accuracy of their apparent coincidence at $M_{\rm GUT}$ in terms of experimental errors is an academic issue. Much more important effects come from the GUT-scale threshold corrections which depend on the particle spectra above $M_{\rm GUT}$. For each of the

[9] The least precisely determined $\alpha_3(M_Z) = 0.1184 \pm 0.0007$ [19] is known with a 0.6% accuracy.

three couplings α_i we have

$$\alpha_i(M_{\rm GUT}) \;=\; \alpha_{\rm GUT}(M_{\rm GUT}) \;+\; c_i\,\alpha^2_{\rm GUT}(M_{\rm GUT}) \;+\; \ldots\;, \tag{1.41}$$

with the numbers c_i being of order unity, and the ellipses standing for higher order corrections. Thus,

$$\frac{1}{\alpha_i(M_{\rm GUT})} \;=\; \frac{1}{\alpha_{\rm GUT}(M_{\rm GUT})} \;-\; c_i \;+\; \ldots\;. \tag{1.42}$$

By convention, we define $M_{\rm GUT}$ in such a way that $c_1 = c_2$, and then test the unification quality by calculating $\Delta_c \equiv c_3 - c_2$ in a particular GUT model. If the physics above $M_{\rm GUT}$ is not specified, we can only verify whether Δ_c is not too large as for an order-unity number. The example in Fig. 1.5 implies that Δ_c in the MSSM can be arbitrarily small. However, in generic points of the MSSM parameter space, one usually finds $\Delta_c \sim -1$. On the other hand, the left plot of Fig. 1.4 implies that in the SM one would need $\Delta_c \sim +5$, which might be difficult to obtain. Thus, the gauge coupling unification issue speaks in favour of the MSSM (as compared to the SM) as a candidate for the correct effective theory below $M_{\rm GUT}$. However, it is not a decisive argument. The main motivation for SUSY in the GUT context comes from the hierarchy problem.

The scale $M_{\rm GUT}$ in the MSSM turns out to be significantly higher than $M^{1970s}_{\rm GUT}$, which is easily seen by comparing the two plots in Fig. 1.4. This is a welcome feature because the superheavy gauge boson contributions to the proton decay rate scale like $m_p^5/M^4_{\rm GUT}$, where m_p is the proton mass. With $M_{\rm GUT} \sim 10^{16}\,{\rm GeV}$, such contributions are not in conflict with the experimental lower bounds on the proton lifetime. However, SUSY implies existence of potentially dangerous contributions to the proton decay rate that scale like $m_p^5/(M^2_{\rm GUT}\mu^2_{\rm sp})$. They may originate from the $SU(3)$-triplet higgsinos that are present in the H_5 and $H_{\bar5}$ Higgs superfields of the $SU(5)$ SUSY GUT (see, e.g., Ref. [37]). The role of such contributions depends on the way how the so-called doublet-triplet splitting problem is solved in a given GUT model, i.e. how the superheavy masses are generated for the triplets without being simultaneously generated for the usual MSSM Higgs doublets. After the GUT symmetry is broken, the triplets might receive masses from trilinear superpotential terms that do *not* depend simultaneously on *both* H_5 and $H_{\bar5}$, at the cost of introducing extra $\mathbf{5}$ and $\overline{\mathbf{5}}$ superfields non-interacting with the MSSM matter. In such a case, no dangerous contributions to the proton decay would be generated by the heavy triplet higgsinos. There are also alternative methods of suppressing the unwanted contributions to the proton decay, the simplest of which is making the triplet higgsinos significantly heavier than $M_{\rm GUT}$.

In the present work, we shall analyse the GUT-constrained MSSM without specifying the details of the theory above $M_{\rm GUT}$. The doublet-triplet splitting problem will not be addressed. Apart from what has been mentioned above, we shall not consider any specific mechanism of avoiding the triplet higgsino contributions to the proton decay. We shall work under the assumption that the problem gets resolved in some way, and that the proton lifetime satisfies the current experimental bounds.

1.5 Yukawa coupling unification in the MSSM

Motivated by the successful gauge coupling unification, we assume the MSSM to be a correct effective theory below $M_{\rm GUT}$. Moreover, we assume that the SUSY theory above $M_{\rm GUT}$ can

be described in terms of the $SU(5)$ gauge symmetry, and that the Yukawa interactions of the MSSM matter and Higgs fields are generated in a minimal manner, i.e. they originate from the following part of the $SU(5)$ GUT superpotential

$$\mathcal{W} \ni \Psi_{10}\mathbf{Y^{de}}\Psi_{\bar{5}}H_{\bar{5}} + \Psi_{10}\mathbf{Y^{u}}\Psi_{10}H_5. \tag{1.43}$$

Here, $\Psi_{\bar{5}}$ and Ψ_{10} are the GUT superfields that contain the MSSM matter ones, according to the embeddings given in Eq. (1.21). The Higgs superfields $H_{\bar{5}}$ and H_5 contain the MSSM ones H_d and H_u, respectively.

All the SM fermion masses are thus given by only two independent 3×3 matrices: $\mathbf{Y^{de}}$ and $\mathbf{Y^{u}}$. In other words, the considered SUSY $SU(5)$ GUT induces a boundary condition for the Yukawa couplings of the MSSM. Thus, we should address a question whether the Yukawa sector under such a constraint is compatible with the low-energy data. Our boundary condition for the MSSM RGEs is given by the equality of the matrices $\mathbf{Y^{d}}$ and $\mathbf{Y^{e}}^T$ at $M_{\rm GUT}$. This requirement is true up to possible one-loop threshold corrections at this scale. In our numerical analysis, we are going to allow for moderate threshold corrections at the GUT scale without investigating their origin, as we do not specify details of the model above $M_{\rm GUT}$. Once the minimal form (1.43) of the GUT Yukawa terms is assumed, the GUT-scale threshold corrections to the corresponding MSSM Yukawa couplings are protected by the non-renormalization theorem. It means that they can only originate from threshold effects in the field renormalization. In consequence, they are naturally of moderate size, as long as one assumes that Eq. (1.43) is the only source of flavour violation above the GUT scale.

The unification conditions for $\mathbf{Y^{d}}$ and $\mathbf{Y^{e}}$ take the simplest form in a basis where the superpotential flavour mixing is entirely included in $\mathbf{Y^{u}}$, while $\mathbf{Y^{d}}$ and $\mathbf{Y^{e}}$ are real and diagonal. In such a case, it is enough to require (approximate) equality of the diagonal entries at the GUT scale,

$$Y^d_{ii}(M_{\rm GUT}) \;\simeq\; Y^e_{ii}(M_{\rm GUT}), \qquad i = 1, 2, 3. \tag{1.44}$$

Let us illustrate the problem with the case of the strange quark and muon Yukawa couplings, as they require the largest relative threshold corrections at $\mu_{\rm sp}$. As shown by the dotted lines in Fig. 1.6, in a situation when the SUSY-scale threshold corrections are set to zero, the considered Yukawa couplings differ by a factor of around three at $M_{\rm GUT}$.

An important fact is that the RGEs for the superpotential couplings are independent of the soft terms.[10] In general, no dimensionful couplings can influence the RG-evolution of dimensionless couplings. Thus, for the gauge and Yukawa couplings of the MSSM we have

$$Q\frac{d}{dQ}\begin{pmatrix} g_i(Q) \\ Y_i(Q) \end{pmatrix} = f(g_i(Q), Y_i(Q)). \tag{1.45}$$

The MSSM RGEs have therefore a subsystem that can be solved independently of the remaining equations, as long as the boundary conditions for $g_i(\mu_{\rm sp})$ and $Y_i(\mu_{\rm sp})$ are fixed. Because of that, the gauge coupling running cannot be modified by manipulating the soft terms, which implies that these terms can have only a minor influence on the gauge coupling unification issue. Analogously, neither the Yukawa coupling running can be affected by the

[10] For a reference, the complete two-loop MSSM RGEs can be found in Ref. [38].

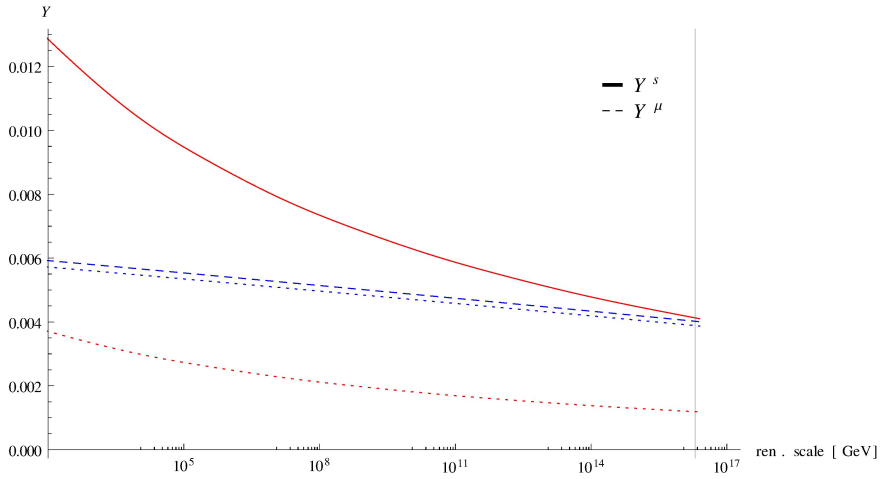

Figure 1.6: RG-running of Y_s (red lines) and Y_μ (blue lines) between $\mu_{\rm sp} = M_Z$ and $M_{\rm GUT}$ for two sample points in the MSSM parameter space. Dotted lines describe a situation with vanishing threshold corrections at $\mu_{\rm sp}$. For the solid (red) and dashed (blue) lines, the threshold corrections at $\mu_{\rm sp}$ have been adjusted to achieve unification at the GUT scale.

soft terms. However, in the case of the first two generation Yukawa couplings, huge effects can be generated by the soft terms via their effects on the boundary conditions at $\mu_{\rm sp}$.

Of course, the SUSY-scale threshold corrections are not the only way to resolve the Yukawa matrix unification problem. Another well-known approach is to relax the assumption about the minimal form (1.43) of the interactions that generate the MSSM Yukawa couplings at $M_{\rm GUT}$. Modifications of the GUT field content aiming at solving this problem were considered already in the 1970's for the non-supersymmetric case, and are known as the Georgi-Jarlskog mechanism [39]. The most exhaustively studied alterations of the MSSM Yukawa coupling ratios at the GUT scale originate from assuming either various versions of the Georgi-Jarlskog mechanism, or non-negligible effects from higher-dimensional operators in the $SU(5)$ model Lagrangian. Different quark and lepton mass ratios obtained by such manipulations are summarised, e.g., in Refs. [40–42]. Departures from the minimal assumption (1.43) have been considered also in the case of the bottom-tau unification [43].

On the other hand, the low-energy boundary conditions turn out to give us more freedom that one might have naively expected. The SM Yukawa couplings are fixed by the mass measurements in the SM. However, their translation to the MSSM renormalised couplings is affected by contributions involving the soft terms. It has been observed that such threshold corrections at the superpartner decoupling scale $\mu_{\rm sp}$ can significantly change or even generate the light fermion masses [44]. An application of this mechanism in the context of grand unification was reported in Ref. [45]. In particular, an adjustment of the lower-end boundary values of Y_s and Y_μ can lead to their unification, as illustrated in Fig. 1.6.

However, in most of the contemporary phenomenological analyses, the Yukawa coupling unification has been exhaustively studied only in the third generation case. A quantitative study that obtained $Y_s(M_{\rm GUT}) = Y_\mu(M_{\rm GUT})$ within the renormalisable R-parity-conserving MSSM was performed in Ref. [46]. It considered only the threshold corrections coming from gluino and higgsino loops, and pointed out that a tension arises between the Yukawa unification and flavour observables. That was to be expected, as the flavour off-diagonal soft terms were used there to generate the Cabibbo angle, too. The analysis was later expanded

and simplified to the flavour-diagonal case in Ref. [2]. It contained examples of points in the MSSM parameter space where the $SU(5)$ Yukawa unification was achieved for $\tan\beta \leq 20$. In another publication [47], where the leading MSSM threshold corrections were investigated, the problem of proton decay was addressed by making the Higgs soft masses greater than 30 TeV.

In the present work, as already stated above, we shall insist on the minimal GUT Yukawa terms (1.43), and study whether the SUSY-scale threshold effects can make the approximate condition (1.44) feasible for all the three generations. The analysis will be restricted to the soft terms not exceeding a few TeV, and we shall allow for the Cabibbo angle being generated by the flavour-violating terms in $\mathbf{Y^u}$. Most importantly, the up-to-date experimental constraints, including the Higgs boson mass, will be taken into account.

CHAPTER 2

Two MSSM scenarios for the SU(5) Yukawa matrix unification

In this chapter, we define the two MSSM scenarios that we are going to investigate in the context of the Yukawa coupling unification. The scenarios will differ in the specific assumptions about soft terms at $M_{\rm GUT}$, on the top of the $SU(5)$ symmetry constraints. Even after imposing the latter constraints, the MSSM has a large number of free parameters ($\mathcal{O}(50)$ real ones), so some extra assumptions need to be made for manageable scans over the parameter space.

2.1 Large diagonal A terms

The main phenomenological motivation behind our first scenario is to achieve the Yukawa matrix unification and fulfil the experimental constraints in the simplest possible manner, adjusting as few parameters as possible. We start from the observation that to independently influence the ratios Y^d_{ii}/Y^e_{ii} for all the three families, one has to adjust at least three real parameters. The diagonal entries of the trilinear $\mathbf{A^{de}}$ terms in the super-CKM basis can well serve this purpose, as they have a strong influence on the relevant threshold corrections.

As it is common in the MSSM analyses, we will adjust the modulus of the superpotential μ-parameter to get a correct value of the VEV that gives masses to the W- and Z-bosons. Moreover, to obtain a correct mass of the lightest Higgs boson for given sparticle masses, one has to adjust A^u_{33} that governs the stop mixing [48], see Sec. 3.2. Both the Higgs soft mass terms and $\tan\beta = \frac{v_u}{v_d}$, which we employ to parameterise the Higgs sector, are unconstrained by the $SU(5)$ unification conditions, and can serve well other phenomenological purposes.

As far as the gaugino and the soft sfermion masses at the GUT scale are concerned, we restrict ourselves to the common gaugino mass $M_{1/2}$ (which is the simplest choice among relations that naturally arise in the framework of SUSY $SU(5)$ GUTs), and a universal soft mass m_0 for all the sfermions (but not the Higgs doublets). This choice reduces the number of free parameters and makes the analysis transparent. However, it is not necessary for achieving the Yukawa matrix unification, so these assumptions could be relaxed, if a need would arise.

In total, our large-diagonal-A-term scenario will be characterised in terms of 9 free parameters: $\tan\beta$, $M_{1/2}$, m_0, m_{h_u}, m_{h_d}, A^{de}_{11}, A^{de}_{22}, A^{de}_{33}, A^{u}_{33}. As far as the remaining A-terms in the super-CKM basis are concerned, they are inessential for our problem, so we shall set them to zero for simplicity. Of course, apart from the above-mentioned free parameters, we need to take into account the measured SM gauge couplings and fermion masses. The (adjusted) superpotential μ-parameter will be assumed to be real, not to introduce flavour-blind sources of CP-violation.[1] Choosing a negative sign of μ will appear to be preferable (see Sec. 2.3 below).

2.2 General Flavour Violating MSSM

Despite being consistent with the Yukawa matrix unification requirement, the regions delivered by the first scenario will turn out to suffer from the MSSM vacuum stability problem. Though this problem has a phenomenologically acceptable solution, namely the long lifetime of a metastable Universe, there is no reason for which it would need to be the unification's necessary cost.

In principle, the soft masses and trilinear terms do not need to be flavour-blind. They could involve mixing terms between the squark generations, as long as it does not lead to contradictions with experimental data. Such a case is often referred to as the *General Flavour Violating* (GFV) MSSM. If the flavour-violating soft terms are sizeable, they could generate too large contributions to processes known as the Flavour Changing Neutral Currents (FCNCs). We shall discuss this issue in more detail in Sec. 3.1.

The phenomenology of models with $SU(5)$ symmetry at the GUT scale and flavour mixing in the squark mass matrices has been studied in various contexts. Ref. [49–51] analysed possible signatures of their spectra at the LHC. Ref. [52] investigated properties of the dark matter (DM) candidate, while the consequences for the Higgs mass, B-physics and electroweak (EW) observables were discussed in Refs. [53–57].

We shall start our analysis by defining a general set of SUSY parameters at $M_{\rm GUT}$. A priori, we do not know which GFV parameters in the down-squark sector are indispensable to achieve the Yukawa coupling unification, and which can be skipped. Therefore, initially, we allow all of them to assume non-zero values, and perform a preliminary numerical scan, to identify those parameters that are essential. Next, we pass to our final scan, described in Chapter 6, where both the Yukawa unification and the experimental constraints are tested.

We shall assume for simplicity that the soft SUSY-breaking parameters are real, therefore neglecting the possibility of new SUSY sources of CP-violation. The GUT-scale $SU(5)$ boundary conditions for the soft masses are as follows:

$$(m^2_{\tilde l})_{ij} = (m^2_{\tilde d})_{ij} \equiv (m^2_{dl})_{ij}, \qquad (m^2_{\tilde q})_{ij} = (m^2_{\tilde u})_{ij} = (m^2_{\tilde e})_{ij} \equiv (m^2_{ue})_{ij}. \tag{2.1}$$

We do not impose any additional conditions on the relative sizes of the diagonal entries. The off-diagonal elements of the down-squark matrix are required to satisfy the bound $|(m^2_{dl})_{ij}/(m^2_{dl})_{33}| \leq 1$.

We assume as well that

$$(m^2_{ue})_{ij} = 0, \;\; i \neq j. \tag{2.2}$$

[1] Such effects are not excluded, but strongly constrained, e.g., by the neutron EDM.

Such a condition is not expected to cause any significant loss of generality because relatively large off-diagonal elements of $(m^2_{\tilde{q}})_{ij}$ are generated radiatively at the scale[2] $M_{\rm SUSY}$ due to the RG-running in the super-CKM basis. It will turn out later that $(m^2_{\tilde{q}})_{23}(M_{\rm SUSY}) > 0$ and $(m^2_{\tilde{q}})_{13}(M_{\rm SUSY}) < 0$ are the desired properties for the Yukawa unification. As we will see in Chapter 2.3, when those inequalities are satisfied, the dominant gluino threshold correction turns out to be negative for the strange quark, and positive for the down quark, as long as the trilinear term A^{de}_{33} is greater than zero. For similar reasons we restrict our study to the case $(m^2_{dl})_{ij} > 0$. At this point, we can introduce a short-hand notation

$$m^{dl}_{ij} \equiv \sqrt{(m^2_{dl})_{ij}}, \qquad m^{ue}_{ij} \equiv \sqrt{(m^2_{ue})_{ij}}. \tag{2.3}$$

The GUT-scale $SU(5)$ boundary conditions for the trilinear terms are, similarly as for the Yukawa matrices, given by

$$A^d_{ij} = A^e_{ji} \equiv A^{de}_{ij}. \tag{2.4}$$

We constrain the relative magnitude of the diagonal entries by the corresponding Yukawa couplings

$$\frac{|A^f_{ii}|}{|A^f_{33}|} < \frac{Y^f_{ii}}{Y^f_{33}}. \tag{2.5}$$

Doing so, we aim at relaxing the strong tension between the EW vacuum stability condition and the Yukawa unification that has been mentioned above in the context of large diagonal A-terms. We also impose that

$$A^u_{ij} = 0, \;\; i \neq j. \tag{2.6}$$

On the other hand, the off-diagonal entries in the down-sector trilinear matrix are not constrained to scale proportionally to the corresponding Yukawa matrix entries. They are only required to satisfy $|(A^{de}_{ij})/(A^{de}_{33})| \leq 0.5$.

Finally, as in the first scenario, we take a negative μ, and assume that the gaugino mass parameters are universal at $M_{\rm GUT}$,

$$M_1 = M_2 = M_3 \equiv M_{1/2}. \tag{2.7}$$

Our usage of the squark mixing terms is a tactic to enhance and control the threshold corrections to the down-type quark Yukawa couplings. Consistent SU(5) symmetry conditions at $M_{\rm GUT}$ force us though to include also a mixing between the corresponding sleptons, as in Eq. (2.1). The latter is in general severely constrained by Lepton Flavour Violating (LVF) observables. Thus, we split the analysis into two sub-scenarios:

1. GFV_{23}:
   First, we want to use only one additional parameter, the (strange squark)-(bottom squark) mixing term, to unify the Yukawa couplings of the second and third generations. Therefore, the only non-zero off-diagonal entry of m^{dl} matrix at $M_{\rm GUT}$ in this sub-scenario is m^{dl}_{23}.

2. GFV_{123}:
   Then, we turn to a more general setup and address the complete SU(5) Yukawa matrix unification, allowing all the off-diagonal entries of m^{dl} matrix to be non-zero at $M_{\rm GUT}$.

[2] The scale $M_{\rm SUSY}$ is defined as the geometric average of masses of the two top-squark (*stop*) mass eigenstates: $M_{\rm SUSY} = \sqrt{m_{\tilde{t}_1} m_{\tilde{t}_2}}$.

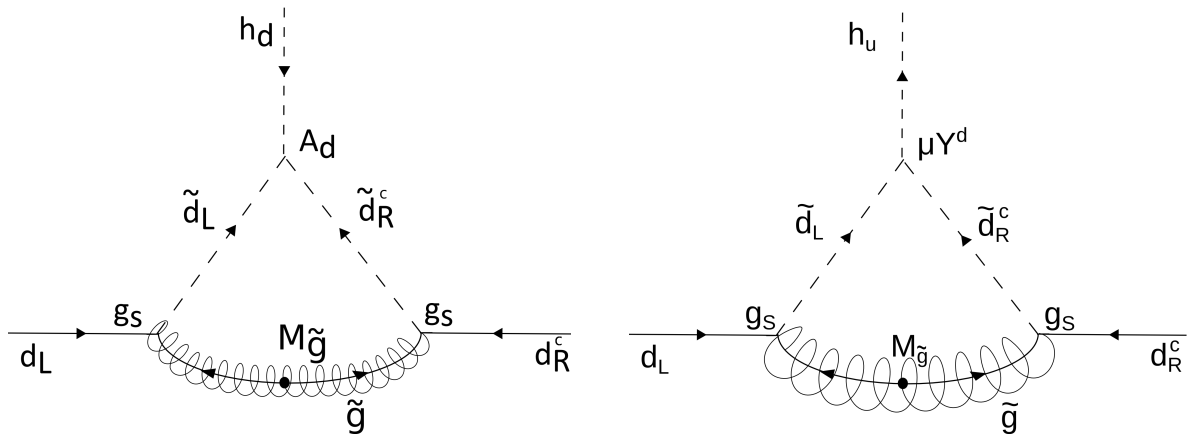

Figure 2.1: Diagrams describing the gluino-mediated one-loop threshold corrections to the Yukawa couplings at $\mu_{\rm sp}$.

2.3 Threshold corrections in the diagonal soft term case

In this section, we present and analyse explicit expressions for the SUSY-scale threshold corrections to the Yukawa couplings. We investigate their form in the two previously defined scenarios. In the first scenario, which depends on a lower number of free parameters, we shall plot the GUT-scale Yukawa coupling ratios as functions of selected pairs of the relevant soft parameters.

The diagonal entries of the Yukawa couplings are constrained by measurements of the quark and lepton masses that are performed at or below the electroweak scale. Therefore, these entries are most easily first fixed within the SM. One needs, though, to determine their renormalised values in the MSSM. This is done by evaluating threshold corrections Σ^f_{ii} at the matching scale μ_{sp}. Such corrections depend on values of the soft supersymmetry-breaking terms. Examples of the relevant Feynman diagrams are shown in Figs. 2.1 and 2.2. For $f = u, d, e$ (and denoting $v_e \equiv v_d$), one can write

$$v_f Y^{f\,MSSM}_{ii} = v_f Y^{f\,SM}_{ii} - \Sigma^f_{ii}(\alpha_s, \mu, Y^{f'}_{jj}, A^{f'}_{jj}, (m^2_{\tilde{f}'})_{jj}, m_{\tilde{g}}), \tag{2.8}$$

where we have explicitly indicated dependence on those parameters that matter for the numerically dominant effects in the flavour-diagonal case. Once the threshold corrections are evaluated, the MSSM Yukawa coupling values at $M_{\rm GUT}$ are determined by solving their MSSM RGEs (that do not depend on the soft parameters). Next, the Yukawa unification for a given set of parameters can be tested.

The experimentally determined values of fermion masses can give a qualitative feeling about the problems encountered in achieving the full Yukawa matrix unification. As it is well known, the condition $Y_b(M_{\rm GUT}) = Y_\tau(M_{\rm GUT})$ can be satisfied without large threshold corrections at $\mu_{\rm sp}$, at least for moderate $\tan\beta$. On the other hand, achieving strict unification of the Yukawa couplings for the remaining families ($Y_s(M_{\rm GUT}) = Y_\mu(M_{\rm GUT})$ and $Y_d(M_{\rm GUT}) = Y_e(M_{\rm GUT})$) forces the threshold corrections to be of the same order as the leading terms. It does not contradict perturbativity of the model because the considered Yukawa couplings are

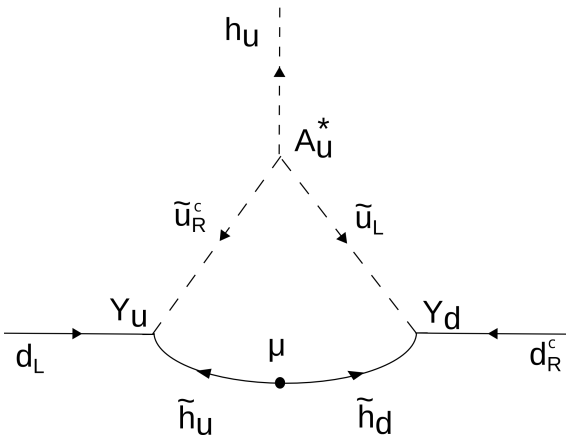

Figure 2.2: A diagram contributing to the higgsino-mediated threshold correction to the down-type quark Yukawa couplings at $\mu_{\rm sp}$.

small enough, $Y_{s,d} \ll 1$. To satisfy the minimal $SU(5)$ boundary conditions for the Yukawas, the MSSM tree-level strange-quark mass needs to be larger than the SM one (see Fig. 1.6), whereas the threshold correction effect in the down-quark case should have an opposite sign.

The leading SUSY-scale threshold corrections to the Yukawa couplings beyond the small $\tan\beta$ limit have been calculated in Ref. [58]. It was shown that in the SUSY-decoupling limit, the chirality-flipping parts of the renormalised quark (lepton) self energies Σ are linear functions of the Yukawa couplings, with a proportionality factor ϵ and an additive term $\Sigma_{\not Y}$,

$$m_i^{d(\ell)\,SM} - v_d Y_{ii}^{d(\ell)MSSM} \;=\; \Sigma_{ii}^{d(\ell)\,LR} \;=\; \Sigma_{ii\not Y}^{d(\ell)\,LR} + \epsilon_i^{d(\ell)}\, v_u\; Y_{ii}^{d(\ell)MSSM} \;+\; O(\tfrac{v^2}{M_{SUSY}}), \quad (2.9)$$

where $m_i^{d,SM}$ is the SM quark mass at $\mu_{\rm sp}$. In this approximation, the relation can easily be inverted, and the corrected MSSM Yukawa couplings in the super-CKM basis read

$$Y_{ii}^{d(\ell)MSSM} = \frac{m_i^{d(\ell)\,SM} - \Sigma_{ii\not Y}^{d(\ell)\,LR}}{v_d(1+\tan\beta\cdot\epsilon_i^{d(\ell)})}. \quad (2.10)$$

What are the possible patterns of soft terms and Yukawa couplings at the matching scale μ_{sp} in the first scenario? Given our choice of the GUT-scale parameters, the only origin of flavour violation at this scale is the Yukawa matrix $\mathbf{Y^u}$. As it affects the RGE for the remaining parameters, neither $\mathbf{Y^d}$ nor the soft terms are going to remain strictly flavour-diagonal below $M_{\rm GUT}$. Nevertheless, the corresponding flavour violation is going to be given by the CKM matrix, and remain genuinely small. Although such flavour violation is taken into account in our numerical study, we shall neglect it for simplicity in the following discussion where large corrections to the flavour-diagonal terms are of main interest. Within this approximation, it is sufficient to consider only real diagonal Yukawa matrices $\mathbf{Y^d} \equiv \mathrm{diag}(Y_d, Y_s, Y_b)$ and $\mathbf{Y^e} \equiv \mathrm{diag}(Y_e, Y_\mu, Y_\tau)$ at all the renormalisation scales.

The threshold corrections $\Sigma_{\not Y}^{d,LR}$ to the down-type quark Yukawa couplings in Eq. 2.10 can be enhanced by either $\tan\beta$ or large values of the A-terms. For the first two generations, the most significant contribution comes from loops with the gluino shown in Fig. 2.1. The resulting correction in the flavour-diagonal case is given by

$$(\Sigma_{ii}^d)^{\tilde g} = \frac{2\alpha_s m_{\tilde g} v_d}{3\pi}\left(A_{ii}^d - Y_{ii}^d \mu\tan\beta\right) C_0(m_{\tilde g}^2, m_{\tilde q_i^L}^2, m_{\tilde d_i^R}^2), \quad (2.11)$$

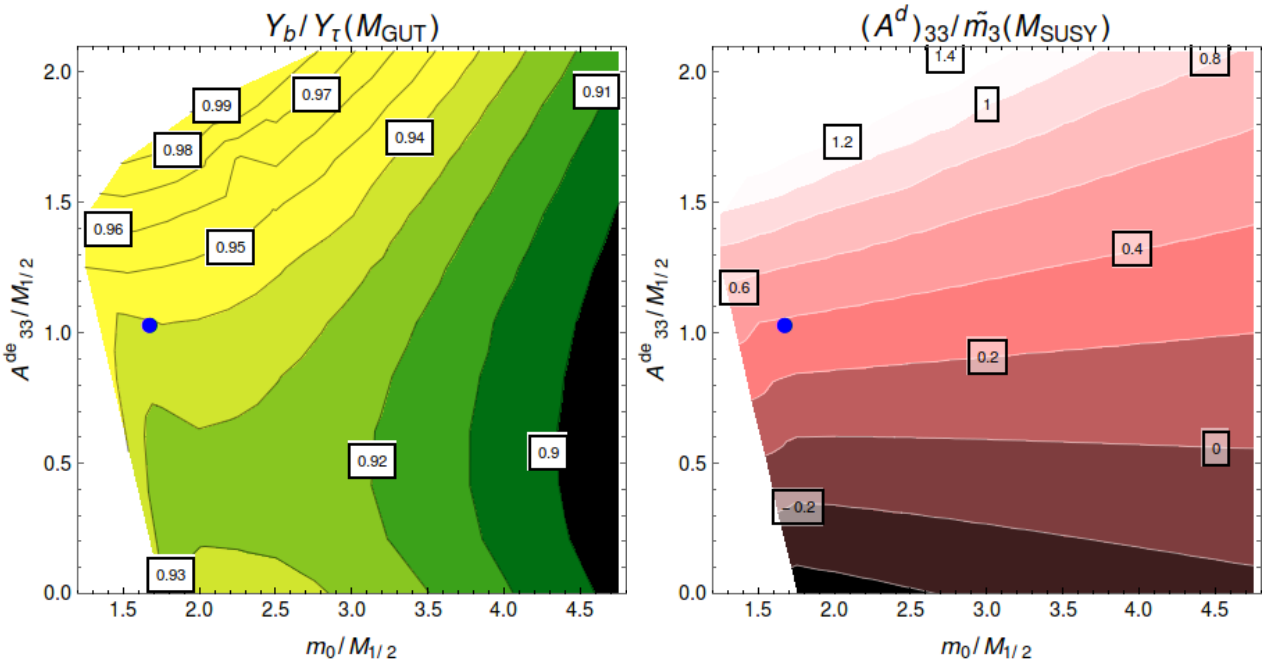

(a) (b)

Figure 2.3: Left: The ratio Y_b/Y_τ shown as a function of A^{de}_{33} and m_0. Right: The corresponding values of $A^d_{33}/\tilde{m}_3$ at $M_{\rm SUSY}$. They are presented around point 3 from Tab. 5.1 (marked by a blue dot). Both A^{de}_{33} and m_0 are normalized to $M_{1/2}$ which equals to around 815 GeV at that point.

where

$$C_0\left(m_1^2, m_2^2, m_3^2\right) = \frac{m_1^2 m_2^2 \ln\frac{m_1^2}{m_2^2} + m_2^2 m_3^2 \ln\frac{m_2^2}{m_3^2} + m_3^2 m_1^2 \ln\frac{m_3^2}{m_1^2}}{\left(m_1^2 - m_2^2\right)\left(m_2^2 - m_3^2\right)\left(m_3^2 - m_1^2\right)}\,. \tag{2.12}$$

As we can see, two parameters play a major role here: the soft trilinear coupling A^d_{ii} and the superpotential μ-parameter. Interestingly, for the third family, the expression given in Eq. (2.11) often tends to cancel with the higgsino-mediated contribution generated by the diagram in Fig. 2.2. This fact makes the ratio Y_b/Y_τ relatively stable with respect to the SUSY threshold corrections. On the contrary, for the first and second generations, the gluino contribution is dominant, and can be used to fix the ratios of the corresponding Yukawa couplings at $\mu_{\rm sp}$. Such a possibility was considered in Refs. [2, 46].

Importantly, while μ affects corrections to all the Yukawa couplings in a correlated manner, the diagonal A terms can be used to tune them independently for each family. Still, a large and negative μ for a high $\tan\beta$ is decisively helpful for unification of the second family down-type quark and lepton Yukawa couplings.

In Figs. 2.3–2.5, we illustrate how the ratios Y^d_{ii}/Y^e_{ii} (at the GUT scale) and $A^d_{ii}/\tilde{m}_i$ (at the SUSY scale) depend on the most important GUT-scale soft parameters. Here, $\tilde{m}_i$ are defined by

$$\tilde{m}_i = \sqrt{\frac{m^2_{\tilde{q}_i} + m^2_{\tilde{d}_i} + m^2_{H_d}}{3}}. \tag{2.13}$$

Using the point no. 3 from Tab. 5.1 (Sec. 5.1) as a reference, we have varied only two

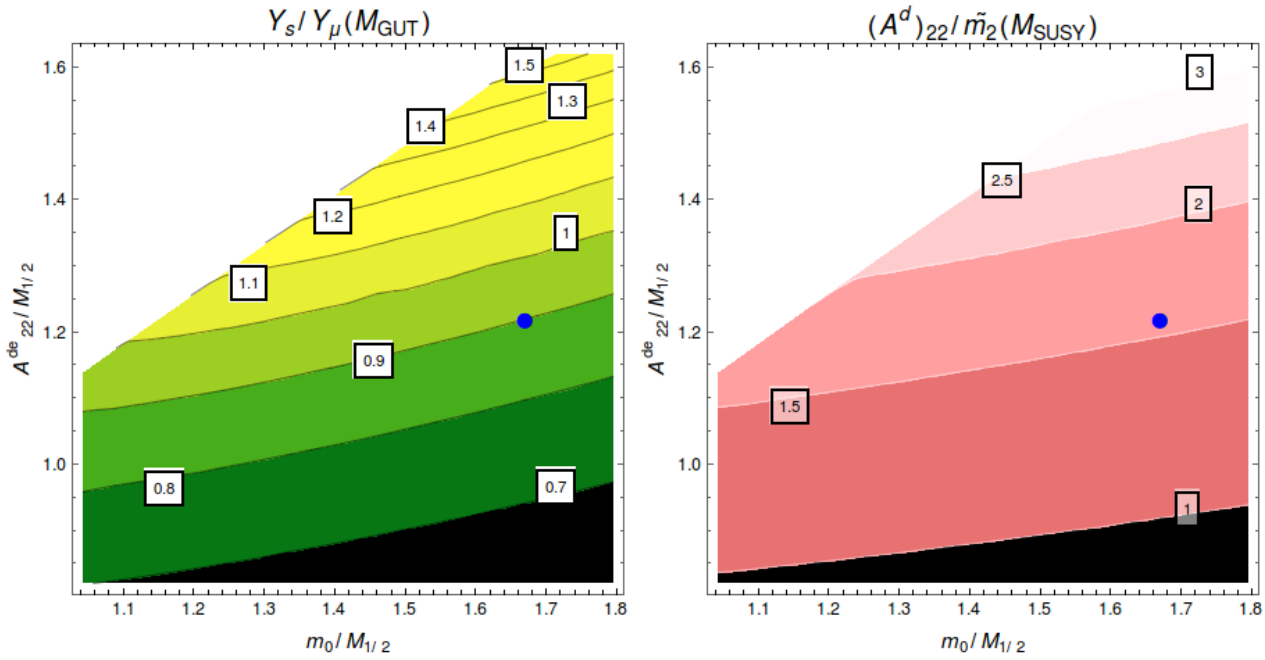

(a) (b)

Figure 2.4: Left: The ratio Y_s/Y_μ presented as a function of A^{de}_{22} and m_0. Right: The corresponding values of $A^d_{22}/\tilde{m}_2$ at $M_{\rm SUSY}$. They are shown around point 3 from Tab. 5.1 (marked by a blue dot).

parameters at a time, which gives some estimates of the shape of the parameter correlations in the vicinity of the considered point. In all these plots, we display only the points which fulfil all the necessary phenomenological requirements, in particular that the Higgs vacuum is a local minimum of the scalar potential,[3] and that no Landau poles exist below $M_{\rm GUT}$. White regions in the plots signal that either one of above conditions was not fulfilled, or that the applied program, `SOFTSUSY` [59], rejected the point because its iterative algorithm had not converged.

Beginning with the largest couplings, we notice that three parameters play a crucial role in the case of bottom-tau unification: A^{de}_{33}, μ and m_0 (which for given $M_{1/2}$ governs masses of the third family sfermions). The non-universal sfermion masses, independent for each family, could add some additional freedom to our model. Although they are not necessary for achieving the Yukawa unification, relaxation of the universality could facilitate finding points with even higher $\tan\beta$ than presented in the next section.

The obtained values of the ratio Y_b/Y_τ at $M_{\rm GUT}$ are shown in the left panel of Fig. 2.3 as functions of A^{de}_{33} and m_0. The equality of Y_b and Y_τ at that scale might in general require an adjustment of all the parameters, as the excluded points tightly surround the allowed region.

In the second family case, the unification of Y_s and Y_μ is normally possible by a manipulation of just one parameter, namely A^{de}_{22}, despite the fact that it influences both the Yukawa couplings. For the first two families, μ has no noticeable influence on the unification in the considered region because the higgsino loop, being $\sim Y^u_{ii}$, gives a much smaller contribution, due to $m_{u,c} \ll m_t$.

[3] No scalar tachyons appear in the spectrum, meaning that no m^2 terms are negative.

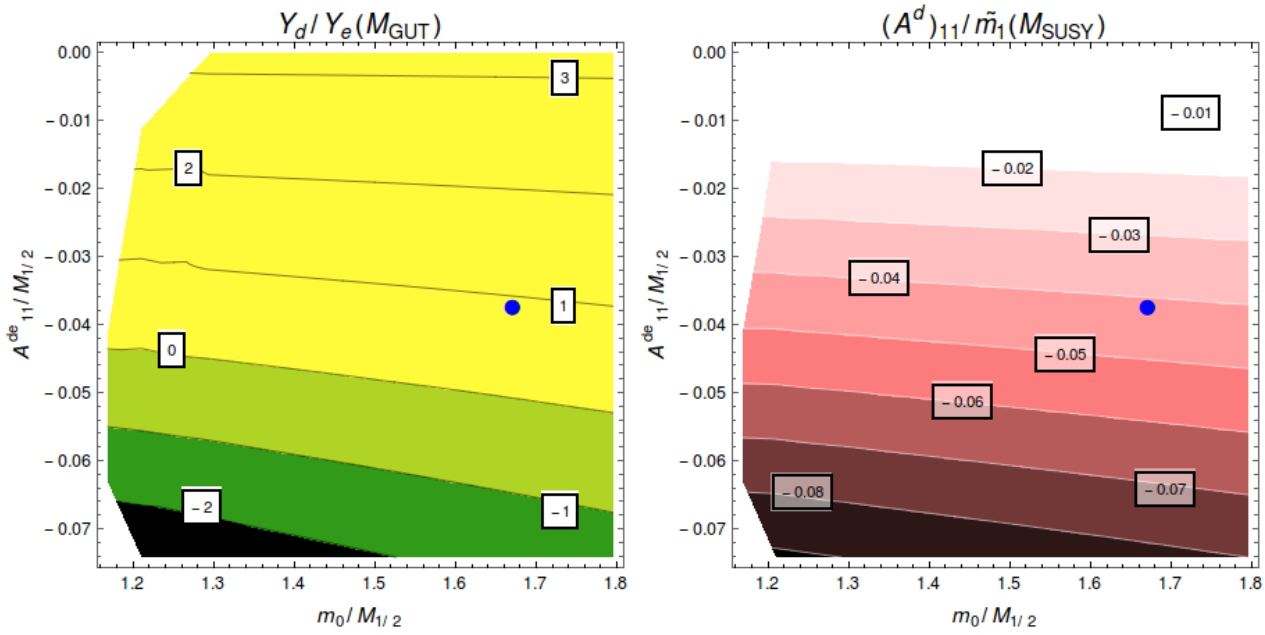

(a) (b)

Figure 2.5: Left: The ratio Y_d/Y_e as a function of A^{de}_{11} and m_0. Right: The corresponding values of $A^d_{11}/\tilde{m}_1$ at $M_{\rm SUSY}$. They are shown around point 3 from Tab. 5.1 (marked by a blue dot).

The ratio Y_s/Y_μ at $M_{\rm GUT}$ is plotted in the left panel of Fig. 2.4 against m_0 and A^{de}_{22}. The plot shows that a large value of A^{de}_{22} is necessary to achieve the unification. The corresponding values of $A^d_{22}/\tilde{m}_2$ at $M_{\rm SUSY}$ are shown in the right panel of Fig. 2.4. Such ratios will be relevant in the context of our discussion of the vacuum metastability in Sec. 5.3.

Analogous plots that describe unification of the down-quark and electron Yukawa couplings are presented in Fig. 2.5. It is the simplest case because the necessary adjustment of the respective A-term neither triggers phenomenological problems, nor influences any parameters that are relevant for other families.

2.4 Threshold corrections with flavour mixing in the soft terms

Now, after we have described the most important features of the flavour-diagonal soft term case, let us explore the more general framework of GFV MSSM. The dependence of threshold corrections on the GFV parameters is non-trivial. The flavour-off-diagonal soft mass matrix elements enter Eq. (2.9) through rotation matrices that diagonalise the very sfermion mass matrices. On the other hand, the off-diagonal trilinear couplings appear explicitly in the expressions for the threshold corrections given in Ref. [58]. Such a treatment of the flavour-violating terms is correct in the SUSY-decoupling limit, in which case the sfermion mass matrix diagonalisation can be performed prior to considering the EWSB.

To gain some intuition about the functional dependence of Eq. (2.9) on various entries in the sfermion mass matrices, let us consider again an example of threshold corrections to

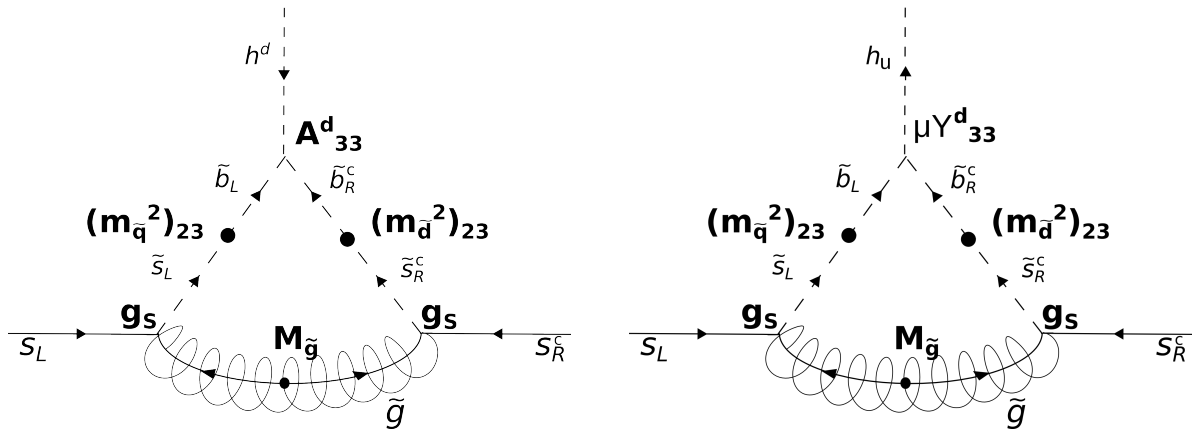

Figure 2.6: Diagrams contributing to the gluino-mediated threshold correction to the strange-quark Yukawa coupling at $\mu_{\rm sp}$. It arises when flavour mixing is present in the soft mass matrix.

the self-energy of down-type quarks. A relatively simple analytic expression for $(\Sigma^d_{22})^{\tilde{g}}$ can be obtained when the first-family couplings are still assumed to be flavour-diagonal, while the second and third family mixing is generated by $(m^2_{dl})_{23}(M_{\rm GUT})$ alone.[4] In such a case, the dominant GFV contribution to the strange quark self-energy is associated with a gluino loop. The relevant diagrams are shown in Fig. 2.6. They give [58]

$$(\Sigma^d_{22})^{\tilde{g}} = \frac{2\alpha_s m_{\tilde{g}} v_d}{3\pi}(A^d_{33} - Y_b\,\mu\tan\beta)\sum_{m,n=2,3} C_0(m^2_{\tilde{g}}, m^2_{\tilde{q}^L_m}, m^2_{\tilde{d}^R_n}) \times \frac{(m^2_{\tilde{q}})_{23}}{\sqrt{\left[(m^2_{\tilde{q}})_{22} - (m^2_{\tilde{q}})_{33}\right]^2 + 4((m^2_{\tilde{q}})_{23})^2}} \frac{(m^2_{\tilde{d}})_{23}}{\sqrt{\left[(m^2_{\tilde{d}})_{22} - (m^2_{\tilde{d}})_{33}\right]^2 + 4((m^2_{\tilde{d}})_{23})^2}}, \tag{2.14}$$

where it has been assumed that $(m^2_{\tilde{q}})_{23}$ and $(m^2_{\tilde{d}})_{23}$ are real. It follows from Eq. (2.14) that the chirality-conserving GFV interactions $[(m^2_{\tilde{q}})_{23}\,\tilde{s}^*_L\tilde{b}_L + \text{h.c.}]$ and $[(m^2_{\tilde{d}})_{23}\,\tilde{s}^*_R\tilde{b}_R + \text{h.c.}]$ generate a threshold correction to Y_s of the order of $\Delta Y_s \sim \alpha_s A^d_{33}/M_{\rm SUSY}$, which in general can be large enough to enable a satisfactory Yukawa coupling unification for the second family, even when A^d_{22} is small.

The above discussion, however, should be treated only as a simplified qualitative illustration. In a general case, other off-diagonal elements of the squark mass matrix can significantly differ from zero, which makes the mixing among all the three generations important. To make sure that all the relevant effects are properly taken into account, we shall perform a complete numerical analysis of the GFV scenario in Chapters 6 and 7.

[4] As we have already mentioned, not only $(m^2_{\tilde{d}})_{23}$ but also $(m^2_{\tilde{q}})_{23}$ gets then generated at the SUSY scale, thanks to the RG-evolution effects.

CHAPTER 3

Phenomenological constraints

In this chapter, some of the phenomenological low-energy constraints that matter for our analysis are described. They are selected according to their relevance for the discussion of the considered scenarios.

3.1 Flavour Changing Neutral Currents

This section is devoted to recalling basic properties of those Flavour Changing Neutral Current (FCNC) processes that are going to serve as experimental tests in the following chapters. The name FCNC refers to processes where flavour is not conserved, but each open fermion line has particles with the same electric charges on its ends. In the SM and MSSM, there are no FCNCs at the tree level because all the flavour-changing vertices involve a change in the electric charge, too. Historically, this was a postulate that allowed to explain the FCNC suppression via the so-called Glashow-Iliopoulos-Maiani (GIM) mechanism [60]. This mechanism implies that the FCNCs involving the first two generations of quarks alone are suppressed not only by loop factors and small coupling constants but, in addition, by tiny ratios of the light quark masses squared to the W-boson mass squared.[1] The GIM suppression by mass ratios is not in place for loops with the top quark because $m_t > M_W$. However, other numerically small factors often enter in this case, e.g., the CKM matrix element V_{td}.

The generic smallness of FCNC amplitudes in the SM renders them sensitive to possible new physics effects, making all the beyond-SM theories with tree-level FCNCs severely constrained. In the MSSM, no such tree-level effects are present, but we encounter new loop contributions to the FCNC amplitudes. We need to test the corresponding experimental constraints, keeping in mind though that the SUSY FCNC effects tend to zero (decouple) when all the superpartners become much heavier than the electroweak scale. This is contrary to the Yukawa threshold corrections that may remain large also in the heavy SUSY limit.

[1] The same mechanism makes the FCNC processes in the lepton sector completely negligible in the SM, due to tiny masses of the neutrinos.

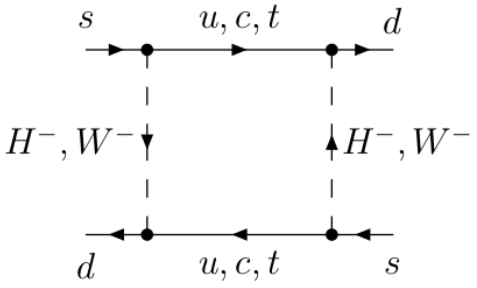

(A): W and charged Higgs exchanges

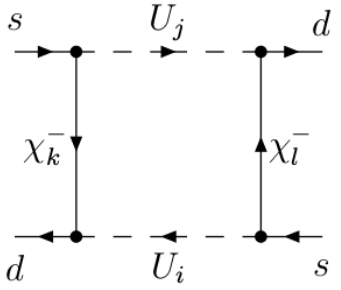

(B): chargino exchange

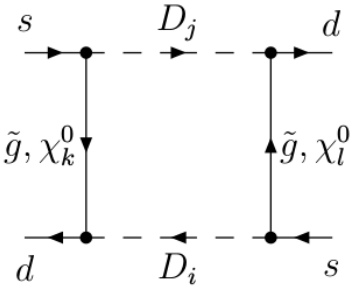

(C): neutralino and gluino exchanges

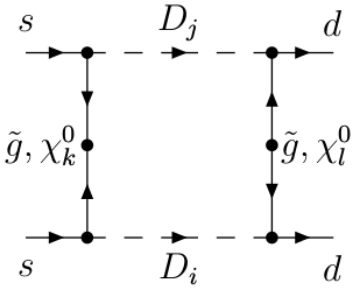

(D): neutralino and gluino exchanges

Figure 3.1: The MSSM Feynman diagrams contributing to $\bar{K}^0$-K^0 mixing. In this figure, U_i and D_i denote respectively the up- and down-squarks of any family. The drawings have been adopted from Ref. [61].

3.1.1 Kaon mixing

The lightest mesons containing an (anti)strange quark, called *kaons*, are a significant object of study, both at present and in the past. The kaon system was the first where CP-violation was observed [62]. A mixing of the two neutral kaon flavour eigenstates ($K^0 \sim (d\bar{s})$ and $\bar{K}^0 \sim (s\bar{d})$) produces two mass eigenstates K_S and K_L that are detected in experiments. An important observable used to quantify CP-violation in the mixing phenomenon is the ratio ϵ_K of the decay amplitudes of K_S and K_L into two-pion states with vanishing total isospin:

$$\epsilon_K = \frac{\mathcal{A}[K_L \to (\pi\pi)_{I=0}]}{\mathcal{A}[K_S \to (\pi\pi)_{I=0}]}. \tag{3.1}$$

Here, $|(\pi\pi)_{I=0}\rangle = \frac{1}{\sqrt{3}}(|\pi^+\pi^-\rangle + |\pi^-\pi^+\rangle - |\pi^0\pi^0\rangle)$. One-loop diagrams contributing to K^0-$\bar{K}^0$ mixing in the MSSM are presented in Fig. 3.1.

The current experimental result for $|\epsilon_K|$ which we adopt for our analysis reads [19]:

$$|\epsilon_K^{\rm exp}| = (2.228 \pm 0.011) \times 10^{-3}. \tag{3.2}$$

The present status of the SM calculations of $|\epsilon_K|$ is discussed in Ref. [63]. The theoretical uncertainty is much larger than the experimental one. Until several years ago, it had originated mainly from the non-perturbative parameter B_K that is being determined using lattice QCD simulations. Nowadays, the lattice QCD errors are subdominant, and the main theory uncertainty in $|\epsilon_K|$ stems from poor convergence of the QCD perturbation series for the double-charm contributions in Fig. 3.1(A), as well as from the CKM matrix element $|V_{cb}|$

which enters in the fourth power into the expression for $|\epsilon_K|$. The value of $|V_{cb}|$ can be quite accurately extracted either from the inclusive or exclusive semileptonic B-meson decay data. However, a long-standing discrepancy between the two methods persists. If the inclusive method for $|V_{cb}|$ is used, the SM result for $|\epsilon_K|$ in Ref. [63] agrees with Eq. (3.2) within the theory uncertainty of $\pm 2.3 \times 10^{-4}$. On the other hand, a 3.4σ discrepancy is found (with $\sigma \sim 1.8 \times 10^{-4}$) when the exclusive method is followed. The discrepancy is going to decrease after taking into account the very recent experimental update of the exclusive semileptonic results at the EPS-HEP 2015 conference [64], as it shifts the exclusive $|V_{cb}|$ towards the inclusive one.

Our numerical analysis here and in Ref. [4] relies on the calculation of Ref. [65] where the SM result

$$|\epsilon_K^{\rm SM}| = (1.81 \pm 0.28) \times 10^{-3} \tag{3.3}$$

was obtained employing the 2010 weighted average of the exclusive and inclusive $|V_{cb}|$, namely $|V_{cb}| = 0.0406(13)$. We do not make any use of the SM central value from Eq. (3.3), but rather calculate $|\epsilon_K|$ in the MSSM from the outset, using the code `SUSY_FLAVOR v2.10` [66]. As far as the SM parameters are concerned, we adopt the SM values and uncertainties for all of them but the Wolfenstein parameters ρ and η in the CKM matrix description. In our numerical treatment, each point of the MSSM scan corresponds to a particular value of (ρ, η), and it is tested against SUSY-sensitive loop observables that matter for determining the allowed regions in the (ρ, η) plane. At the same time, our initial ranges for ρ and η are adopted from the so-called 'new physics fit' by the UTFit collaboration [67] where only tree-level observables are included.

Once $|\epsilon_K|$ is calculated for a given point in the MSSM parameter space, it needs to be tested against the experimental result (3.2), taking into account the theory uncertainty. To do so, we subtract the Wolfenstein-parameter-induced error from the one in Eq.(3.3), which reduces the theory uncertainty to $\pm 1.7 \times 10^{-4}$. The latter error is treated as the theory one for particular values of ρ and η in our MSSM scan. To accept or reject a given point, we check its consistency with Eq. (3.2) at the desired level (see Chapter 6), after adding the theory error in quadrature to the experimental one. An identical approach is followed for all the other flavour observables for which the dependence on ρ and η (varied within their initial tree-level-determined ranges) is non-negligible when compared to other uncertainties.

3.1.2 B-meson mixing

Similarly to the neutral kaon mixing, an analogous phenomenon occurs for the neutral B-mesons whose flavour contents are

$$B_d^0 \sim (d\bar{b}), \qquad \bar{B}_d^0 \sim (b\bar{d}), \qquad B_s^0 \sim (s\bar{b}), \qquad \bar{B}_s^0 \sim (b\bar{s}). \tag{3.4}$$

They are the lightest eigenstates of the strong interaction Hamiltonian which possess these very flavour contents.

There are several observables in the neutral B-meson mixing which we shall use for tests of our Yukawa unification scenarios. First, we shall consider mass differences ΔM_{B_d} and ΔM_{B_s} between the corresponding mass eigenstates. Their experimentally determined values

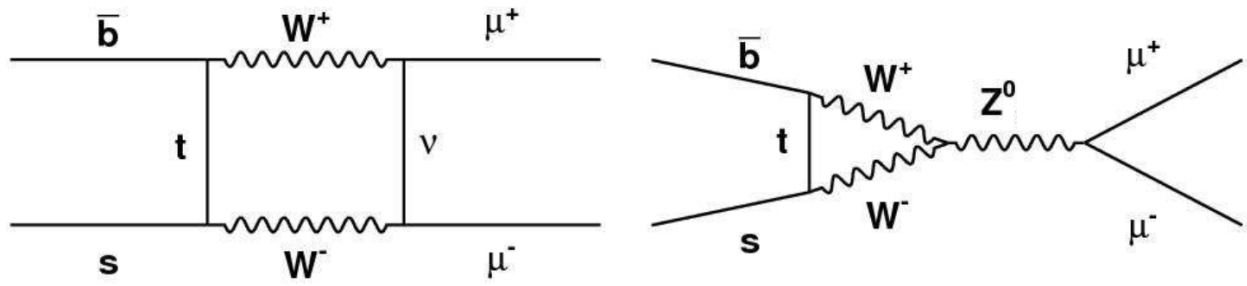

Figure 3.2: Examples of SM diagrams contributing to $\mathcal{B}(B_s \to \mu^+\mu^-)$. The drawings have been adopted from Ref. [70].

are as follows [19]:

$$\Delta M_{B_s}^{\rm exp} = (1.1691 \pm 0.0014) \times 10^{-11}\,{\rm GeV}, \tag{3.5}$$
$$\Delta M_{B_d}^{\rm exp} = (3.357 \pm 0.033) \times 10^{-13}\,{\rm GeV}. \tag{3.6}$$

Their theoretical estimates for fixed ρ and η receive the main uncertainties[2] from overall factors that are determined in lattice QCD simulations – see, e.g., Ref. [68]. These uncertainties cancel to a large extent in the ratio $\Delta M_{B_d}/\Delta M_{B_s}$. In consequence, this ratio has a smaller theory uncertainty, and will be considered as a supplementary observable. Its experimental value reads [69]

$$(\Delta M_{B_d}/\Delta M_{B_s})^{\rm exp} = (2.87 \pm 0.02) \times 10^{-2}. \tag{3.7}$$

Another important observable is the CP-violating phase β of the B_d^0-$\bar{B}_d^0$ mixing amplitude. Measurements of CP-asymmetries in $B_d^0 \to J/\psi K_S$ and similar processes imply that [69]

$$\sin(2\beta)_{\rm exp} = 0.682 \pm 0.019. \tag{3.8}$$

The above result provides a valuable constraint in the GFV case because the experimental error is small, and the theory uncertainty is even smaller, in fact practically negligible at present.

3.1.3 Rare B decays

Another set of precisely measured flavour observables is provided by rare decays of the B-mesons. Among them, we select three branching ratios to be investigated more closely when testing our scenarios:

1. $\overline{\mathcal{B}}_{s\mu} \equiv \mathcal{B}(B_s \to \mu^+\mu^-)$
   As for any FCNC process, contributions to this branching ratio arise only at one-loop level in the SM and MSSM. Two sample SM diagrams are presented in Fig. 3.2. Apart from loop factors, the branching ratio gets additionally suppressed by $m_\mu^2/m_{B_s}^2$ where m_μ is the muon mass. An analogous suppression occurs in all the other decays of the neutral B-mesons into lepton pairs. Current measurements by CMS and LHCb give

[2] Numerical estimates of all such uncertainties are collected in Tab. 6.1 of Chapter 6.

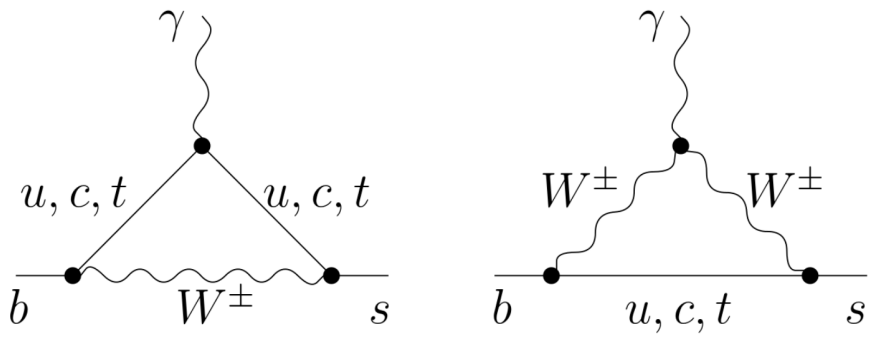

Figure 3.3: Leading order diagrams contributing to $\mathcal{B}(\bar{B} \to X_s\gamma)$. The drawings have been adopted from Ref. [73].

the following weighted average [71]:

$$\mathcal{B}(B_s \to \mu^+\mu^-)_{\text{exp}} = \left(2.8^{+0.7}_{-0.6}\right) \times 10^{-9}, \tag{3.9}$$

whereas the SM prediction reads [72]

$$\mathcal{B}(B_s \to \mu^+\mu^-)_{\text{SM}} = (3.65 \pm 0.23) \times 10^{-9}. \tag{3.10}$$

2. $\overline{\mathcal{B}}_{d\mu} \equiv \mathcal{B}(B_d \to \mu^+\mu^-)$
This is an analogous process involving the B^0_d meson. The CMS and LHCb experiments have published the following average of their branching ratio measurements [71]:

$$\mathcal{B}\left(B_d \to \mu^+\mu^-\right)_{\text{exp}} = (3.9^{+1.6}_{-1.4}) \times 10^{-10}, \tag{3.11}$$

while the SM calculation returns [72]

$$\mathcal{B}\left(B_d \to \mu^+\mu^-\right)_{\text{SM}} = (1.06 \pm 0.09) \times 10^{-10}. \tag{3.12}$$

3. $\mathcal{B}_\gamma \equiv \mathcal{B}(\bar{B} \to X_s\gamma)$
This process is an inclusive decay of $\bar{B}^0$ ($\bar{d}b$) or B^- ($\bar{u}b$) into a photon and charmless hadrons with non-zero overall strangeness.[3] The leading SM contributions to this process are shown in Fig. 3.3, whereas a few examples of the MSSM contributions can be seen in Fig. 3.4. The inclusive branching ratio $\mathcal{B}(\bar{B} \to X_s\gamma)$ was first measured in 1995 by the CLEO collaboration [74]. The current experimental world average reads [69]:

$$\mathcal{B}(\bar{B} \to X_s\gamma)^{\text{exp}}_{E_\gamma > 1.6\,\text{GeV}} = (3.43 \pm 0.22) \times 10^{-4}. \tag{3.13}$$

It agrees very well with the SM prediction [75]

$$\mathcal{B}(\bar{B} \to X_s\gamma)^{\text{SM}}_{E_\gamma > 1.6\,\text{GeV}} = (3.36 \pm 0.23) \times 10^{-4}. \tag{3.14}$$

It is an untypical FCNC process, as the GIM mechanism in the SM does not provide any extra suppression except for the loop factor and the electromagnetic coupling.

[3] It means that *none* of these hadrons is allowed to contain a valence c-quark, while the non-vanishing strangeness requirement refers to the total hadronic state X_s.

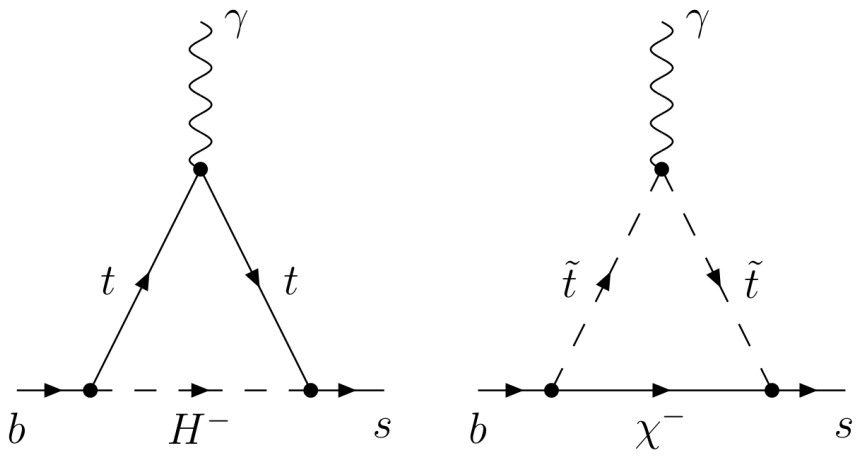

Figure 3.4: Sample MSSM diagrams contributing to $\mathcal{B}(\bar{B} \to X_s\gamma)$. The drawings have been adopted from Ref. [61].

In effect, the branching ratio is of the same order as $\alpha_{\rm em}/(4\pi) \simeq 6 \times 10^{-4}$. Such a "big" branching ratio helps in performing accurate measurements. On the other hand, the sensitivity to beyond-SM effects remains exceptional. To understand the latter point one needs to recall that the leading contributions to the B-meson decay originate from three-body partonic processes ($b \to c\ell\bar{\nu}$, $b \to cd\bar{u}$, etc.), while the radiative decay is generated by a two body transition $b \to s\gamma$ that comes with a CKM factor of practically the same size. The phase-space enhancement of the two-body mode gets compensated by the chirality suppression factor, namely by the fact that $b \to s\gamma$ proceeds via a dipole-type interaction that changes chirality of the quarks. In the SM, the chirality shift results in an extra factor of m_b/M_W in the amplitude. However, in the second MSSM diagram of Fig. 3.4, the factor of m_b/M_W gets replaced by (roughly) $m_b \tan\beta \, \sin\theta_\chi \, m_{\chi^-}/\max(m^2_{\chi^-}, m^2_{\tilde{t}})$ where θ_χ is the higgsino-wino mixing angle. Thus, the SUSY contributions can get enhanced by $\tan\beta$, which acts against the usual suppression by the superpartner masses. For heavy superpartners, one additionally needs to take into account that the higgsino-wino mixing angle tends to zero in the SUSY decoupling limit.

3.1.4 Lepton Flavour Violation

Lepton Flavour Violating (LFV) processes belong to the observables that provide the most severe constraints on GUT-motivated models with new sources of flavour mixing. In the SM, mixing between different lepton generations comes only through higher-dimensional operators.[4] One of such operators has been given in Eq. (1.10). It is responsible for generating the observed neutrino masses and mixings. These tiny masses and sizeable mixing angles do imply existence of charged-lepton LVF processes but with extremely low rates. If the neutrino mixings are the only source of LFV then, for instance, the branching ratio of $\mu^+ \to e^+\gamma$ decay is estimated at the level of 10^{-54} [76]. Thus practically no SM background

[4] By writing "in the SM" we understand working under the assumption that all the beyond-SM degrees of freedom are much heavier than the electroweak scale and could have been decoupled.

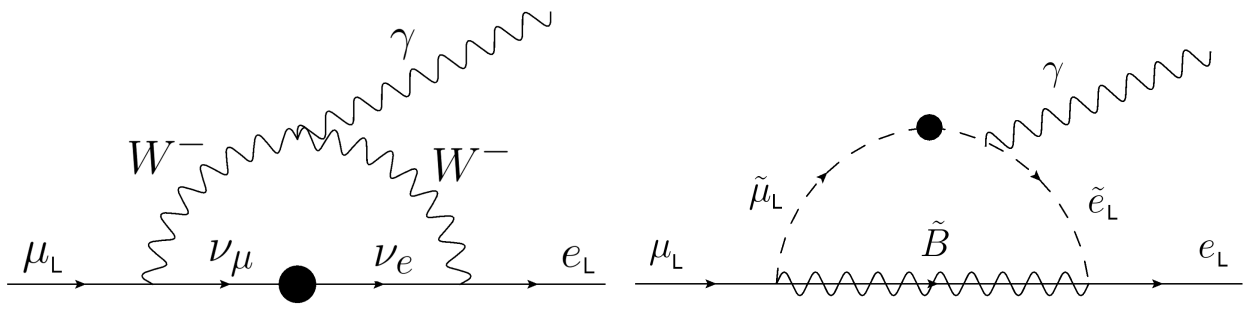

Figure 3.5: Sample diagrams generating the $\mu^+ \to e^+\gamma$ decay. The relevant flavour changing vertex is marked by a dot. Left: decay via neutrino mixing. Right: A possible decay mechanism in the GFV MSSM.

is present in using this process for testing new physics models with LFV parameters.

Two experimental bounds on LFV are of special importance for our scenario with flavour mixing in the soft mass terms:

1. $\mathcal{B}(\mu^+ \to e^+\gamma)$
   Sample diagrams contributing to this process are presented in Fig. 3.5 for the SM (left) and GFV MSSM (both). The first historical search was reported in Ref. [77], and the upper limit has been continuously improving over the following decades. The choice of μ^+ rather than μ^- has a technical motivation: μ^+ does not get captured by nuclei, which helps to simplify the experimental background subtraction as compared to the μ^- decays. The present upper bound comes from the MEG experiment. It reads [78]

   $$\mathcal{B}(\mu^+ \to e^+\gamma) < 5.7 \times 10^{-13}. \tag{3.15}$$

2. $\mathcal{B}(\tau^\pm \to \mu^\pm\gamma)$

   The mechanism of this decay is analogous to the previous one. The current upper bound reads [79]

   $$\mathcal{B}(\tau^\pm \to \mu^\pm\gamma) < 4.4 \times 10^{-8}. \tag{3.16}$$

3.2 Higgs boson mass measurement

In the years surrounding the official announcement of the Higgs boson discovery by the LHC experiments ATLAS and CMS in 2012 [80, 81], the main aim in most of the supersymmetric phenomenology research was to correctly reproduce the observed Higgs boson mass m_{h^0}. The combined measurements as of March 2015 yield [82]

$$m_{h^0}^{\text{exp}} = 125.09 \pm 0.21(\text{stat.}) \pm 0.11(\text{syst.})\,\text{GeV}. \tag{3.17}$$

As previously mentioned, it is not straightforward to obtain this number in a simple supersymmetric extension of the SM. The MSSM requires certain adjustment of parameters to provide a correct prediction. At the tree level, the mass of the lightest neutral Higgs boson

is lower than M_Z. Only the higher-order contributions can raise it to the observed value. If the pseudoscalar A^0 is much heavier than M_Z, the expression for $m^2_{h^0}$ including the leading one-loop corrections is given by [83]

$$m^2_{h^0} \approx M_Z^2 \cos^2 2\beta + \frac{3m_t^4}{2\pi^2 v^2}\left[\log\frac{M^2_{\rm SUSY}}{m_t^2} + \frac{X_t^2}{M^2_{\rm SUSY}}\left(1 - \frac{X_t^2}{12M^2_{\rm SUSY}}\right)\right], \tag{3.18}$$

with $v \simeq 246\,\text{GeV}$, $X_t = A^u_{33}/Y_t - \mu\cot\beta$ and $M_{\rm SUSY} = \sqrt{m_{\tilde{t}_1} m_{\tilde{t}_1}}$. The QCD-running couplings (Y_t, A^u_{33}) and masses (m_t, $m_{\tilde{t}_i}$) in the above equations should be taken at the scale $M_{\rm SUSY}$ to minimize higher-order effects. One can observe that to maximise the Higgs mass, a high $\tan\beta$ should be chosen, both stops should be heavy, and the stop mixing encoded in the parameter $|X_t|$ should be large, i.e. $|X_t|$ should be close to $M_{\rm SUSY}\sqrt{6}$. This is the reason why for given soft mass terms it is the A^u_{33} parameter that can be used to adjust the Higgs mass.

An extant phenomenological trouble is the theoretical uncertainty of the Higgs mass predictions. It has been estimated at the level of $\pm 3\,\text{GeV}$ [84] (i.e. much larger than the current experimental error) on the basis of differences between results obtained in various approximations by several of the available spectrum generators.

3.3 LHC SUSY searches

After decades of searches for supersymmetry at various colliders, the LHC has provided the most recent constraints on particular MSSM parameters or specific configurations of them. The results collected at the center-of-mass energy of 7 and 8 TeV clearly indicate that the superpartners should have masses of at least $\mathcal{O}(\text{TeV})$. Each of the constraints is based on particular simplifying assumptions, which makes the overall picture extremely complex. However, the basic fact is that no search has provided any significant signal in favour of supersymmetry. The most stringent and model-independent constraints are observed for the gluino being the particle that should be most abundantly produced at the LHC.

The summaries of searches at 8 TeV performed by the CMS and ATLAS collaborations are presented in Figs. 3.6 and 3.7. They provide a good illustration of the current frontier of direct SUSY searches.

3.4 Electroweak vacuum stability

To discuss another important requirement imposed on the MSSM, let us briefly recall the issue of the EW vacuum stability. In the Minkowski spacetime, a construction of the Hilbert space over which the operator fields act starts from a Lorentz invariant *vacuum state*. In the local and perturbative QFT case, we begin with determining the configuration of fundamental scalar fields that minimises their classical Hamiltonian. The positive definiteness of the scalars' kinetic terms in the Hamiltonian ensures that only constant fields can be non-vanishing in the minimum. By minimising the potential with respect to them, we find tree-level approximations for the *vacuum expectation values* (VEVs) of the scalar fields $\phi(x) = v_\phi = \text{const}$. Next, builiding up a perturbative QFT around the tree-level minimum, we find the loop-corrected effective potential and, order-by-order, the loop-corrected VEVs.

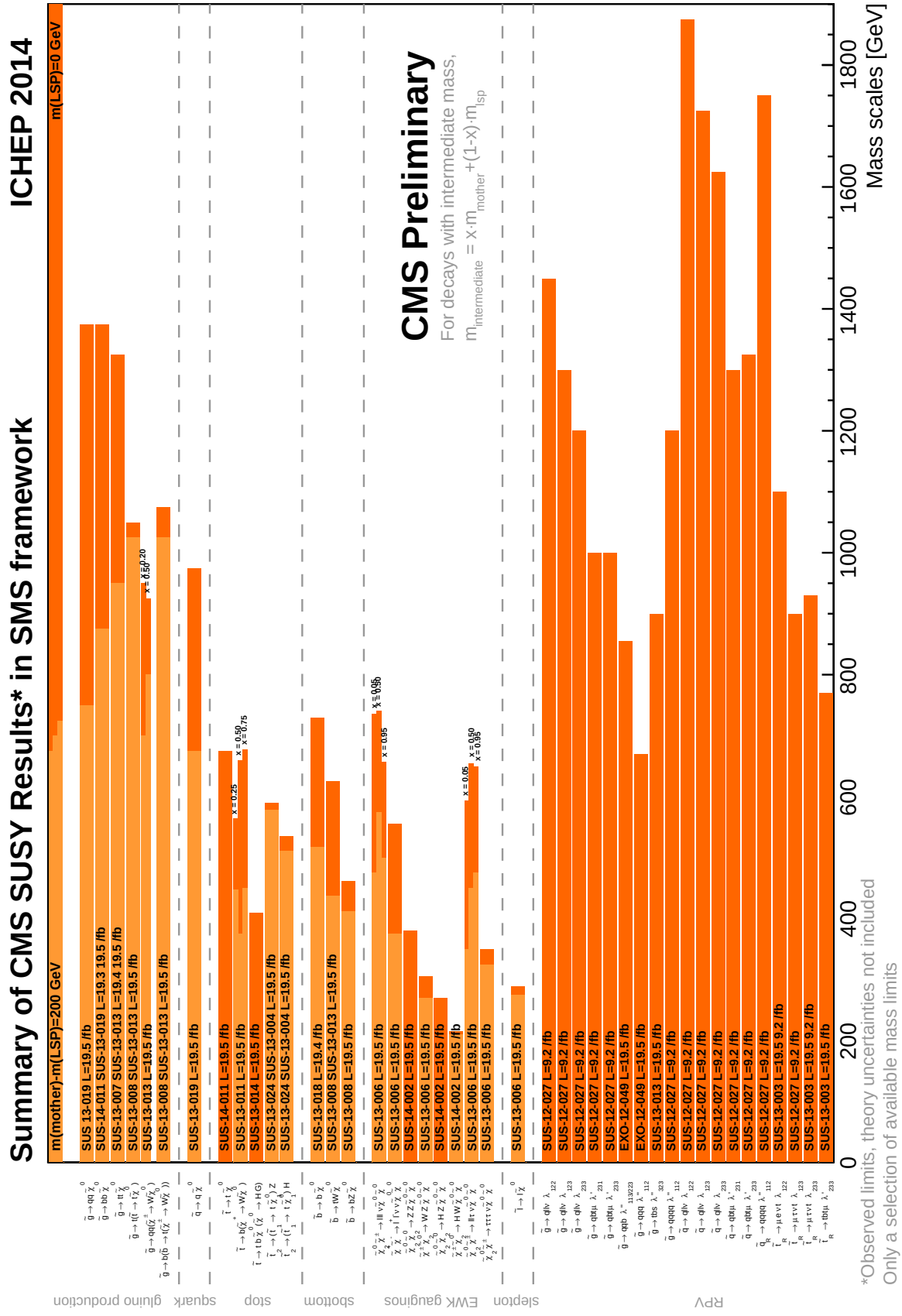

Figure 3.6: Plot summarising the SUSY searches performed by the CMS collaboration with 8 TeV data. It shows the best exclusion limits for masses of the mother particles when $m_{\mathrm{LSP}} = 0$ (dark shades) and $m_{\mathrm{mother}} - m_{\mathrm{LSP}} = 200\,\mathrm{GeV}$ (light shades). The indicated values are to be interpreted as upper bounds on the mass limits. The plot has been adopted from Ref. [85].

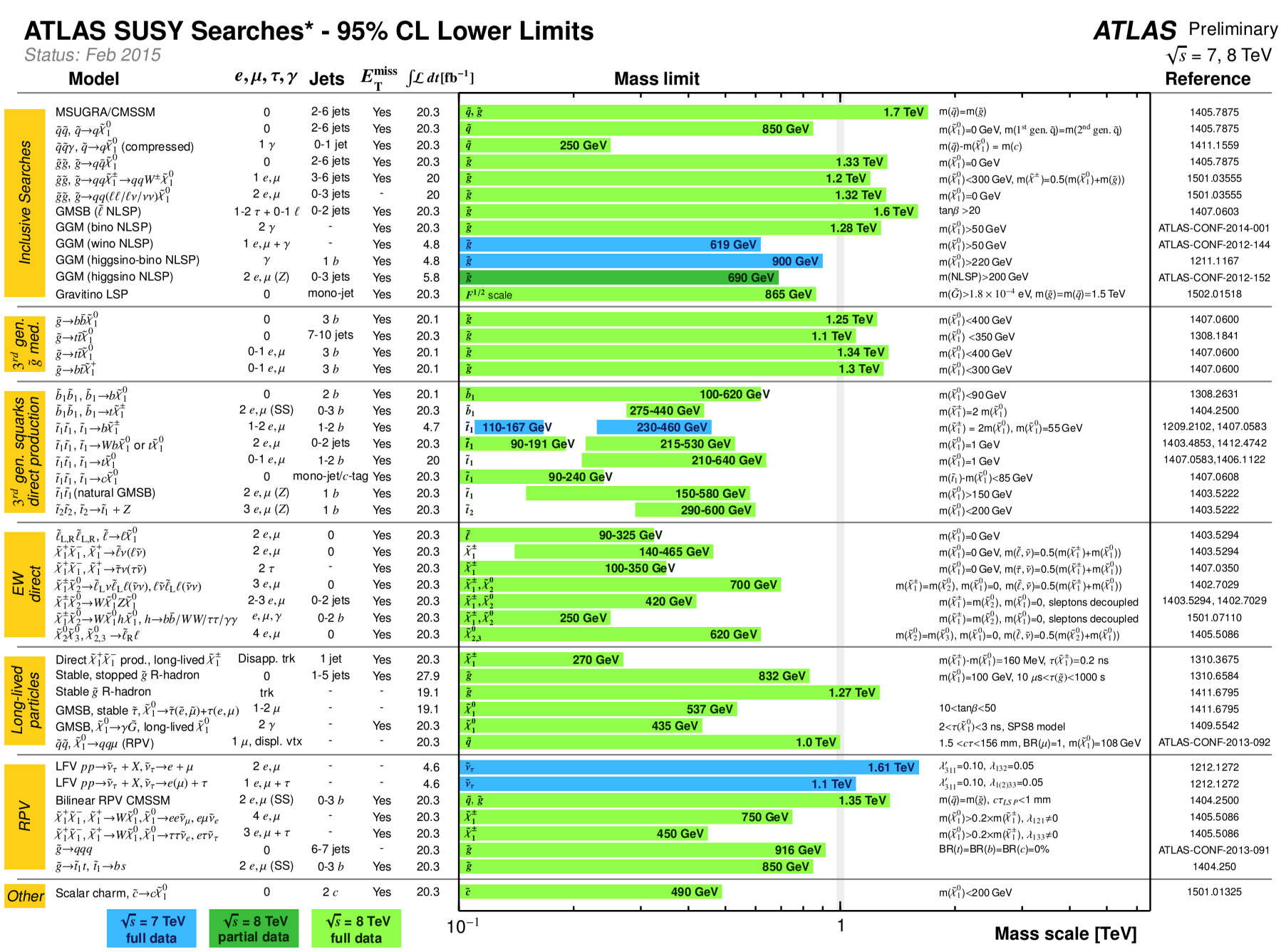

Figure 3.7: Plot summarising the SUSY searches performed by the ATLAS collaboration with 8 TeV data. It shows exclusion limits for masses of the sparticles under the assumptions stated adjacent to each bar. The plot has been adopted from Ref. [86].

The problem of finding a set of tree-level VEVs in the MSSM for arbitrary values of its parameters has not been solved so far due to immense dimensionality of the field space. In practice, one only tests particular menaces at certain classes of directions in this space, namely whether the potential is unbounded from below (UFB) or has deeper minima than the standard Higgs one. In the latter case, the VEVs in the global minimum would necessarily involve electrically charged scalars or the sneutrinos (having $L \neq 0$), which would stand against the experimental evidence. Such non-standard deeper minima are called Charge- or Colour-Breaking (CCB) vacua, as the sneutrino alone (without any charged scalar VEV) cannot produce a negative contribution to the classical vacuum energy. The appearance of a CCB minimum or the UFB configuration does not necessarily exclude the considered set of the MSSM parameters. One can assume that the cosmological history started with descending into a metastable vacuum state (in our case – the standard Higgs minimum). Then, as long as the standard Higgs vacuum lives longer than the age of the Universe, the model would not contradict any of our observations. There is a vast literature on testing the vacuum stability conditions in the MSSM. Some of the most dangerous field configurations have been considered in Ref. [87].

3.5 Dark matter

In this section, we briefly sketch the main facts about Dark Matter (DM) which belongs to the main unsolved puzzles of contemporary fundamental science. Particle physics offers possible explanations to the problem by means of introducing a beyond-SM stable particle. In this work, we find interesting correlations of the DM issue with our GFV scenario.

The existence of DM was postulated for the first time when astronomers could not explain velocities of stars in Milky Way relying only on masses of visible objects [88]. The same problem arose also for the galaxies in the Coma cluster [89]. By now, there is a vast amount of data consistently pointing that a yet-unknown type of gravitationally interacting matter exists (see e.g., Ref. [90]). Two examples are shown in Fig. 3.8.

Still, it is not known what kind of matter constitutes the DM. Many astronomical-scale objects and all the SM particles are excluded as viable candidates [93]. A range of proposals to explain the nature of DM exists. A notable position among them have the ones that assume that it consists of yet unknown elementary particles. This could have an impact on our quantum theories of fundamental interactions, especially if the DM candidate interacts not only gravitationally with the SM fields. An immensely popular idea advertises new Weakly Interacting Massive Particles (WIMPs) that would be consistent with present data coming from astronomy and particle physics, yet could be described with the means of the familiar perturbative QFT techniques. Moreover, a generic model involving such matter, Λ_{CDM}, is able to perfectly fit also the well-studied observational data that come from the Cosmic Microwave Background (CMB) [94].

One of the phenomenological side-effects of the R-parity assumption in the MSSM is that it provides a viable DM candidate. The R-parity implies that the Lightest Supersymmetric Particle (LSP) cannot decay to possibly lighter SM particles and, being stable, it is bound to permeate the Universe. There still remains, however, a quantitative test that is highly non-trivial to pass. This crucial observable is the current DM density in the Universe.

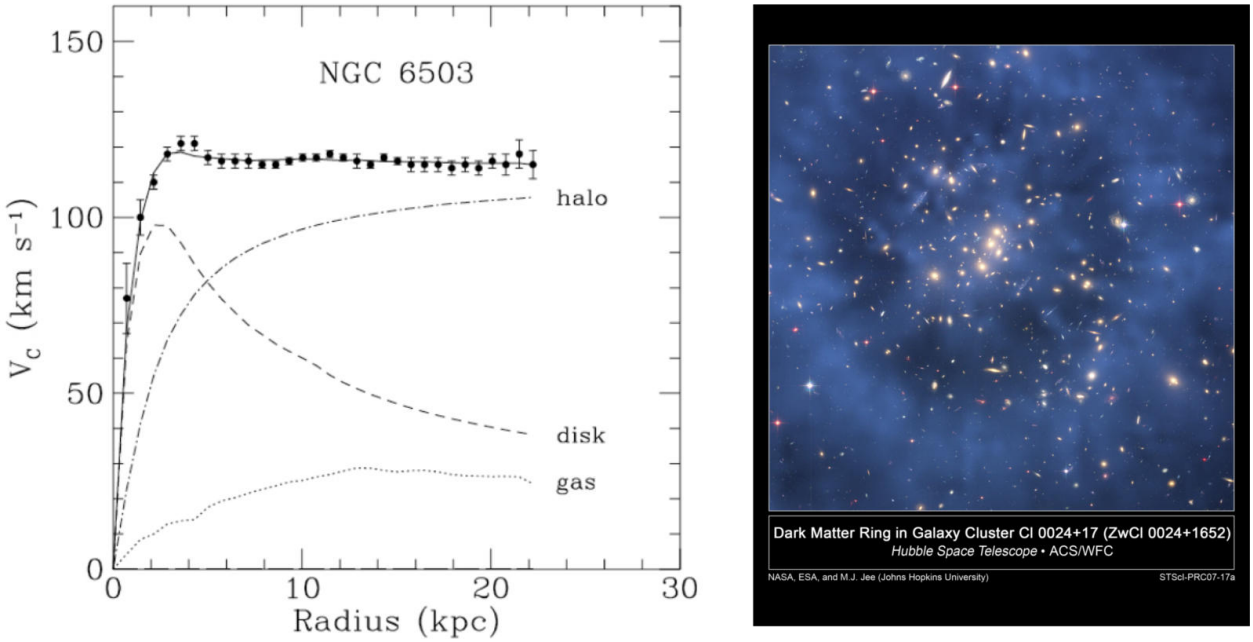

Figure 3.8: Examples of observational evidence for the dark matter existence. Left: the rotation curve of NGC 6503 galaxy – the data points and a fit split into contributions from the light-emitting components (disk), gas, and the missing dark component (halo) [91]. Right: a blue map of the cluster Cl 0024+17 dark matter distribution superimposed on the Hubble Space Telescope image of the cluster. The map was inferred from the observed gravitational lensing (source: Ref. [92]).

The DM relic density can be calculated in the MSSM, as long as a cosmological model is selected. The so-called *standard cosmological model* relies on the assumption that the Universe on sufficiently large scales is homogeneous and isotropic. It can be then described by the Friedman-Lemaître-Robertson-Walker (FLRW) metric

$$ds^2 = -dt^2 + a^2(t)d\Sigma^2, \tag{3.19}$$

where Σ is a metric on a 3-dimensional Euclidean manifold of uniform curvature. In the polar coordinates r, θ, ϕ, we have

$$d\Sigma^2 = \frac{dr^2}{1 - kr^2} + r^2(d\theta^2 + \sin^2\theta d\phi^2), \tag{3.20}$$

with $k \in \{-1, 0, 1\}$ describing the curvature type. The dynamics of the Universe is captured in the term $a(t)$, and computable given the universal energy density in the Universe $\rho(t)$. If the Universe is spatially flat ($k = 0$), the total energy density is said to be *critical* and obeys the following equation:

$$\rho_{\text{crit}} = \frac{3}{8\pi G}\left(\frac{\dot{a}}{a}\right)^2, \tag{3.21}$$

with G being the Newton's gravitational constant ($6.70837 \times 10^{-39}\,\text{GeV}^{-2}$).

The Λ_{CDM} model that currently provides the best fit to the CMB data splits the energy density ρ into three parts:

$$\rho = \rho_b + \rho_\chi + \frac{\Lambda}{8\pi G}, \tag{3.22}$$

where ρ_b is the baryonic matter energy density (including also small contributions from electrons, photons and neutrinos), ρ_χ is that of dark matter, and Λ is the cosmological constant. The energy density ρ_χ is usually expressed in units of the critical density via

$$\Omega_\chi \equiv \frac{\rho_\chi}{\rho_{\rm crit}}. \tag{3.23}$$

The $\Lambda_{\rm CDM}$ fit in Ref. [94] returns the dark matter relic abundance in terms of the parameter

$$\Omega_\chi h^2 = 0.1199 \pm 0.0027 \tag{3.24}$$

which additionally contains the dimensionless constant $h = 0.673(12)$ [19] that parameterises the current expansion rate of the Universe

$$\frac{\dot{a}}{a}(\text{now}) = h \times 100\ \tfrac{\text{km/s}}{\text{Mpc}}. \tag{3.25}$$

The relic abundance of dark matter is often the most stringent constraint in GUT-constrained SUSY scenarios. The lightest neutralino (see Sec. 1.4.4) is a favoured candidate for the LSP. It is well known that the properties of this DM candidate strongly depend on its composition. If the lightest neutralino is almost purely a bino, the relic density is generally too large.

In the cosmological past, the neutralinos could have been produced thermally. Their present density depends on their annihilation rates to other particles. Since in the bino case the neutralino relic abundance is too high, its annihilation cross-section needs to be enhanced by a particular mechanism. A good solution is a co-annihilation with the lightest sfermion, or a resonance annihilation through one of the Higgs bosons. On the other hand, a significant higgsino component of the neutralino opens a possibility of efficient annihilation into gauge bosons. In fact, the annihilation cross-section in such a case is usually too large, and it leads to the DM underabundance.

Complementary to indirect estimates, a range of direct searches for WIMP DM have been performed. Typically, an underground tank filled with a noble gas (e.g., xenon), well isolated from other particle sources, is observed over a long period of time in expectation for an interaction with a DM particle. For a review of results and techniques applied in various experiments, see, e.g., Ref [95]. In this work, we consider only the currently most stringent bounds on the spin-independent neutralino-proton scattering cross section $\sigma_p^{\rm SI}$ from the LUX experiment [96].

CHAPTER 4

Numerical Tools

4.1 Spectrum generators

Let us briefly summarise the problem we face when quantitatively testing the Yukawa matrix unification in the MSSM. In principle, we could specify each point of the parameter space in terms of the gauge, superpotential and soft couplings at $M_{\rm GUT}$. Next, we could check whether it is acceptable using the low-energy SM determinations of the gauge and Yukawa couplings, the Higgs boson mass, and its quartic coupling. Finally, we could test all the other observational constraints: the direct search limits, flavour and electroweak observables, as well as the predicted dark matter relic density.

In practice, the problem is somewhat more complicated because some of the input parameters need to be initially specified at the low-energy scale, to avoid inefficient scans over the multi-dimensional parameter space. This refers not only to the gauge and Yukawa couplings but also to the μ and $B\mu$ parameters that are necessary for a proper EWSB. For every point in the parameter space, we employ an iterative procedure that determines the complete MSSM mass spectrum, as well as values of all the couplings at $M_{\rm GUT}$.

As a first step to be made, one has to numerically solve the nonlinear MSSM RGEs with boundary conditions subsequently specified at three different scales:

1. $\mu_{\rm sp}$ where the SM gauge and Yukawa couplings are translated into the MSSM ones (with the threshold corrections being calculated in an iterative manner, assuming no such corrections at the first step),

2. $M_{\rm EWSB} \equiv M_{\rm SUSY} = \sqrt{m_{\tilde{t}_1} m_{\tilde{t}_2}}$ where the minimisation of the MSSM scalar potential is performed. This scale is chosen with the aim to reduce the sensitivity of the EWSB conditions to higher-order perturbative corrections.

3. $M_{\rm GUT}$ where the soft terms are specified as the input parameters that determine the superpartner spectra and, consequently, the threshold corrections for the next steps of the iteration.

Public programs, called *spectrum generators*, implement this iterative algorithm in a generically similar manner, but with convention-dependent details. The procedure used by

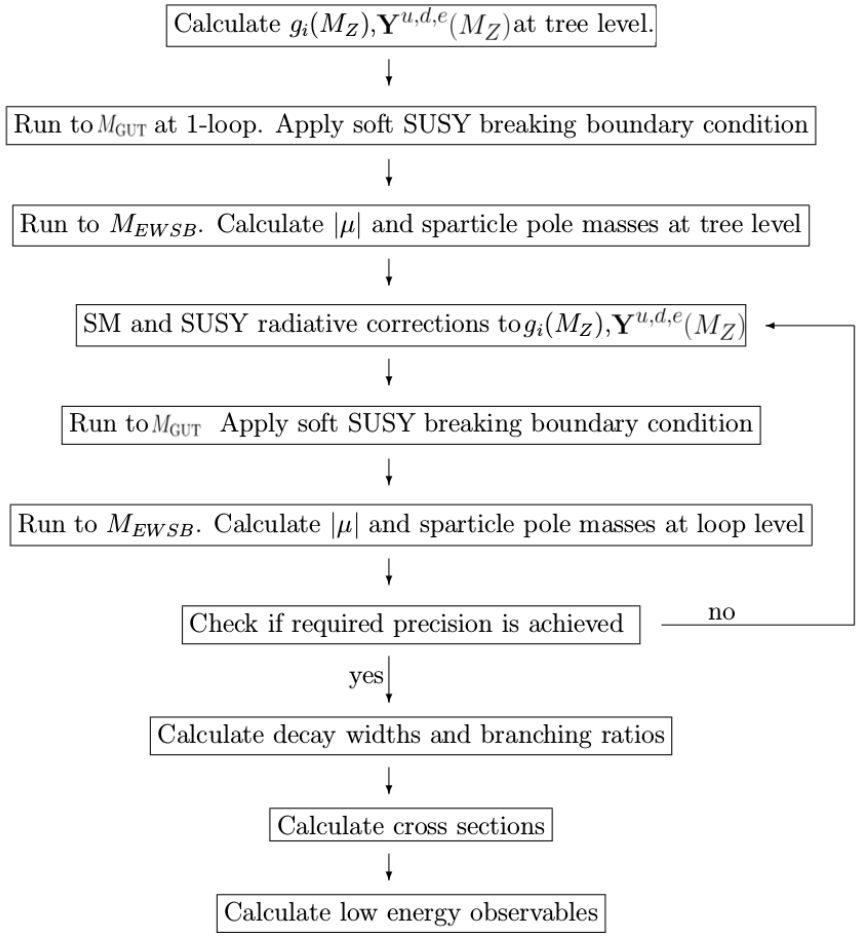
Calculate $g_i(M_Z)$,$\mathbf{Y}^{u,d,e}(M_Z)$at tree level.
Run to $M_{\rm GUT}$ at 1-loop. Apply soft SUSY breaking boundary condition
Run to M_{EWSB}. Calculate $|\mu|$ and sparticle pole masses at tree level
SM and SUSY radiative corrections to$g_i(M_Z)$,$\mathbf{Y}^{u,d,e}(M_Z)$
Run to$M_{\rm GUT}$ Apply soft SUSY breaking boundary condition
Run to M_{EWSB}. Calculate $|\mu|$ and sparticle pole masses at loop level
Check if required precision is achieved
no
yes
Calculate decay widths and branching ratios
Calculate cross sections
Calculate low energy observables

Figure 4.1: An iterative algorithm finding a solution of the RGE problem in the MSSM. The illustration has been adopted from the `SPheno` manual [97].

the code `SPheno` [97] is sketched in Fig. 4.1. The boundary with the SM (i.e. the scale $\mu_{\rm sp}$) is currently set by most of the public programs to be at M_Z. Such a choice has considerable disadvantages, one of which is excluding too many parameter points from the analysis. For instance, some scalar fields may become formally tachyonic (having a negative mass squared) only well below their proper decoupling scale but above M_Z, which is still acceptable, though most programs usually reject such points.

Another caveat is that there may exist acceptable points in the GUT-scale parameter space to which such an iterative procedure can never converge. In other words, since the starting-point data are not specified in terms of single-scale boundary conditions, the problem may have multiple solutions. Examples of such situations have been presented in Ref. [98]. This fact is of phenomenological relevance, as it affects the MSSM dark matter analyses performed with the standard iterative codes [99]. However, this problem hardly matters for our present investigation, as we only demonstrate existence of regions in the parameter space where the Yukawa unification constraint is satisfied.

4.2 Numerical setup for the large A-term scenario

For the purpose of the analysis of the large A-term scenario, we have modified `SOFTSUSY 3.3.8` [59] that distinguishes itself among other spectrum generators by possessing a technical documentation and clear structure. Following Ref. [58], we modified this code by implementing threshold corrections to the first and second family Yukawa couplings, as well as to the CKM matrix. It was necessary because such corrections were missing in `SOFTSUSY` at the time when the work was performed. As a by-product, we found some points to correct in both `SOFTSUSY` and `SPheno` which were then implemented by the authors [100].

$\alpha_s^{\overline{MS}}(M_Z)$	$\alpha_{em}^{-1}(M_Z)$	G_F $\left[\text{GeV}^{-2}\right]$		M_Z^{pole}	m_e^{pole}	m_μ^{pole}
0.1184	127.944	1.16638×10^{-5}		91.19 GeV	511 keV	106 MeV
m_τ^{pole}	$m_u^{\overline{MS}}$	$m_d^{\overline{MS}}$	$m_s^{\overline{MS}}$	$m_c^{\overline{MS}}(m_c)$	$m_b^{\overline{MS}}(m_b)$	m_t^{pole}
1.777 GeV	2.3 MeV	4.8 MeV	95 MeV	1.275 GeV	4.18 GeV	173.5 GeV

Table 4.1: Standard Model parameters [101] used in our numerical calculations for the diagonal A-term scenario. The light (u, d, s) quark masses are $\overline{\text{MS}}$-renormalised at 2 GeV.

Our input values of the SM parameters are collected in Tab. 4.1. Flavour observables are calculated with the help of `SUSY_FLAVOR v2.10` [66]. This code evaluates the renormalised MSSM Yukawa matrices and obtains the proper CKM matrix also according to the prescriptions of Ref. [58], taking the previously determined soft parameters as input.

For the purpose of the final scan that delivered the regions consistent with the Yukawa unification, we used the BayesFITSv3.2 [102] numerical package that interfaces several publicly available codes. Except the above-mentioned programs, it uses `MultiNest v2.7` [103] which allows for fast and efficient Markov Chain Monte Carlo (MCMC) scanning according to a pre-defined likelihood function. For the $SU(5)$ boundary condition in Eq. (1.44), we assume a Gaussian likelihood distribution

$$\mathcal{L}_{\text{Yuk}} = \sum_{i=1,2,3} \exp\left[-(1 - Y_{ii}^e(M_{\text{GUT}})/Y_{ii}^d(M_{\text{GUT}}))^2/2\sigma_{\text{Yuk}}^2\right], \tag{4.1}$$

with σ_{Yuk} set to 5% to allow for deviations from the exact unification condition.

4.3 Numerical tools for the GFV MSSM scenario

To investigate the second scenario, we have employed the same package BayesFITSv3.2. It was first developed in Ref. [102], and then modified to incorporate the full GFV structure of the soft SUSY-breaking sector in Ref. [57]. The package uses for sampling the `MultiNest v2.7` [103] code which allows for fast and efficient scanning according to a predefined likelihood function using the MCMC algorithms. The likelihood corresponding to the $SU(5)$ boundary condition (1.44) is modelled as in Eq. (4.1), with the same allowed deviation from the exact unification condition, $\sigma_{\text{Yuk}} = 0.05$.

m_t^{pole}		$m_b^{\overline{MS}}(m_b)$		$\alpha_s^{\overline{MS}}(M_Z)$		$\alpha_{\text{em}}^{-1}(M_Z)$	
173.34 ± 0.76 GeV		4.18 ± 0.03 GeV		0.1184 ± 0.0007		127.944 ± 0.015	
$m_u^{\overline{MS}}$	$m_d^{\overline{MS}}$	$m_s^{\overline{MS}}$	$m_c^{\overline{MS}}(m_c)$	m_e^{pole}	m_μ^{pole}	m_τ^{pole}	M_Z^{pole}
2.3 MeV	4.8 MeV	95 MeV	1.275 GeV	511 keV	106 MeV	1.777 GeV	91.19 GeV
$\bar{\rho}$		$\bar{\eta}$		A		λ	
0.159 ± 0.045		0.363 ± 0.049		0.802 ± 0.020		0.22535 ± 0.00065	

Table 4.2: Standard Model parameters [19, 67] used in our numerical calculations for the GFV scenario. The light (u, d, s) quark masses are $\overline{\text{MS}}$-renormalised at 2 GeV.

When our calculations for the first scenario were being performed, another version of `SPheno` was released. It offered us several necessary features that had not been available before. In particular, a more accurate treatment of the threshold corrections to the Yukawa couplings was implemented. The mass spectra in our GFV analysis are therefore calculated with `SPheno v3.3.3` [104] and checked against results obtained with the modified `SOFTSUSY 3.3.8` that has been mentioned earlier. Four SM parameters (m_t^{pole}, $m_b^{\overline{MS}}(m_b)$, $\alpha_{\text{em}}^{-1}(M_Z)$ and $\alpha_s^{\overline{MS}}(M_Z)$) are treated as nuisance parameters, and randomly drawn from a Gaussian distribution centered around their experimentally measured values [19]. The elements of the CKM matrix in the Wolfenstein parameterisation ($\bar{\rho}$, $\bar{\eta}$, A, λ) are scanned as well, with central values and errors given by the UTfit Collaboration for the scenario allowing new physics effects in loop observables [67]. The other SM parameters which are passed as an input to `SPheno` ($m_s^{\overline{MS}}$, $m_c^{\overline{MS}}(m_c)$, $m_d^{\overline{MS}}$, $m_u^{\overline{MS}}$, m_τ^{pole}, m_μ^{pole}, m_e^{pole}, M_Z^{pole}) are fixed at their experimentally measured values. Our SM input is collected in Table 4.2.

The relic density and the spin-independent neutralino-proton cross section σ_p^{SI} have been calculated with the help of `DarkSUSY v5.0.6` [105]. For the EW precision constraints `FeynHiggs v2.10.0` [106–109] has been used. To include the exclusion limits from Higgs boson searches at LEP, Tevatron, and LHC, as well as the χ^2 contributions from the Higgs boson signal rates from Tevatron and LHC, we applied HiggsBounds `v4.0.0` [110–112] interfaced with HiggsSignals `v1.0.0` [113]. Like in the previous scenario, all the flavour observables have been evaluated with the code `SUSY_FLAVOR v2.10` [66].

CHAPTER 5

Large diagonal A terms – numerical results

5.1 Regions with the successful SU(5) Yukawa matrix unification

In this chapter, following our article in Ref. [3], we describe sample regions in the MSSM parameter space that are consistent with the unification condition $\mathbf{Y}^d \simeq \mathbf{Y}^{eT}$ at $M_{\rm GUT}$ in the flavour-diagonal A-term scenario. Due to the large dimensionality of the considered parameter space, our description of these regions will amount to showing a few of their projections onto surfaces spanned by the most relevant parameters, as well as to presenting selected benchmark points.

In Figs. 5.1–5.2 and in Tab. 5.1, we present sample parameter-space regions and benchmark points where a proper Yukawa matrix unification has been achieved in our setup. In selecting these regions and points, we aimed at fulfilling the unification constraints and reproducing the lightest Higgs particle mass (up to the theoretical uncertainty of 3 GeV) for a broad range of $\tan\beta$. We have chosen the sparticle masses so that the gluino is heavy enough to have evaded the current bounds, but could possibly be detected in the second LHC phase.

Plots in Figs. 5.1–5.2 show points investigated in our MCMC scans performed for three $\tan\beta$ intervals: [5,20], [15,30], and [30,45]. Different colours are used to indicate successful Yukawa matrix unification, either for all the three families or for some of them only. We observe that Yukawa unification for all the three generations can be achieved for a wide range of $\tan\beta$. Generically, larger values of the A-terms are necessary for larger $\tan\beta$ because the down-type quark Yukawa couplings (and thus the required threshold corrections) scale proportionally to $\tan\beta$. For this reason, finding acceptable points for larger values of $\tan\beta$ in each random scan required collecting much more statistics.

Tabs. 5.1-5.4 contain information on the input parameters and particle spectra in four sample points with a proper Yukawa matrix unification. We also present the ratios m_{h_d}/m_0 and m_{h_u}/m_0 at the GUT scale that quantify departures from the scalar mass universality for each of the points. Tab. 5.2 shows the corresponding SUSY-scale threshold corrections

$$\delta Y_x \equiv \frac{v_d Y_x^{MSSM} - m_x^{\rm SM}}{m_x^{\rm SM}}, \qquad x = d, s, b, e, \mu, \tau, \tag{5.1}$$

	$\tan\beta$	$\frac{M_{1/2}}{\text{GeV}}$	$\frac{m_0}{M_{1/2}}$	$\frac{m_{h_u}}{m_0}$	$\frac{m_{h_d}}{m_0}$	$\frac{A^{de}_{11}}{M_{1/2}}$	$\frac{A^{de}_{22}}{M_{1/2}}$	$\frac{A^{de}_{33}}{M_{1/2}}$	$\frac{A^{u}_{33}}{M_{1/2}}$
1	7.47	1032.27	2.28	0.49	2.35	-0.008	0.63	1.63	-2.13
2	16.4	815.081	1.72	0.37	2.46	-0.017	0.89	1.30	-1.23
3	30.3	2733.63	1.67	0.19	1.79	-0.037	1.22	1.04	1.96
4	40.4	2663.45	1.72	0.26	2.58	-0.055	1.53	1.65	1.56

Table 5.1: Examples of points with a successful Yukawa unification. They are given by their defining sets of MSSM parameters: $\tan\beta$, common gaugino mass $M_{1/2}$, common sfermion mass m_0, soft masses of Higgs doublets m_{h_u} and m_{h_d}, and soft trilinear couplings $A_{ii}(M_{\text{GUT}})$.

	δY_d	δY_s	δY_b	$\frac{Y_d}{Y_e}$	$\frac{Y_s}{Y_\mu}$	$\frac{Y_b}{Y_\tau}$
1	-0.6	2.4	0.19	1.10	0.94	0.97
2	-0.66	2.3	0.089	0.95	0.91	0.90
3	-0.69	2.1	0.085	0.92	0.90	0.94
4	-0.66	2.1	0.13	1.01	0.92	1.08

Table 5.2: Values of the threshold corrections and other characteristics of the points from Tab. 5.1 (see the text).

as well as the GUT-scale ratios Y^d_{ii}/Y^e_{ii} which parameterise the unification quality. The observed small deviations of the latter ratios from unity determine sizes of the necessary GUT-scale threshold corrections.

5.2 Flavour observables

In this section, we discuss the impact of large A-terms on a few selected flavour observables. The MSSM scenario we consider does not include any sources of flavour- and CP- violation at M_{GUT} other than the CKM matrix. Therefore, flavour off-diagonal entries of the soft terms remain small, as they arise solely from the RGE running.[1]

In the following, we shall illustrate how the flavour observables change when the A-terms grow from 0 to 150% of the value that is necessary for the Yukawa unification $\mathbf{Y}^d(M_{\text{GUT}}) = \mathbf{Y}^{eT}(M_{\text{GUT}})$ to take place. Among the observables calculable with the help of `SUSY_FLAVOR v2.10`, only three turn out to be significantly altered:

$$\mathcal{B}_\gamma \equiv \mathcal{B}(\bar{B} \to X_s\gamma), \quad \overline{\mathcal{B}}_{s\mu} \equiv \mathcal{B}(B_s \to \mu^+\mu^-) \quad \text{and} \quad \overline{\mathcal{B}}_{d\mu} \equiv \mathcal{B}(B_d \to \mu^+\mu^-).$$

[1] `SOFTSUSY 3.3.8` assumes that all the MSSM parameters are real, i.e. it neglects the CP-violating phases. A separate numerical evaluation of the soft term imaginary parts has been performed with the help of `SPheno 3.3.3` [97,104]. No observable impact on CP-violating observables has been found for the MSSM parameter space points discussed in the previous section.

	$m_{\tilde{s}_L}$	$m_{\tilde{s}_R}$	$m_{\tilde{\mu}_L}$	$m_{\tilde{\mu}_R}$	$m_{\tilde{t}_1}$	$m_{\tilde{t}_2}$	$m_{\tilde{b}_1}$	$m_{\tilde{b}_2}$	$m_{\tilde{\tau}_1}$	$m_{\tilde{\tau}_2}$
1	2031.	1856.	1433.	1433.	1328.	1649.	1603.	1652.	1130.	1185.
2	3049.	2958.	2579.	2579.	1542.	2085.	2068.	2154.	1916.	2011.
3	5999.	4944.	3752.	3752.	5596	4933	5620	5698	3937	4180.
4	5700.	4290.	3714.	3714.	4902	4951	4904.	3984.	2658.	2658.

Table 5.3: Masses of selected sfermions (in GeV) corresponding to the points from Tab. 5.1. In the case of the second generation, where the left-right mixing is negligible, mass eigenstates are labeled according to their largest interaction eigenstate component.

	$m_{\tilde{g}}$	$m_{\chi_1^0}$	$m_{\chi_2^0}$	$m_{\chi_3^0}$	$m_{\chi_4^0}$	$m_{\chi_1^\pm}$	$m_{\chi_2^\pm}$	m_{A_0}	μ
1	2350.	453.	865.	2688.	2688.	865.	2689.	5192.	-2698.
2	1858.	350.	670.	1626.	1626.	670.	1628.	2981.	-1626.
3	5719.	1223.	2269.	4529.	4530.	2270.	4531.	5523.	-4521.
4	5545.	1189.	2205.	3690.	3691.	2205.	3692.	6958.	-3686.

Table 5.4: Masses of the gluino, neutralinos, charginos, pseudoscalar A_0 and the value of μ parameter (in GeV) corresponding to the points from Tab. 5.1.

Moreover, the only A-term component they noticeably depend on is A_{33}^{de}. Another important parameter to which these observables are sensitive is $\tan\beta$.

In Fig. 5.3, we show the dependence of $\delta\mathcal{B}_\gamma \equiv (\mathcal{B}_\gamma^{\rm MSSM} - \mathcal{B}_\gamma^{\rm SM})/\mathcal{B}_\gamma^{\rm SM}$ on A_{33}^{de} and $\tan\beta$. For each example listed in Tab. 5.1 (and also for 17 other examples), we have plotted $\delta\mathcal{B}_\gamma$ keeping all the parameters but A_{33}^{de} fixed. As one can see, SUSY contributions in our examples can enhance $\mathcal{B}_\gamma$ by up to 25% with respect to the SM prediction. Moreover, up to 10% relative differences are observed between points with vanishing and maximal A_{33}^{de}. These conclusions are practically insensitive to whether the calculation is performed with the very recently updated SM prediction that was quoted in Eq. (3.14) or rather with the previous one

$$\mathcal{B}_\gamma^{\rm SM,2006} = (3.15 \pm 0.23) \times 10^{-4} \quad [114]. \tag{5.2}$$

The two predictions differ mainly due to an additive correction to the $b \to s\gamma$ amplitude from diagrams with the charm quark loops, which are the same in the SM and MSSM.

Our actual results displayed in Fig. 5.3 were obtained in Ref. [3] with the use of Eq. (5.2). This fact has little effect on the plotted data points, but strongly affects the position of the horizontal lines marking the (unchanged) experimental world average (3.13). The solid horizontal lines corresponds to the central value of this average, while the dashed lines describe the 1σ range that is obtained after adding the experimental and theoretical uncertainties in quadrature. With the new SM result of Eq. (3.14), all the horizontal lines would shift downwards by around 0.07, with the distances among them remaining unchanged. This would move around half of the displayed points outside the 1σ range. However, most of them would remain in the 2σ range. We can thus see that the observed significant variation of $\mathcal{B}_\gamma$ could lead to a possible exclusion of some of our points once the uncertainties get reduced.

	$\frac{A_d}{\widetilde{m}_1}$	$\frac{A_s}{\widetilde{m}_2}$	$\frac{A_b}{\widetilde{m}_3}$
1	-0.0064	0.49	1.26
2	-0.016	0.89	1.01
3	-0.041	1.56	0.38
4	-0.048	1.54	0.18

Table 5.5: Values of the ratios $A^d_{ii}/\widetilde{m}_i$ at the scale M_{SUSY} for the points from Tab. 5.1.

Analogous plots for $\delta\overline{\mathcal{B}}_{s\mu} \equiv (\overline{\mathcal{B}}^{\rm MSSM}_{s\mu} - \overline{\mathcal{B}}^{\rm SM}_{s\mu})/\overline{\mathcal{B}}^{\rm SM}_{s\mu}$ are shown in Fig. 5.4. All our sample results for $\overline{\mathcal{B}}^{\rm MSSM}_{s\mu}$ fall within the 1σ band above the experimental average (3.9), and the branching ratio can be smaller by about 15% compared to the SM prediction (3.10).

As far as $\overline{\mathcal{B}}_{d\mu}$ is concerned, it undergoes an almost identical alteration with respect to the SM. However, it remains in perfect agreement with the present experimental result (3.11) within its large uncertainties. The experimental sensitivity would need to be improved by more than an order of magnitude to distinguish between the SM prediction (3.12) and the corresponding MSSM results for our sample points.

The three considered decays share the crucial property of being sensitive to supersymmetric contributions even if no sources of flavour violation beyond the CKM matrix are present. It follows from the fact that they are all chirally suppressed in the SM.

5.3 Electroweak symmetry breaking

As described in Sec. 3.4, the MSSM contains a large number of scalar fields. In a proper analysis of the electroweak symmetry breaking, one would need to prove that only the neutral Higgs fields acquire non-zero values in the global minimum of the MSSM scalar potential. However, it is well known that there exist large regions in the MSSM parameter space where other, deeper minima arise. At such minima, also sfermions develop non-vanishing VEVs.

In particular, along the direction in the MSSM scalar field space where $|H_1| = |\tilde{s}_L| = |\tilde{s}_R|$, a deeper, CCB minimum arises when $A_s(M_{\rm SUSY})$ is large. Actually, all our examples in Tabs. 5.1-5.2 strongly violate the stability condition [87]

$$\frac{A_{ii}}{Y_{ii}\widetilde{m}_i} < O(1), \tag{5.3}$$

with $\widetilde{m}_i$ defined by Eq. (2.13). Instead, we have $A_s/(Y_s\widetilde{m}_2) \sim 10^2$ at the scale $M_{\rm SUSY}$.

However, the usual Higgs vacuum does not need to be absolutely stable. The standard viability condition is that the its lifetime must be longer than the age of the Universe. According to Ref. [115], such a condition is fulfilled when $A_s/\widetilde{m}_2 < 1.75$. This requirement turns out to be satisfied in all our examples of Yukawa unification. One can verify this by inspecting Tab. 5.5 where the ratios $A^d_{ii}/\widetilde{m}_i$ have been presented for all the three generations.

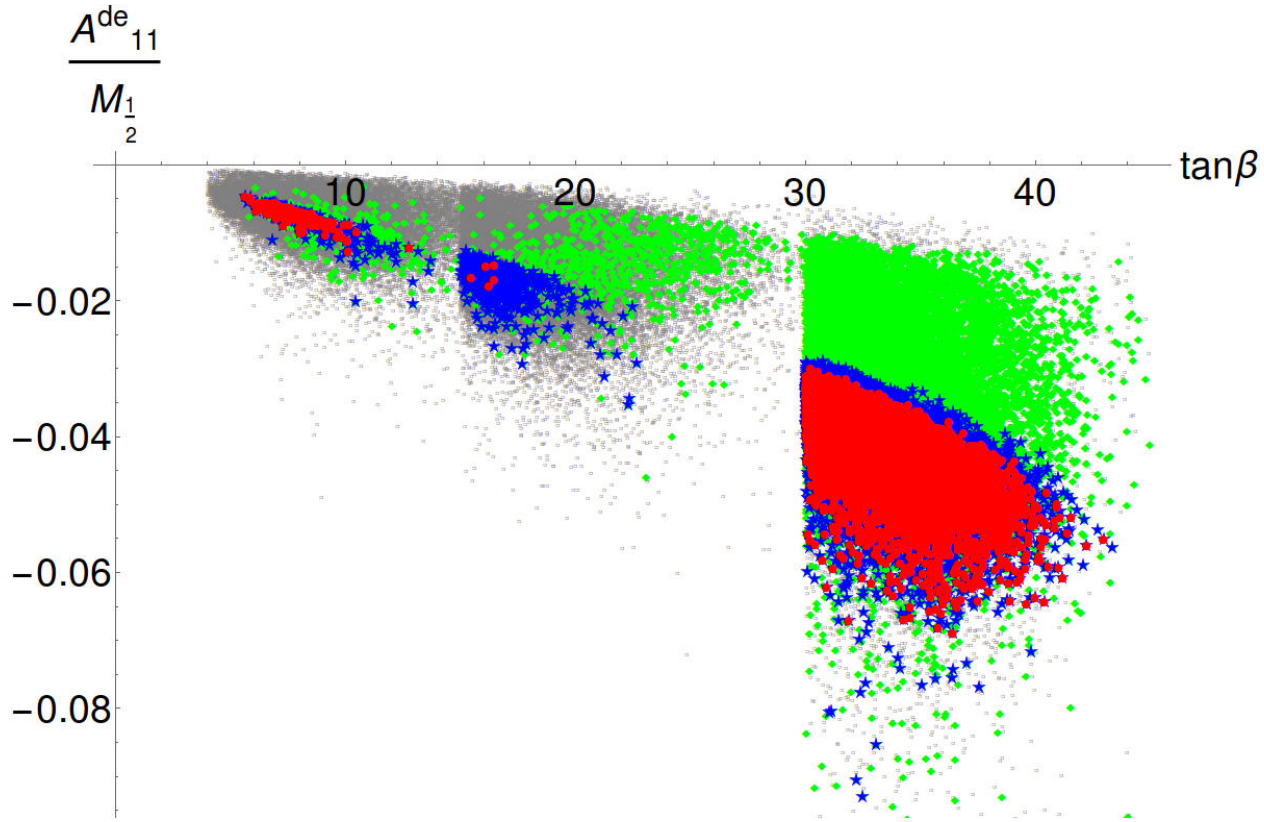

(a)

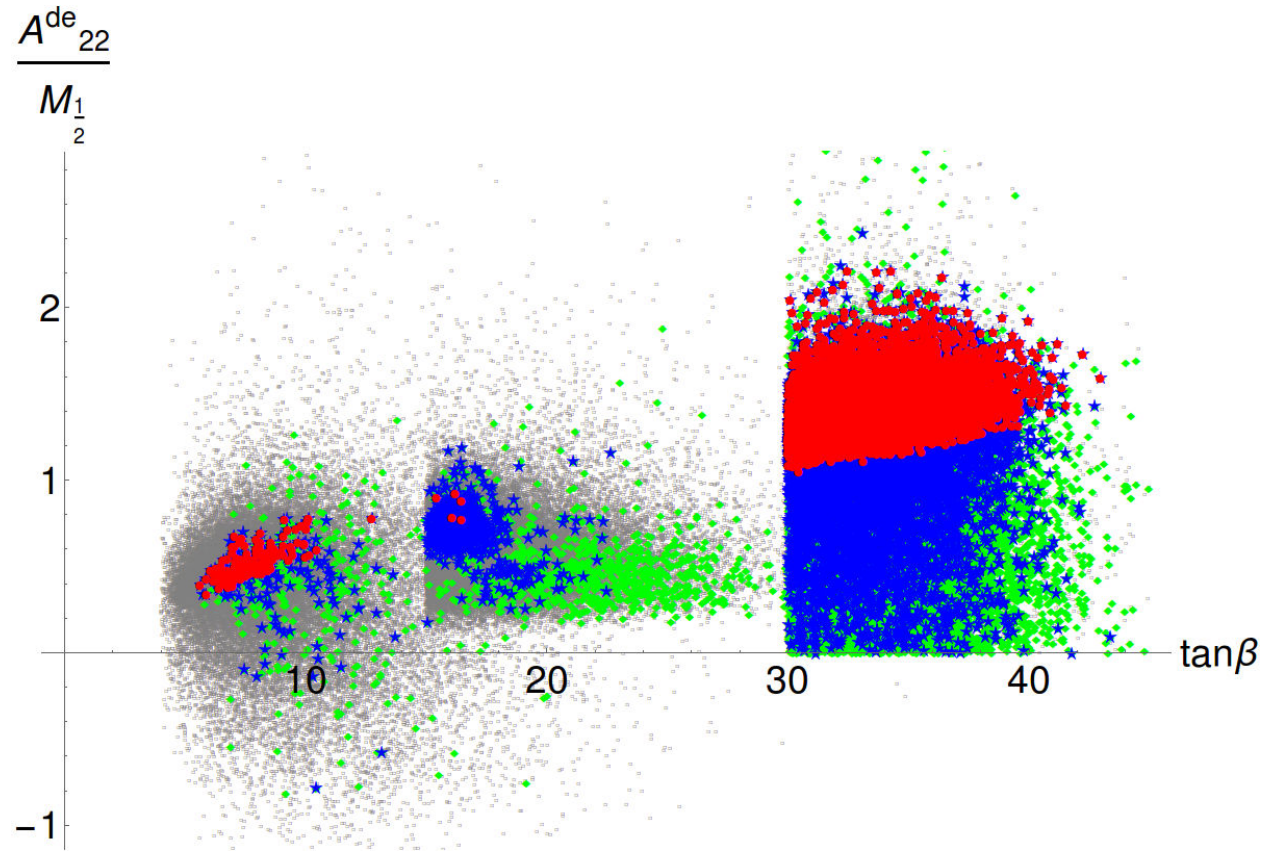

(b)

Figure 5.1: (a): points gathered in three of our MCMC scans (grey), shown in the $\tan\beta \times (A^{de}_{11}/M_{1/2})$ plane. For some of them, the respective Yukawa couplings get unified within a 10% bound and the Higgs boson mass prediction lies in the interval $[122.5, 128.5]$ GeV: green diamonds mark the b–τ unification, blue stars fulfil also the d–e one, while red circles include also the s–μ one (i.e. the full Yukawa matrices get unified). (b): the same data projected onto the $\tan\beta \times (A^{de}_{22}/M_{1/2})$ plane.

For efficiency reasons in covering a broad $\tan\beta$ range, the scans were made in disjoint $\tan\beta$

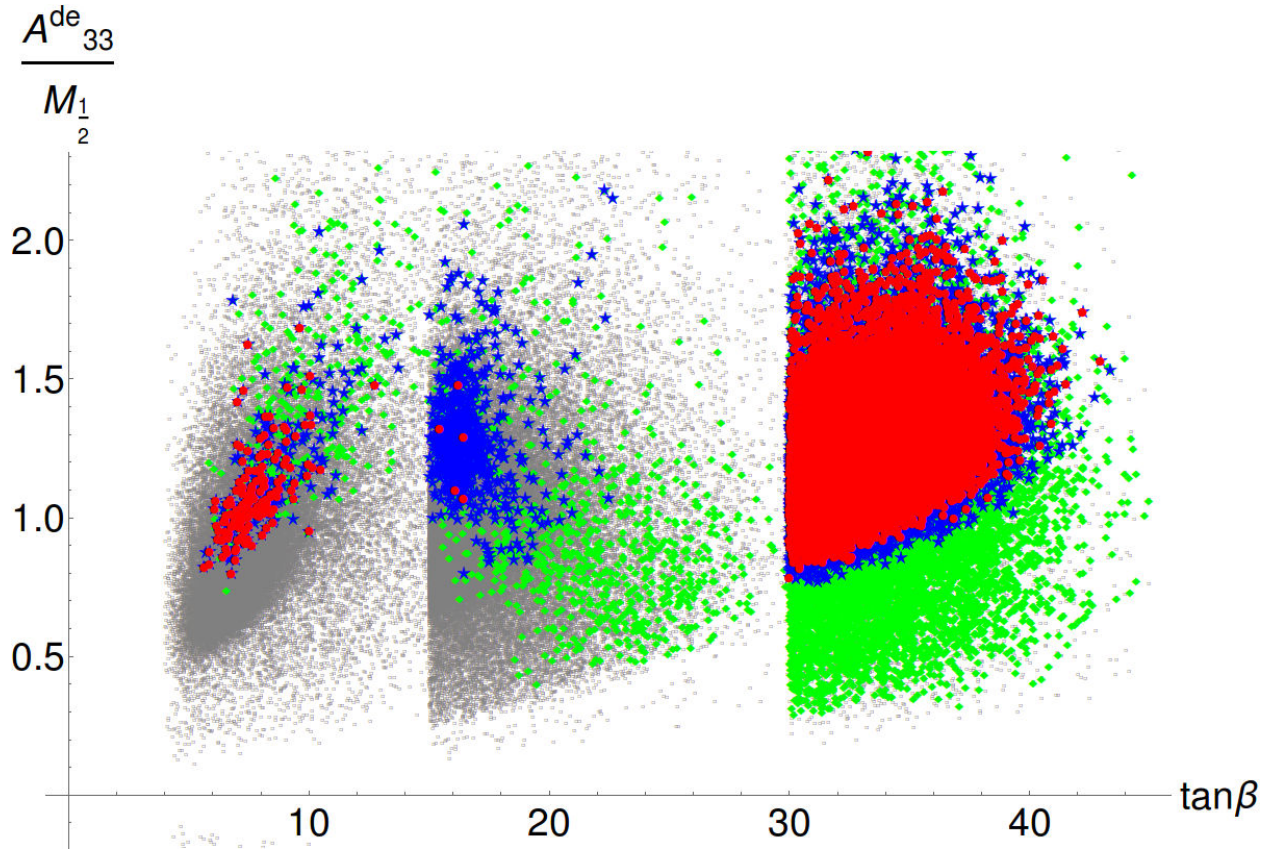

(a)

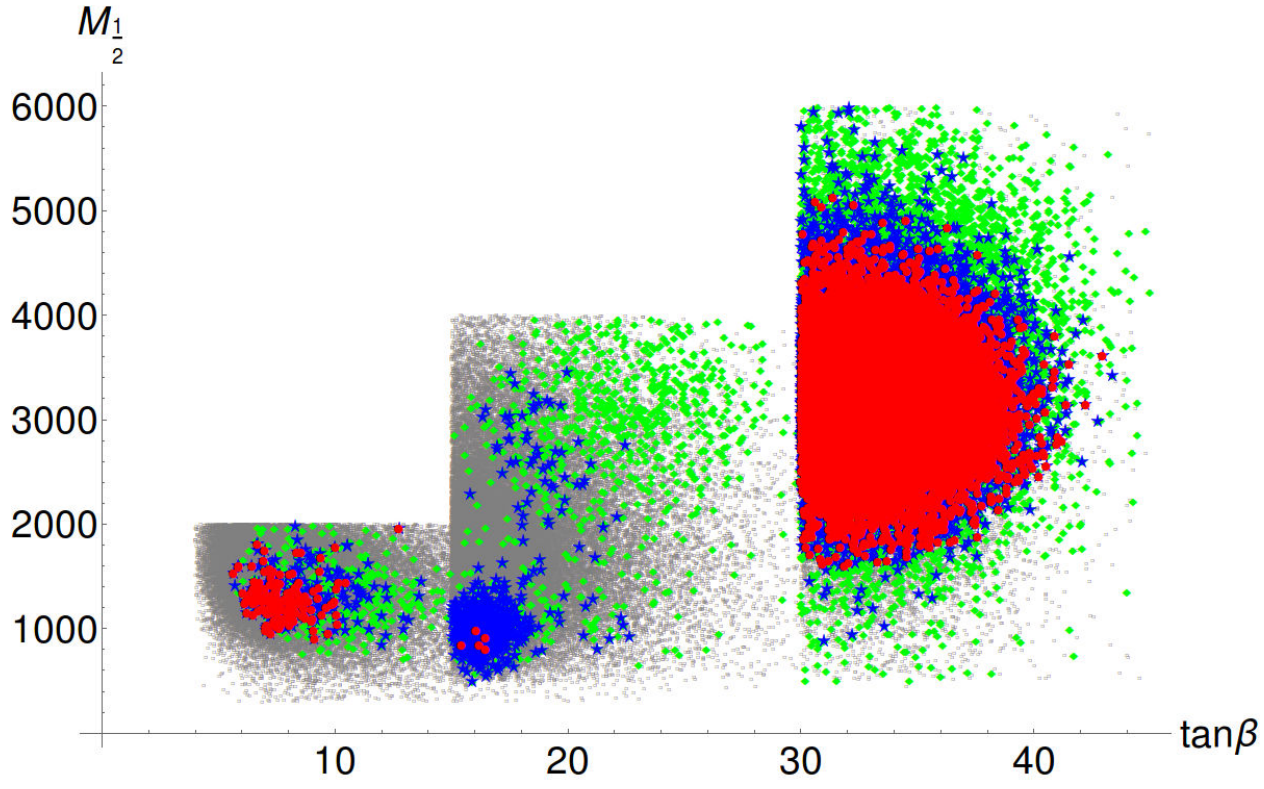

(b)

Figure 5.2: The same data as in Fig. 5.1 projected onto the $\tan\beta \times (A^{de}_{33}/M_{1/2})$ (a) and $\tan\beta \times M_{1/2}$ (b) planes.

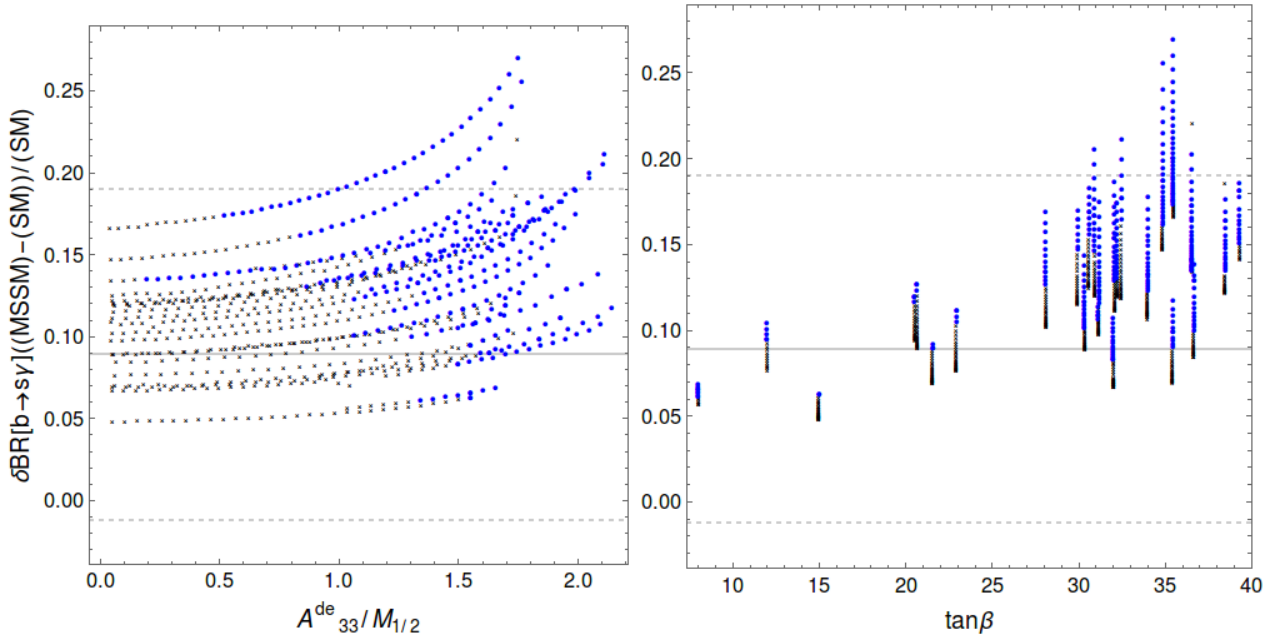

(a) (b)

Figure 5.3: Dependence of $\delta\mathcal{B}_\gamma$ on A_{33}^{de} and $\tan\beta$. Points fulfilling $\mathbf{Y}^d(M_{\rm GUT}) = \mathbf{Y}^{eT}(M_{\rm GUT})$ are marked in blue. The 1σ experimental error band is represented by horizontal lines.

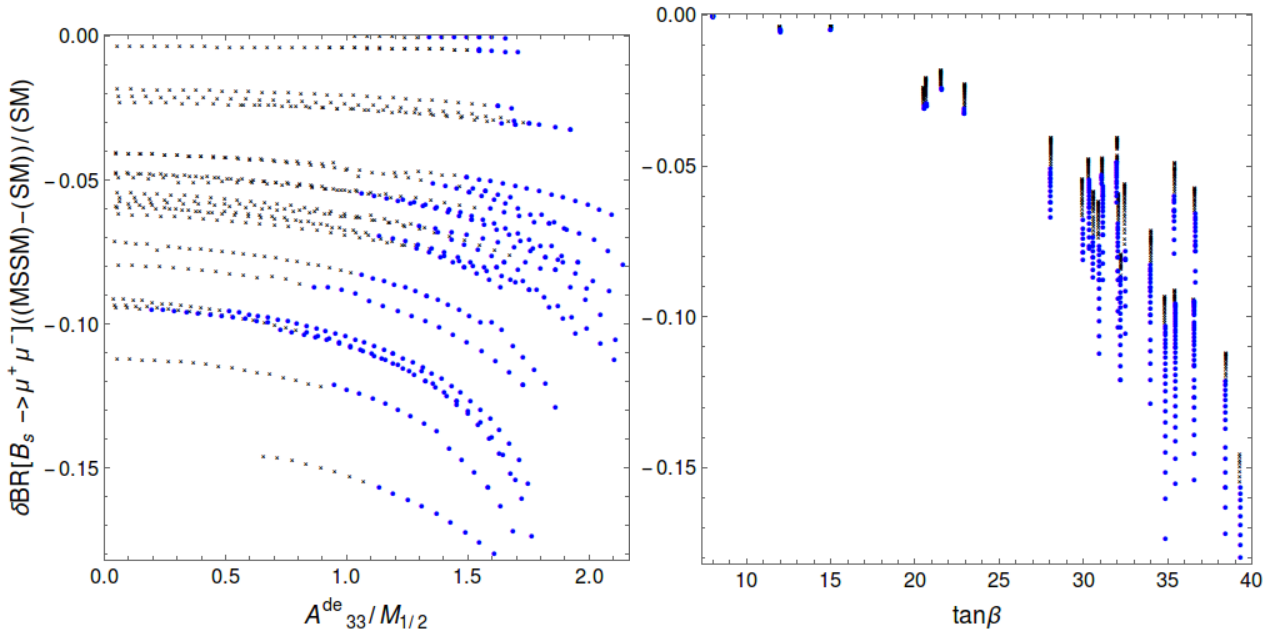

(a) (b)

Figure 5.4: Dependence of $\delta\overline{\mathcal{B}}_{s\mu}$ on A_{33}^{de} and $\tan\beta$. Points fulfilling $\mathbf{Y}^d(M_{\rm GUT}) = \mathbf{Y}^{eT}(M_{\rm GUT})$ are marked in blue. The results for $\delta\overline{\mathcal{B}}_{d\mu}$ are practically identical.

CHAPTER 6

Numerical results for the GFV_{23} scenario

In this chapter, we describe the phenomenological aspects of the GFV_{23} scenario. We do it step by step, describing how the imposed constraints affect the parameter space of the model. We start by presenting the region in which the bottom-tau and strange-muon Yukawa unification is fulfilled. Further, points giving the correct DM relic density are presented (Sec. 6.2.1). Next, it is shown that reproducing the measured Higgs mass and results from flavour physics is not in any tension with the unification condition (Sec. 6.2.2). Finally, we find that having a proper DM candidate means that the GFV_{23} parameter space points with SU(5) Yukawa matrix unification that have been found by our scan turn out to be testable at the LHC with $\sqrt{s} \simeq 14\,\text{TeV}$ (Sec. 6.2.3). In Tab. 6.1, all the experimental constraints discussed in this chapter are collected.

We present the results of our final MCMC scan performed with the software described in Chapter 4. The principal aim of the scan was to verify whether the questionable strange-muon Yukawa coupling unification can be achieved alongside with well tested bottom-tau case when all phenomenological constraints are satisfied. In particular, we focus on fulfilling the flavour physics bounds and the phenomenological patterns that emerge when the observed DM relic density is correctly reproduced. Although deliberately avoiding a CCB scalar potential minimum triggered by the squark fields of the second generation, we did not guide the scan in such a way that the CCB bounds from electroweak vacuum stability on the third family couplings were automatically satisfied. The latter issue, already covered in many other works, is discussed in Sec. 6.2.4. The ranges of input variables defining our search are summarized in Tab. 6.2.

6.1 Regions with the successful bottom-tau and strange-muon unification

The performed scan has returned the MSSM spectrum for 121986 parameter-space points, among which 34758 yield the Yukawa couplings of leptons and down-quarks at M_{GUT} equal within 10% for the second and third generations. Fig. 6.1 presents distributions of the points collected by our scan in the planes ($M_{1/2}$, A^d_{33}) (a), (m_{H_d}/m_{H_u}, $\tan\beta$) (b), and (m^{dl}_{23}/m^{dl}_{33}, m^{dl}_{22}/m^{dl}_{33}) (c). All the points for which the spectrum was returned by `SPheno` are depicted as grey rectangles, whereas those that satisfy the Yukawa unification condition for the third

Measurement	Mean or range	Error [exp., th.]	Reference
$\Omega_\chi h^2$	0.1199	[0.0027, 10%]	[94]
LUX (2013)	See Sec. 3 of [118]	See Sec. 3 of [118]	[96]
m_h (by CMS)	125.7 GeV	[0.4, 3.0] GeV	[119]
$\sin^2\theta_{\rm eff}$	0.23155	[0.00012, 0.00015]	[19]
M_W	80.385 GeV	[0.015, 0.015] GeV	[19]
$\mathcal{B}\left(\overline{B}\to X_s\gamma\right)\times 10^4$	3.43	[0.22, 0.23]	[69]
$\mathcal{B}\left(B_s\to\mu^+\mu^-\right)\times 10^9$	2.8	[0.7, 0.23]	[71]
$\mathcal{B}\left(B_d\to\mu^+\mu^-\right)\times 10^{10}$	3.9	[1.6, 0.2]	[71]
$\Delta M_{B_s}\times 10^{11}$	1.1691 GeV	[0.0014, 0.1580] GeV	[19]
$\Delta M_{B_d}\times 10^{13}$	3.357 GeV	[0.033, 0.340] GeV	[19]
$\Delta M_{B_d}/\Delta M_{B_s}\times 10^2$	2.87	[0.02, 0.14]	[69]
$\sin(2\beta)_{\rm exp}$	0.682	[0.019, 0.003]	[19]
$\mathcal{B}\left(B_u\to\tau\nu\right)\times 10^4$	1.14	[0.27, 0.07]	[19]
$\mathcal{B}(K^+\to\pi^+\nu\bar{\nu})\times 10^{10}$	1.73	[1.15, 0.04]	[19]
$\lvert d_n\rvert\times 10^{26}$	< 2.9 e cm	[–, 30%]	[120]
$\lvert\epsilon_K\rvert\times 10^3$	2.228	[0.011, 0.17]	[19]
$\mathcal{B}\left(\mu^+\to e^+\gamma\right)\times 10^{-13}$	< 5.7	[–,0]	[78]
$\mathcal{B}\left(\mu^+\to e^+e^+e^-\right)\times 10^{-12}$	< 1.0	[–,0]	[116]
$\mathcal{B}\left(\tau^+\to\mu^+\gamma\right)\times 10^{-8}$	< 4.4	[–,0]	[79]
$\mathcal{B}\left(\tau^+\to\mu^+\mu^+\mu^-\right)\times 10^{-8}$	< 2.1	[–,0]	[117]
LHC $\sqrt{s}=8$ TeV	Sec. 6.2.3	Sec. 6.2.3	[121–123]

Table 6.1: Experimental constraints applied in the analysis.

generation at 2σ ($0.9 < Y_b/Y_\tau < 1.1$) as green diamonds. Finally, blue stars correspond to those points for which both heavier generations are unified at 2σ. The latter points constitute around 28% of the points collected in the scan.

Several observations can now be made. First of all, it is known that a satisfactory unification of the third family Yukawa couplings is possible in the MFV $SU(5)$ with universal scalar masses for moderate values of $\tan\beta$. This is confirmed by Fig. 6.1 where green points can easily be found for vanishing flavour-violation in the GUT-scale soft parameters, and for values of m^{dl}_{22}/m^{dl}_{33} close to 1. One can also observe that the values of $M_{1/2}$ are limited for the points with a successful second- and third-family Yukawa unification. The ratio m_{H_d}/m_{H_u} seems unconstrained by the unification requirement, whereas moderate values of $\tan\beta$ are slightly preferred.

Secondly, the scan includes values of A^d_{33} that are large as compared to the superpartner masses. It is of relevance for the minimisation of the scalar potential, and will be discussed in Sec. 6.2.4.

Finally, the blue points, signalling that the strange-muon Yukawa unification has taken place, appear also for almost vanishing values of the soft-mass element m^{dl}_{23}. The scan has collected 999 points (about 0.8% of all points) with $m^{dl}_{23}/m^{dl}_{33} < 0.005$ for which the bottom-tau and strange-muon Yukawa unification takes place within 10%. As already discussed in the context of Eq. (2.11), large and negative values of μ might decisively contribute to the Yukawa unification issue for sizeable values of $\tan\beta$ and relatively light sfermions (as

Parameter	Scanning Range
$M_{1/2}$	[100, 4000] GeV
m_{H_u}	[100, 8000] GeV
m_{H_d}	[100, 8000] GeV
$\tan\beta$	[3, 35]
$\operatorname{sgn}\mu$	-1
A^{de}_{33}	[−5000, 5000] GeV
A^{u}_{33}	[−9000, 9000] GeV
A^{de}_{11}/A^{de}_{33}	[−0.00028, 0.00028]
A^{de}_{22}/A^{de}_{33}	[−0.065, 0.065]
A^{u}_{22}/A^{u}_{33}	[−0.005, 0.005]
$m^{dl}_{ii},\ i=1,2,3$	[100, 7000] GeV
m^{dl}_{23}/m^{dl}_{33}	[0, 1]
$m^{ue}_{ii},\ i=1,2,3$	[100, 7000] GeV

Table 6.2: Ranges of the input SUSY parameters used in the final GFV_{23} scan. The omitted soft SUSY-breaking parameters at the GUT scale have been set to zero, as discussed in Chapter 2.

compared to $\sqrt{|\mu m_{\tilde{g}}|}$). Such a situation corresponds to the blue points in Fig. 6.2.

6.2 Phenomenology of the GFV_{23} scenario

6.2.1 Dark matter

The DM relic density is influenced by multiple parameters of the model. For the GFV scenario it requires a very specific mass spectrum, which leads to interesting phenomenological conclusions.

In Fig. 6.3, we show distributions of points found by our scanning procedure in the planes (m_A, μ) (a), ($m_{\tilde{\chi}^0_1}$, σ_p^{SI}) (b) and ($\tan\beta$, $M_{1/2}$) (c). All the points collected by our scan are drawn as grey stars, while those that satisfy at 3σ the observational bound on the DM relic density appear as brown dots. Blue diamonds correspond to those scenarios for which also the Yukawa coupling unification holds. The green dashed line indicates the 90% C.L. exclusion bound on the σ_p^{SI} based on the 85-day measurement by the LUX collaboration [96]. The purple dashed line is a projection of XENON1T sensitivity [124]. By comparing the panels (a) and (b) of Fig. 6.3, one can see that in the region where Yukawa unification is achieved, the higgsino mass μ is much larger than the LSP mass, which means that the LSP is bino-like. It corresponds to a relatively low spin-independent proton-neutralino cross-section. In other words, the condition of Yukawa coupling unification strongly disfavours purely or partly higgsino-like neutralino as the LSP. This is due to the fact that the μ parameter value associated with this region is quite large in magnitude ($|\mu| \gtrsim 5\,\mathrm{TeV}$) to enhance the μ-dependent contribution in Eq. (2.14) that aids unification of the second family Yukawa couplings. For this reason, only a bino-like neutralino was found by the scan, which is an important phenomenological feature of our GFV Yukawa unification scenario.

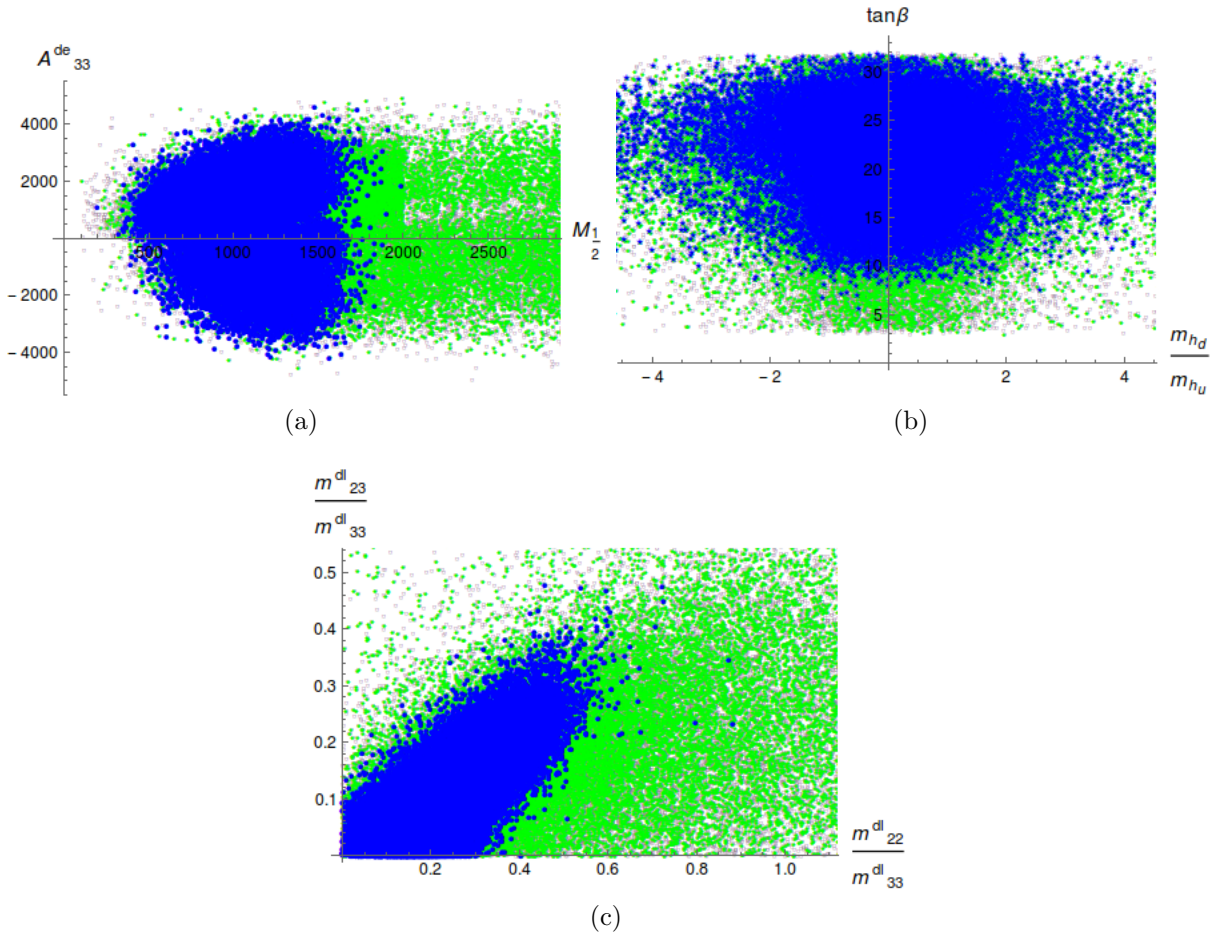

Figure 6.1: Scatter plot of the GFV_{23} points in the planes: (a) ($M_{1/2}$, A^d_{33}), (b) (m_{H_d}/m_{H_u}, $\tan\beta$), (c) (m^{dl}_{23}/m^{dl}_{33}, m^{dl}_{22}/m^{dl}_{33}). Colour code: grey rectangles – all the points for which the spectrum was returned; green diamonds – points satisfying the Yukawa unification condition for the third generation at 2σ; blue stars – points for which both the heavier generations are unified at 2σ.

A unique mechanism that makes the effective increase of the DM annihilation cross-section possible in this case is the neutralino co-annihilation with the lightest sneutrino. The pseudoscalar is too heavy to allow a resonant $\tilde{\chi}^0_1$ annihilation (as can be read from the panel (a) of Fig. 6.3), while the masses of coloured sfermions in the GUT-constrained unification scenarios are always larger than those of the sleptons. It is due to a renormalisation effect, as their RGE running is strongly driven by the gluino. Such a property of the spectrum, however, has important consequences for experimental testability. In Fig. 6.3(b) the dashed lines indicate the present reach of LUX and the expected sensitivity for XENON1T experiment. The region favoured by the relic density constraint in the Yukawa unification scenario remains far beyond the reach for any of them. On the other hand, a light bino-like $\tilde{\chi}^0_1$ and a sneutrino having a similar mass can be tested by the LHC 14 TeV, as will be discussed in Sec. 6.2.3.

The value of $\tan\beta$ favoured by the DM measurement is also strongly limited, $\tan\beta \in [4, 15]$. This is a characteristic feature of the co-annihilation mechanism, as the value of $\tan\beta$ influences the sneutrino mass. It becomes somewhat heavier for larger $\tan\beta$, and the

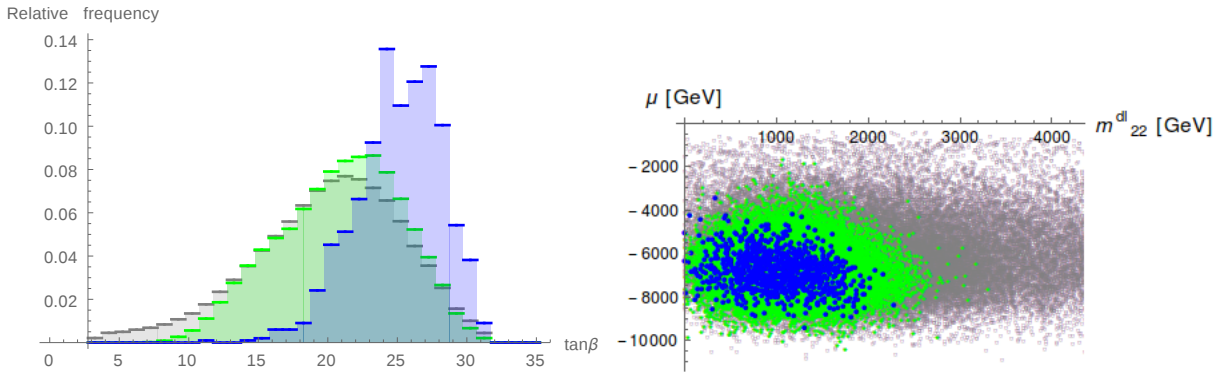

(a) (b)

Figure 6.2: (a) Relative frequencies of $\tan\beta$ values among the points of our GFV_{23} scan; (b) Scatter plot showing these points in the plane (m^{dl}_{22},μ). Colour code: grey – all the points for which a mass spectrum was returned; green – points with the bottom-tau and strange-muon Yukawa unification; blue – points that in addition are characterised by $m^{dl}_{23}/m^{dl}_{33} < 0.005$.

efficiency of neutralino-sneutrino co-annihilation drops. What is interesting, however, is that such a limited value of $\tan\beta$ has important consequences for flavour physics observables, as will be discussed in Sec. 6.2.2.

Fig. 6.4 is devoted to illustrating the dependence of our results on the sfermion-mixing parameter m^{dl}_{23}/m^{dl}_{33}. It can be seen in the left panel of this plot that the DM and Yukawa unification requirements restrict this parameter to remain below around 0.2 for most of the points. As mentioned at the end of the previous section, the GFV_{23} Yukawa unification constraint alone could be satisfied also for very small m^{dl}_{23}/m^{dl}_{33} (smaller than 0.005) thanks to the flavour-diagonal $Y_s\mu\tan\beta$ term in Eq. (2.11). However, the DM constraints reject all but four such points. The corresponding distributions in the $(m^{dl}_{22}/m^{dl}_{33})$ plane are shown in the right panel of Fig. 6.4.

6.2.2 Higgs, flavour and electroweak observables

In Fig. 6.5, we present distributions of points for several relevant observables: $(m_h,\, M_{\rm SUSY})$ (a), $(\mathcal{B}\left(\overline{B}\to X_s\gamma\right),\, \mathcal{B}\left(B_s\to\mu^+\mu^-\right))$ (b) and $(\epsilon_K,\, \Delta M_{B_d}/\Delta M_{B_s})$ (c). Grey stars indicate all the points for which it is possible to achieve the Yukawa coupling unification for the second and third generations. Points that satisfy the relic density constraint at 3σ are shown as blue dots, while red diamonds correspond to those cases where additionally all the other constraints listed in Table 6.1 are met at 3σ (except for the LHC bounds from direct SUSY searches that will be discussed in Sec. 6.2.3).

The Higgs boson mass dependence on the GFV parameters has been discussed in Ref. [54–57]. It was shown that while m_h can be enhanced by non-zero $(2,3)$ entries of the trilinear down-squark matrix, its dependence on the off-diagonal soft-mass elements is negligible. Therefore, in the scenario considered in this study, the only parameters relevant for the Higgs physics remain A^u_{33} and $M_{\rm SUSY}$. That is confirmed by the panel (a) of Fig. 6.5 where no tension between the correct value of the Higgs boson mass and the Yukawa unification constraint (driven by the large GFV parameter m^{dl}_{23}) is observed. The EW observables are not affected either, because the dominant GFV contribution to M_W and $\sin^2\theta_{\rm eff}$ would be

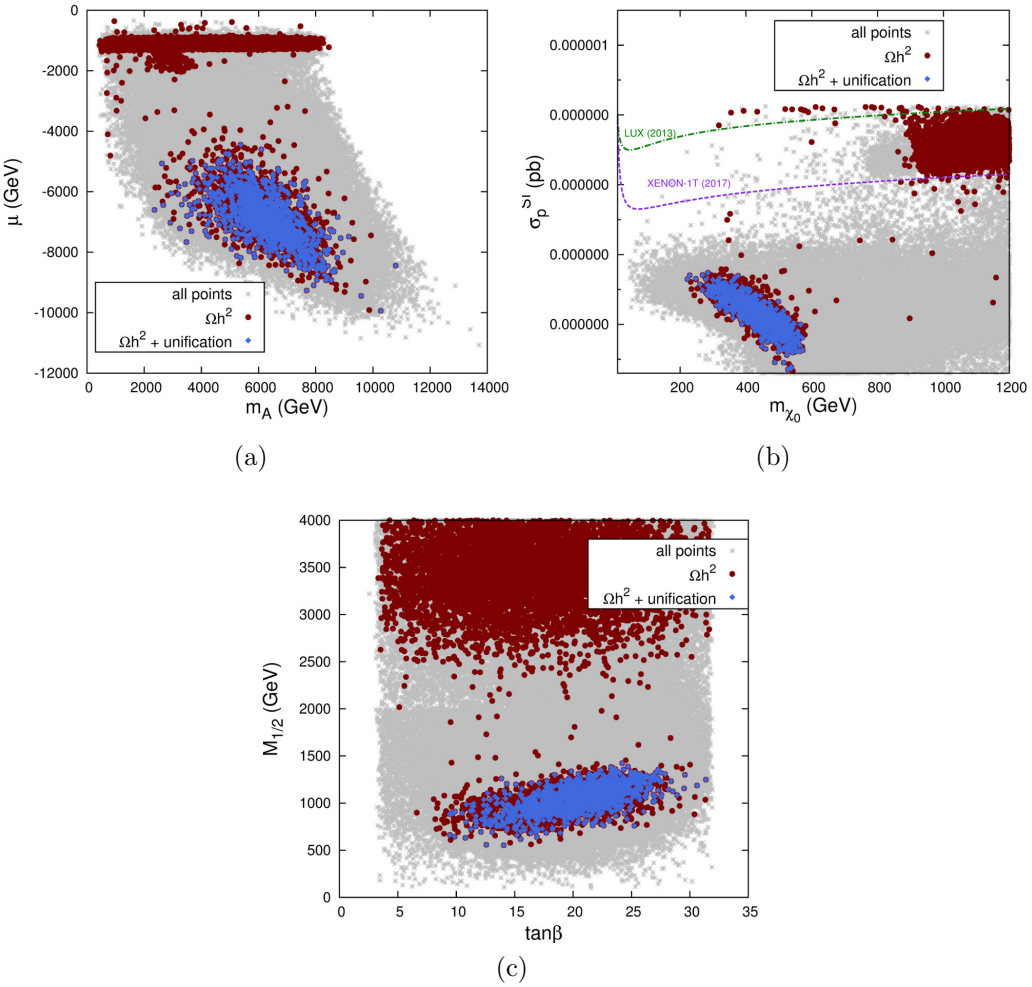

(a) (b) (c)

Figure 6.3: Scatter plot of the GFV_{23} points in the planes $(m_A,\ \mu)$ (a), $(m_{\tilde{\chi}_1^0},\ \sigma_p^{\rm SI})$ (b) and $(\tan\beta,\ M_{1/2})$ (c). Grey stars: all the points collected by the scan; brown dots: points satisfying the DM relic density constraint at 3σ; blue diamonds: points for which additionally the Yukawa unification holds. The meaning of dashed lines is described in the text.

controlled by the element m_{23}^{ue} [53].

On the other hand, the presence of sizeable off-diagonal entries in the squark mass matrices might lead to disastrously high SUSY contributions to FCNC processes. It turns out, however, that in the considered scenario most of the flavour constraints are quite easily satisfied for the points that have survived imposing the DM experimental limit. This is mainly due to the fact that the coloured sfermions are relatively heavy, while $\tan\beta$ needs to be low in our setup, in order to allow an efficient neutralino-sneutrino co-annihilation, as discussed in Sec.6.2.1. In consequence, SUSY contributions to the FCNC processes are suppressed.

A potential threat to the GFV scenario is posed by the LFV observables that severely constrain any non-zero flavour mixing of sleptons [125]. When m_{23}^{dl} is the only non-zero flavour-violating soft term at $M_{\rm GUT}$, the current constraints on the relevant processes are still satisfied without a need to tune any parameters, as can be seen in Fig. 6.6.

In summary, the flavour observables can easily be accommodated into the GFV_{23} scenario, and no tension with either the bottom-tau or strange-muon Yukawa unification is noticed.

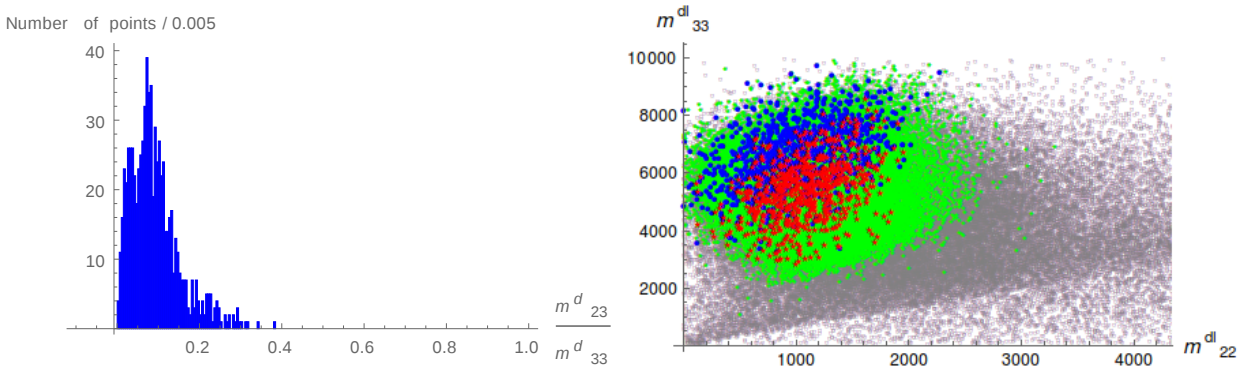

(a) (b)

Figure 6.4: Characteristics of points satisfying the DM relic density constraint in the GFV_{23} scenario: (a) Histogram showing the distribution (as a function m^{dl}_{23}/m^{dl}_{33}) of points that satisfy the Yukawa unification and the DM constraints. (b) Scatter plot in the plane (m^{dl}_{22},m^{dl}_{33}). Grey rectangles – all the points for which the MSSM spectrum was returned; green diamonds – points satisfying the bottom-tau and strange-muon Yukawa unification; red dots – points that fit (in addition) the observed DM relic density; blue stars – those of the Yukawa-unified (green) points that satisfy $m^{d}_{23}/m^{d}_{33} < 0.005$.

6.2.3 LHC direct SUSY searches

All the points from our scan that fulfil the bottom-tau and strange-muon Yukawa unification requirement and satisfy the experimental constraints from Table 6.1 share the same pattern of the light part of the spectrum. Three examples are shown in Fig. 6.7. The Next-to-Lightest SUSY particle (NLSP) is the lightest sneutrino, while one charged slepton, neutralino $\tilde{\chi}^0_2$ and chargino $\tilde{\chi}^{\pm}_1$ are slightly heavier. The presence of light sleptons in the spectrum is very important, as it leads to a characteristic 3-lepton signature at the LHC. The next particle on the mass ladder is the lightest down-type squark which is followed by the gluino. All the other coloured particles, the remaining sleptons and heavy Higgses are much heavier and effectively decoupled.

The strongest limit on the gluino mass comes from the ATLAS no-lepton, 2-6 jets plus Missing Transverse Energy (MET) inclusive search [122]. It provides a stringent 95% C.L. exclusion bound $m_{\tilde{g}} \gtrsim 1400\,\text{GeV}$ when the neutralino LSP is lighter than 300 GeV. The strongest bound on the lightest sbottom mass comes from the CMS no-lepton, 2 jets and MET search [121], while in the electroweakino sector the most stringent experimental exclusion limits are obtained using the 3-lepton plus MET CMS search [123].

However, one needs to keep in mind that the bounds provided by the experimental collaborations are interpreted in the Simplified Model Scenarios (SMS) that make strong assumptions about the hierarchy of the spectrum and the decay branching ratios. Usually it is assumed that there is only one light SUSY particle apart from the neutralino LSP, and only one decay channel of the NLSP with the branching ratio set to 100% is considered. In a more general case, however, the presence of other light particles in the spectrum may alter the decay chain, and the assumption concerning the branching ratio may not hold either. In such a case, the exclusion limits for the SMS should be treated with care, and the actual limits are expected to be weaker.

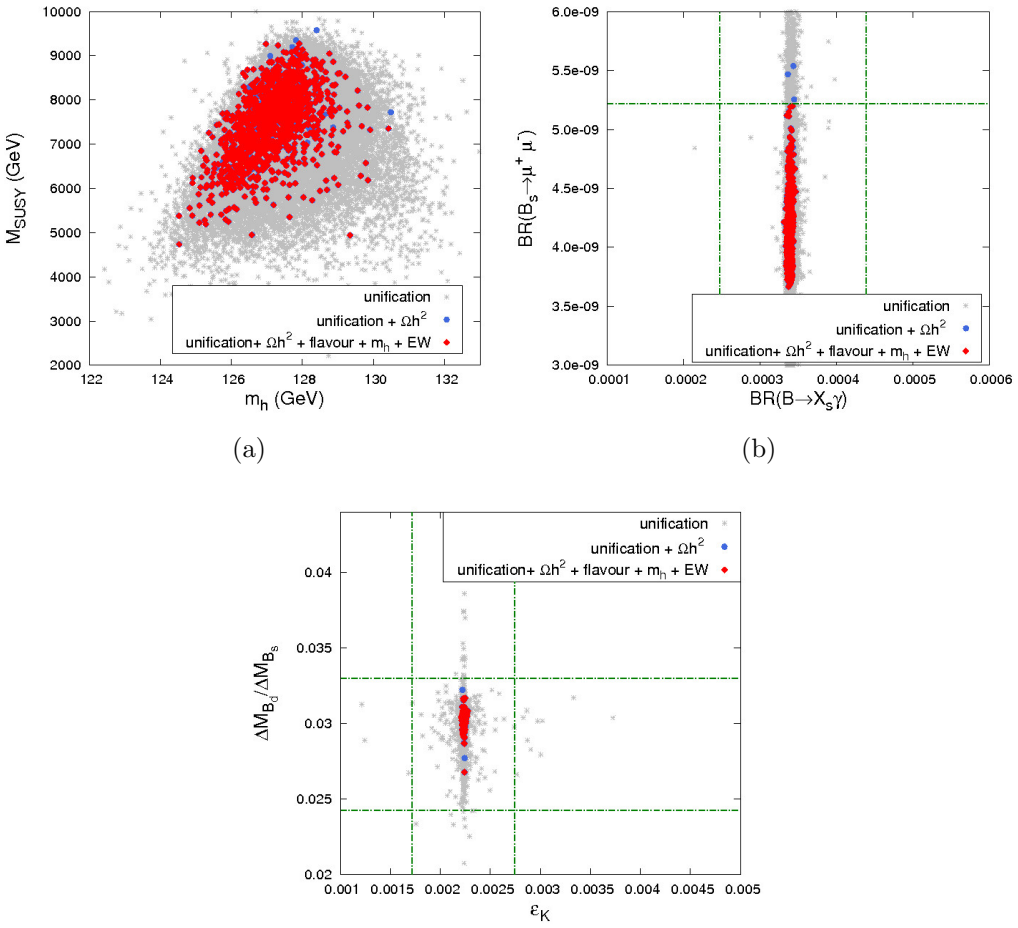

(a) (b)

(c)

Figure 6.5: Scatter plot of the GFV_{23} points in the planes (m_h, $M_{\rm SUSY}$) (a), ($\mathcal{B}\left(\overline{B} \to X_s\gamma\right)$, $\mathcal{B}\left(B_s \to \mu^+\mu^-\right)$) (b), and ($\epsilon_K$, $\Delta M_{B_d}/\Delta M_{B_s}$) (c). Grey stars: all the points that allow the Yukawa coupling unification; blue dots: points satisfying additionally the DM relic density constraint at 3σ; red diamonds: points with good Yukawa coupling unification and all the constraints listed in Table 6.1 satisfied at 3σ (except the LHC). Dashed lines correspond to 3σ experimental limits on the corresponding observables.

In our analysis [4], we have used the experimental exclusion bound for the gluino mass [122] at face value because this search is inclusive, and therefore tests any gluino-driven multijet signature, irrespectively of a particular decay chain. We have also decided to use a direct 95% C.L. limit from the CMS sbottom production search [121]. For the SMS T2bb, it reads $m_{\tilde{b}_1} \gtrsim 700\,\text{GeV}$ for $m_{\tilde{\chi}_1^0} \simeq 150\,\text{GeV}$, and $m_{\tilde{b}_1} \gtrsim 640\,\text{GeV}$ for $m_{\tilde{\chi}_1^0} \simeq 250\,\text{GeV}$. In our scenario, the sbottom decay corresponds exactly to the SMS T2bb, i.e. $\mathcal{B}(\tilde{b} \to b\tilde{\chi}_1^0) = 100\%$. We neglect here a possibility that the actual limit can be weakened due to a significant mixing between the sbottoms and other down-type squarks, and we leave a detailed analysis of the GFV effects in such a case for future studies. We will see, however, that this simplifying assumption is justified by the fact that the limits derived from Ref. [121] are not the dominant ones.

On the other hand, interpretation of the CMS 3-lepton search strongly depends on hierarchy in the considered spectrum, as well as on actual branching ratios for neutralino and chargino decays. Therefore, in order to correctly quantify the effect of this search in the

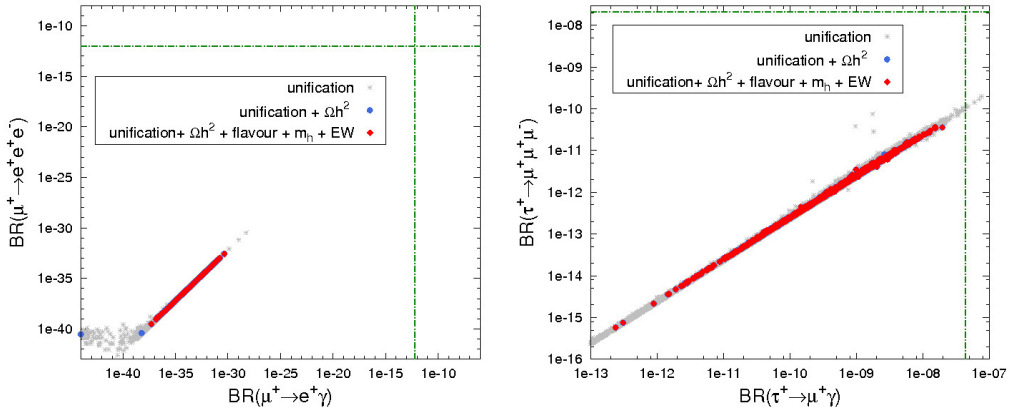

(a) (b)

Figure 6.6: Scatter plot of the GFV_{23} points in the planes $(\mathcal{B}(\mu^+ \to e^+\gamma), \mathcal{B}(\mu^+ \to e^+e^+e^-))$ (a), and $(\mathcal{B}(\tau^+ \to \mu^+\gamma), \mathcal{B}(\tau^+ \to \mu^+\mu^+\mu^-))$ (b). grey stars: all the points that allow the Yukawa coupling unification; blue dots: points satisfying additionally the DM relic density constraint at 3σ; red diamonds: points with good Yukawa coupling unification and all the constraints listed in Table 6.1 satisfied at 3σ (except the LHC). Dashed lines correspond to the upper experimental limits on the corresponding observables.

GFV scenario, a full reinterpretation of the experimental analysis was performed, using the tools developed first in Ref. [**?**], and modified to recast the limits from SMS in Ref. [126]. For the purpose of the present study [4] the previously implemented [127] CMS 3-lepton search was updated to include the full set of data with integrated luminosity of 19.5/fb [123].

In Fig. 6.8, we present a distribution of the model points in the $(m_{\tilde{d}_1}, m_{\tilde{\chi}_1^0})$ plane (a), and in the $(m_{\tilde{d}_1}, m_{\tilde{g}})$ plane (b). All the points for which the Yukawa coupling unification is possible are shown as grey stars, and those that additionally satisfy at 3σ the experimental constraints listed in Table 6.1 (except the LHC) as dark green dots. Finally, red diamonds depict the points that survive (at 3σ) the CMS 3-lepton plus MET search. Dashed lines correspond to the 95% C.L. exclusion bounds from the CMS and ATLAS multijet searches described above, and should be interpreted as lower bounds on the sbottom and gluino masses. One can see that already at the LHC $\sqrt{s} = 8\,\text{TeV}$, the 3-lepton search provides a very strong constraint on the Yukawa unification scenario, much stronger than the limits from Refs. [121] and [122]. It is due to the presence of one generation of light sleptons in the spectrum, although the efficiency of the search is weakened with respect to the corresponding SMS, for which the interpretations are provided in the experimental analysis [123]. Such spectra, however, will be fully tested by the LHC $\sqrt{s} = 14\,\text{TeV}$.

6.2.4 Electroweak symmetry breaking

As already mentioned at the beginning of this chapter, our GFV_{23} scan allows significant values of $A_{33}^{de}/M_{1/2}$ at M_{GUT}. As in the case of the large A-term scenario, some of the points might therefore be characterised by a global CCB minimum of the MSSM scalar potential. Indeed, a large value of $A_{33}^{d}(M_{SUSY})$ makes tuning the threshold corrections to Yukawa couplings easier, and most of the points that are consistent with bottom-tau and

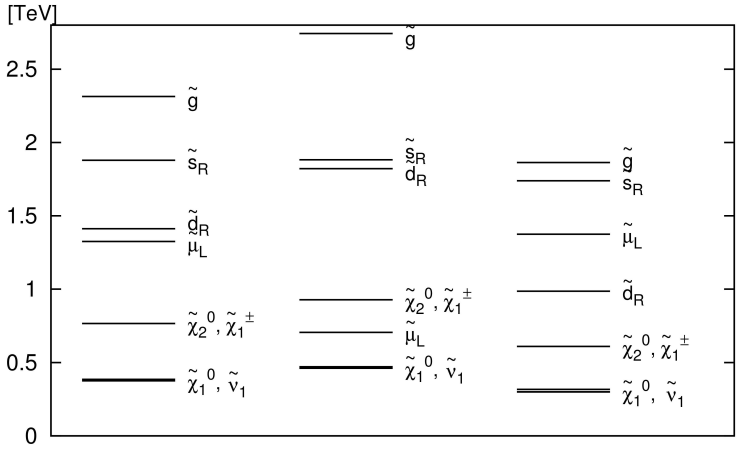

Figure 6.7: Examples of spectra characteristic for the GFV_{23} Yukawa unification scenario.

strange-muon Yukawa coupling unification show $A^d_{33}/(Y^d_{33}\widetilde{m}_3) \sim \mathcal{O}(1)$ at the scale M_{SUSY}, with $\widetilde{m}_i$ defined in Eq. (2.13). For some points however, this ratio is close to zero, as can be seen in Fig. 6.9.

Therefore, we do not see it necessary that the GFV_{23} scenario leads to a metastable vacuum, as the relevant factor $A^d_{33}/(Y^d_{33}\widetilde{m}_3)$ at M_{SUSY} can be fitted to lie an order of magnitude below the coarse bound 5.3. However, this is only a very weak statement, and a more detailed numerical analysis and new scans will be necessary in the future to investigate this issue properly, with inclusion of at least the (already complicated) tree-level stability bounds [87].

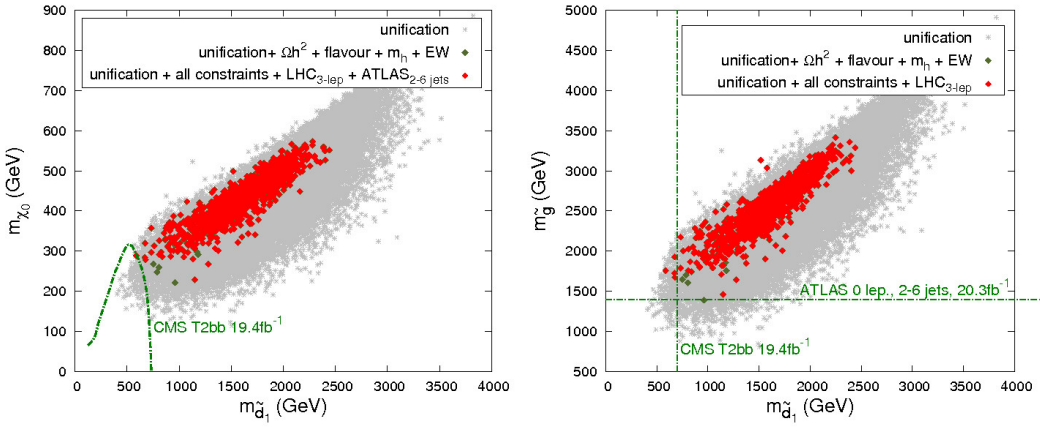
unification
unification+ Ωh² + flavour + m_h + EW
unification + all constraints + LHC3-lep + ATLAS2-6 jets
CMS T2bb 19.4fb-1
m_χ0 (GeV)
m_d̃1 (GeV)
unification
unification+ Ωh² + flavour + m_h + EW
unification + all constraints + LHC3-lep
ATLAS 0 lep., 2-6 jets, 20.3fb-1
CMS T2bb 19.4fb-1
m_g̃ (GeV)
m_d̃1 (GeV)

(a) (b)

Figure 6.8: Scatter plot of the GFV_{23} points in the planes $(m_{\tilde{d}_1}, m_{\tilde{\chi}_1^0})$ (a), and $(m_{\tilde{d}_1}, m_{\tilde{g}})$ (b). grey stars: all the points that allow the Yukawa coupling unification; dark green dots: points with good Yukawa coupling unification and all the constraints listed in Table 6.1 (except the LHC) satisfied at 3σ; red diamonds: points additionally surviving the CMS 3-lepton search at 3σ. Dashed lines correspond to 95% C.L. limits provided by other LHC SUSY searches discussed in the text.

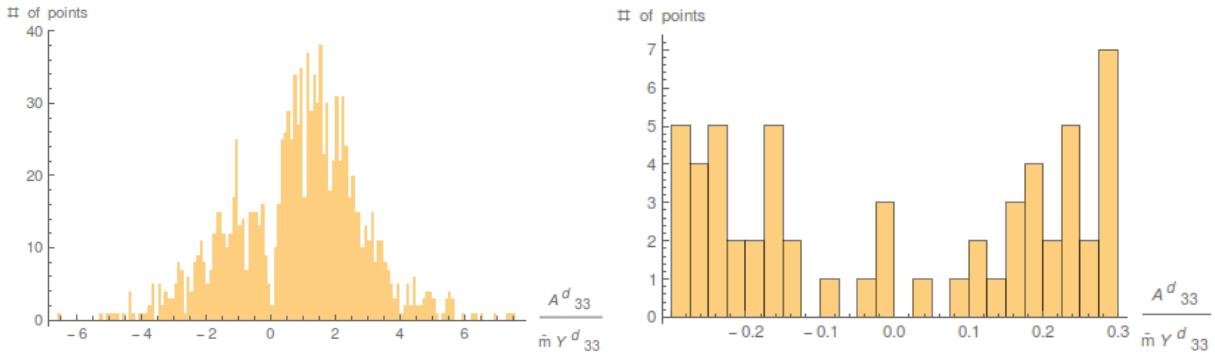

(a) (b)

Figure 6.9: Histograms of points gathered by the GFV_{23} scan as a function of $A^d_{33}/(Y^d_{33}\widetilde{m}_3)$ at the scale M_{SUSY}: (a) all the points gathered by the scan; (b) enlarged vicinity of zero.

CHAPTER 7

Numerical results of the GFV_{123} scenario

In this chapter, we investigate the full 3×3 Yukawa matrix $SU(5)$ unification within the GFV MSSM. We show the numerical results obtained within the GFV_{123} scenario that was introduced in Chapter 2. The scans have returned regions consistent with the unification of lepton and down-type quark Yukawa couplings of all the families, and fulfilling all the imposed experimental constraints except those coming from the LFV observables.

7.1 Regions with the SU(5) Yukawa matrix unification

To find regions consistent with the Yukawa matrix unification, we perform a scan in the parameter space of the GFV_{123} scenario within the bounds presented in Table 7.1.

In Fig. 7.1, we present distributions of the points we collected in our scanning procedure in the planes (m^{dl}_{13}/m^{dl}_{33}, m^{dl}_{12}/m^{dl}_{33}) (a) and (m^{dl}_{23}/m^{dl}_{33}, m^{dl}_{13}/m^{dl}_{33}) (b). All the points that satisfy the Yukawa unification condition for the third generation at 2σ ($0.9 < Y_b/Y_\tau < 1.1$) are depicted as grey stars (they account for 49% of all the points), while those that additionally fulfil 2σ unification of the first family as green diamonds (29% of all the points). Finally, orange dots correspond to those points for which all three generations are unified at 2σ (1.7% of all the points collected by the scan). In Fig. 7.2, similar distributions are shown for the flavour-violating entries of the trilinear down-sector matrix, in the planes corresponding to (A^{de}_{12}/A^{de}_{33}, A^{de}_{21}/A^{de}_{33}) (a), (A^{de}_{13}/A^{de}_{33}, A^{de}_{31}/A^{de}_{33}) (b), and (A^{de}_{23}/A^{de}_{33}, A^{de}_{32}/A^{de}_{33}) (c).

Exactly as in the case of the GFV_{23} scenario, both Fig. 7.1 and Fig. 7.2 confirm, that a satisfactory unification of the third family Yukawa couplings can be easily achieved in the Minimal Flavour Violating $SU(5)$ for moderate values of $\tan\beta$.

The functional form of the threshold correction in Eq. (2.14) might suggest that non-zero soft-mass elements m^{dl}_{23} and m^{dl}_{13} together with the RG-generated $(m^2_{\tilde{q}})_{23}$ and $(m^2_{\tilde{q}})_{13}$ are sufficient to allow the Yukawa unification in both the second and first family cases. Such a simplistic picture, however, is not true, as can be seen from the panel (a) of Fig. 7.1 where large m^{dl}_{12} is clearly favoured. To understand what happens, let us note that the GFV corrections $(\Sigma^d_{22})^{\tilde{g}}$ and $(\Sigma^d_{11})^{\tilde{g}}$ (obtained from Eq. (2.14) by replacing indices "2" with "1") are determined by overlapping sets of parameters, in particular $M_{1/2}$ and A^{de}_{33}. On the other hand, sizes of those corrections, as required by the Yukawa coupling unification, differ by two

Parameter	Scanning Range
$M_{1/2}$	[100, 4000] GeV
m_{H_u}	[100, 8000] GeV
m_{H_d}	[100, 8000] GeV
$\tan\beta$	[3, 45]
$\mathrm{sgn}\,\mu$	-1
A^{de}_{33}	[0, 5000] GeV
A^{u}_{33}	[−9000, 9000] GeV
A^{de}_{11}/A^{de}_{33}	[−0.00028, 0.00028]
A^{de}_{22}/A^{de}_{33}	[−0.065, 0.065]
A^{u}_{22}/A^{u}_{33}	[−0.005, 0.005]
$A^{de}_{ij}/A^{de}_{33},\ i \neq j$	[−0.5, 0.5]
$m^{dl}_{ii},\ i = 1,2,3$	[100, 7000] GeV
m^{dl}_{23}/m^{dl}_{33}	[0, 1]
m^{dl}_{13}/m^{dl}_{33}	[0, 1]
m^{dl}_{12}/m^{dl}_{33}	[0, 1]
$m^{ue}_{ii},\ i = 1,2,3$	[100, 7000] GeV

Table 7.1: Ranges of the input SUSY parameters used in our *initial* GFV_{123} scan. The omitted soft SUSY-breaking parameters at the GUT scale (A^u_{11} as well as A^u_{ij} and m^{ue}_{ij} for $i \neq j$) have been set to zero.

orders of magnitude. Let us now assume that $(\Sigma^d_{11})^{\tilde{g}}$ is fixed by the unification condition for the first family. Thus $M_{1/2}$ and A^{de}_{33}, already constrained by unification of the third family, are even more limited. With such a choice of parameters, however, the correction $(\Sigma^d_{22})^{\tilde{g}}$ is still too small to allow unification of the second family, and needs to be further enhanced by another contribution. Such a contribution comes from a diagram like the one shown in Fig. 2.2, but with the trilinear term A^{de}_{21} in the vertex, and m^{dl}_{12} mixing in the right-handed sector. However, a similar diagram also exists for the first family, and the corresponding contribution should be added to the one driven by m^{dl}_{13}. That explains why all the five parameters m^{dl}_{12}, m^{dl}_{13}, m^{dl}_{23}, A^{de}_{12} and A^{de}_{21} must be adjusted simultaneously. Note also that $A^{de}_{12/21}$ can be kept relatively low, as this contribution is always enhanced by a large value of m^{dl}_{12}.

Flavour-violating parameters are not the only ones constrained by the Yukawa unification condition. In Fig. 7.3, we present distributions of points in the planes ($M_{1/2}$, A^{de}_{33}) (a), (m_{H_d}/m_{H_u}, $\tan\beta$) (b), and (m^{dl}_{11}/m^{dl}_{22}, m^{dl}_{11}/m^{dl}_{33}) (c). The colour code is the same as in Fig. 7.1. One can observe that values of both $M_{1/2}$ and A^d_{33} need to be very limited in order to facilitate unification in the first and second family cases, as they directly enter Eq. (2.14). The ratio m_{H_d}/m_{H_u} in the range $[0, 2]$ allows the unification of the second family for larger values of $\tan\beta$, namely $\tan\beta \in [15, 25]$. Finally, large mass splittings between the diagonal entries of the down-squark mass matrix are disfavoured because they would lead to a strong suppression of SUSY threshold corrections, as can be deduced from Eq. (2.14).

We conclude this section with summarising the allowed ranges of the non-zero GFV parameters that characterise the $SU(5)$ GUT scenario with the full Yukawa coupling unifi-

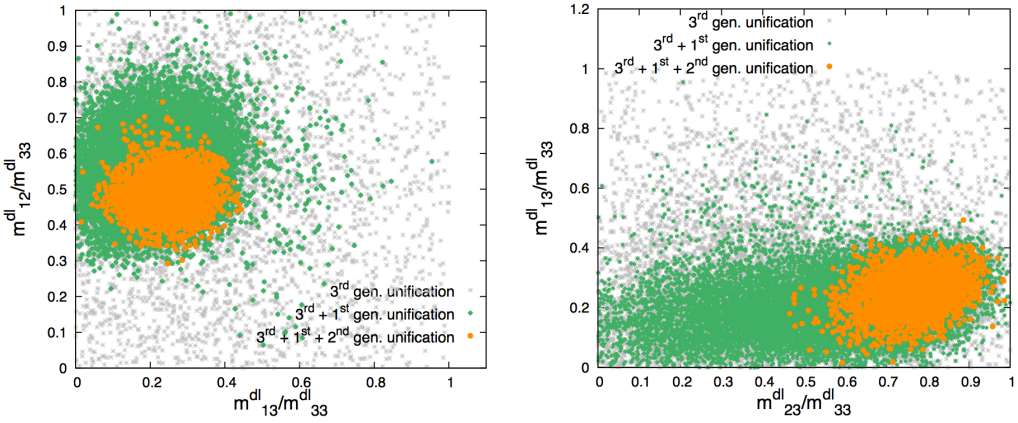

(a) (b)

Figure 7.1: Scatter plot of the GFV_{123} points in the planes $(m^{dl}_{13}/m^{dl}_{33},\ m^{dl}_{12}/m^{dl}_{33})$ (a), and $(m^{dl}_{23}/m^{dl}_{33},\ m^{dl}_{13}/m^{dl}_{33})$ (b). grey stars: all the points satisfying the Yukawa unification condition for the third generation at 2σ; green diamonds: points additionally requiring 2σ unification of the first family; orange dots: points for which all the three generations are unified at 2σ.

cation:

$$0.5 < m^{dl}_{23}/m^{dl}_{33} < 1, \qquad 0 < m^{dl}_{13}/m^{dl}_{33} < 0.5, \qquad 0.3 < m^{dl}_{12}/m^{dl}_{33} < 0.7,$$

$$0 < A^{d}_{12}/A^{d}_{33} < 0.2, \qquad 0 < A^{d}_{21}/A^{d}_{33} < 0.2. \tag{7.1}$$

7.2 Phenomenology of the GFV_{123} scenario

In order to identify points satisfying both the GUT-scale Yukawa unification requirements and the experimental constraints, we use the tools described in Chapter 4, and scan the parameter space specified in Table 7.2. The scanning ranges are chosen to contain the region consistent with full 3×3 Yukawa matrix unification, as discussed in Sec. 7.1. Thus, we restrict our search to $M_{1/2}$ lower than 1 TeV, $\tan\beta < 25$ and A^{de}_{33} in the range of [400, 1100] GeV. The off-diagonal terms A^{de}_{12}/A^{de}_{33}, A^{de}_{21}/A^{de}_{33}, m^{dl}_{23}/m^{dl}_{33}, m^{dl}_{13}/m^{dl}_{33}, m^{dl}_{12}/m^{dl}_{33} are limited according to Eq. (7.1). The remaining parameters are within the initial scanning ranges (cf. Table 7.1), as they do not affect the Yukawa unification. The experimental constraints considered in the analysis are listed in Table 6.1.

7.2.1 Lepton Flavour Violating observables

In the GFV_{123} scenario, the muon-electron conversion observables might be strongly enhanced. All of them are influenced by the relatively large values of m^{dl}_{13}, m^{dl}_{12}, A^{de}_{12}, A^{de}_{21}, A^{de}_{13}, A^{de}_{31} that are required for the electron-(down quark) Yukawa unification. The 90% C.L. upper bound on $\mathcal{B}(\mu^+ \to e^+\gamma)$ reported in Ref. [78] equals 5.7×10^{-13}. All the points of our scan that satisfy the full 3×3 Yukawa matrix unification requirement exceed this bound by five orders of magnitude, as shown in Fig. 7.4.

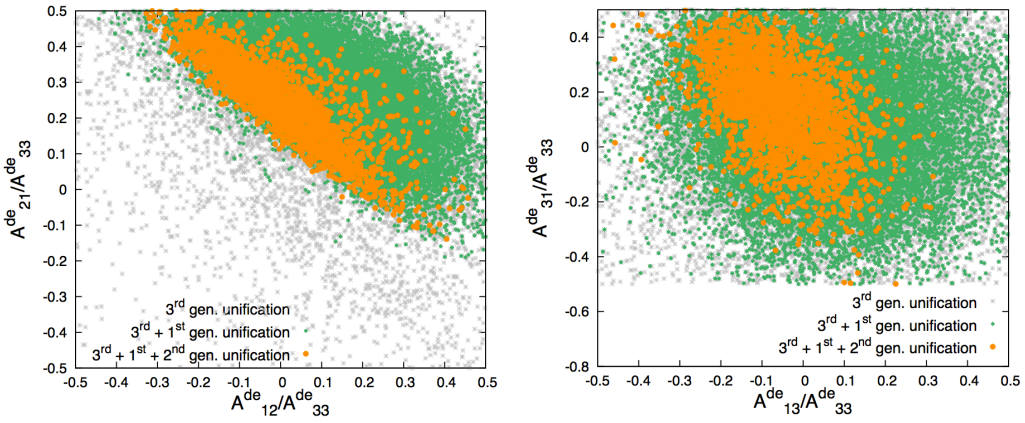

(a)

(b)

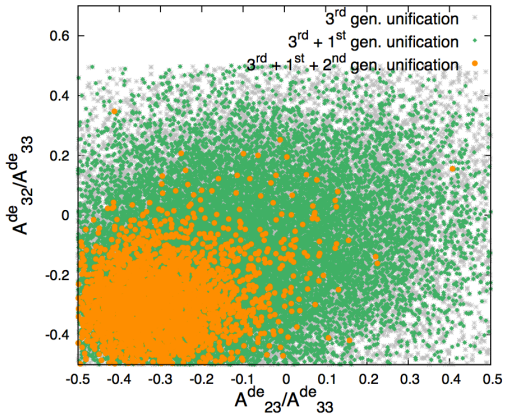

(c)

Figure 7.2: Scatter plot of the GFV_{123} points in the planes $(A^{de}_{12}/A^{de}_{33},\ A^{de}_{21}/A^{de}_{33})$ (a), $(A^{de}_{13}/A^{de}_{33},\ A^{de}_{31}/A^{de}_{33})$ (b), and $(A^{de}_{23}/A^{de}_{33},\ A^{de}_{32}/A^{de}_{33})$ (c). The colour code is the same as in Fig. 7.1.

It is theoretically possible to evade this constraint while unifying the electron and down-quark Yukawa couplings by raising the overall scale of the superpartner masses. However, this could not be achieved with the applied numerical tools that assume $\mu_{sp} = M_Z$. All our scans consistently found values of $M_{1/2}$ to be around 1 TeV at $M_{\rm GUT}$. The fixed condition $\mu_{sp} = M_Z$ is one of the weaknesses of the spectrum generators that were available and widely tested at the moment when our research work at the Yukawa unification problem started.

7.2.2 EW vacuum stability

Let us for the moment assume that if the superpartners were heavier, we could satisfy both the full 3×3 Yukawa matrix unification and all the experimental conditions listed in Table 6.1. There is still an important non-decoupling effect of phenomenological importance, namely the already discussed vacuum (meta)stability problem. Here, we study this issue for the points found in our TeV-scale GFV_{123} scenario.

As mentioned in Sec. 7.1, non-zero elements $A^{de}_{12/21}$ are required to achieve the Yukawa coupling unification for both the first and second family. However, off-diagonal entries of the

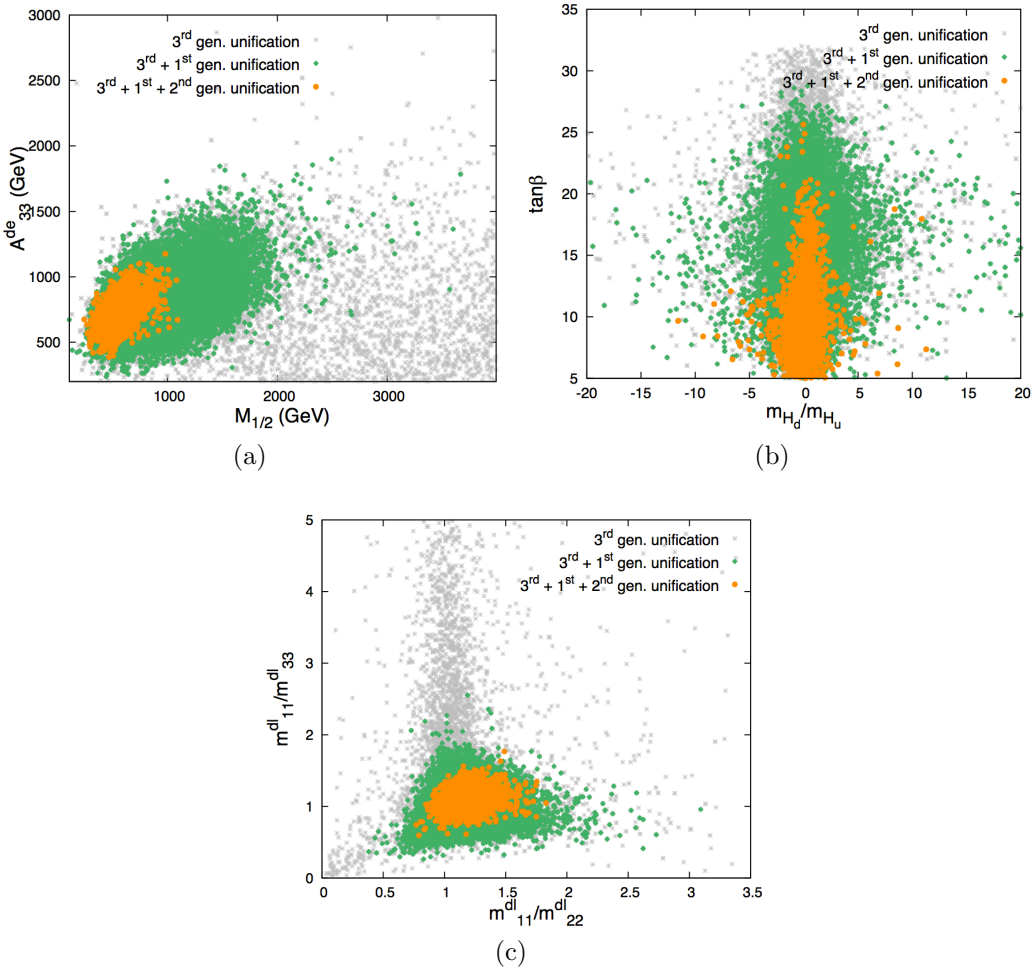

Figure 7.3: Scatter plot of the GFV_{123} points in the planes $(M_{1/2},\ A^d_{33})$ (a), $(m_{H_d}/m_{H_u},\ \tan\beta)$ (b), and $(m^{dl}_{11}/m^{dl}_{22},\ m^{dl}_{11}/m^{dl}_{33})$ (c). The colour code is the same as in Fig. 7.1.

trilinear couplings (as well as the diagonal ones) are strongly constrained by the requirement of EW vacuum stability. When the flavour-violating entries are too large, a CCB minimum may appear in the MSSM scalar potential, and it may become deeper than the standard EW one. The potential may also become unbounded from below (UFB) [87, 128–132]. An important feature of all such constraints is that, unlike the FCNC ones, they do not become weaker when the scale $M_{\rm SUSY}$ is increased.

In the down-squark sector, tree-level formulae for the CCB bounds are given by [132]

$$(v_d/\sqrt{2})A^d_{ij} \ \leq \ m^d_k[(m^2_{\tilde{q}})_{ii} + (m^2_{\tilde{d}})_{jj} + m^2_{H_d} + \mu^2]^{1/2}, \quad k = \mathrm{Max}(i,j). \tag{7.2}$$

The limits on A^e_{ij} have an analogous form, up to replacing the matrix $m^2_{\tilde{d}}$ by $m^2_{\tilde{e}}$. Similarly, the UFB bounds read [132]

$$\begin{aligned} (v_d/\sqrt{2})A^d_{ij} &\leq m^d_k[(m^2_{\tilde{q}})_{ii} + (m^2_{\tilde{d}})_{jj} + (m^2_{\tilde{l}})_{ii} + (m^2_{\tilde{e}})_{jj}]^{1/2}, \\ (v_d/\sqrt{2})A^e_{ij} &\leq \sqrt{3}m^l_k, \quad k = \mathrm{Max}(i,j). \end{aligned} \tag{7.3}$$

In Fig. 7.5, we show to what extent the CCB and UFB limits are satisfied for the points that allow the Yukawa coupling unification and satisfy at 3σ all the experimental constraints

Parameter	Scanning Range
$M_{1/2}$	[200, 1100] GeV
m_{H_u}, m_{H_d}	[100, 8000] GeV
$\tan\beta$	[3, 25]
$\operatorname{sgn}\mu$	-1
A^{de}_{33}	[400, 1100] GeV
A^{u}_{33}	[−9000, 9000] GeV
A^{de}_{11}/A^{de}_{33}	[−0.00028, 0.00028]
A^{de}_{22}/A^{de}_{33}	[−0.065, 0.065]
A^{u}_{22}/A^{u}_{33}	[−0.005, 0.005]
A^{de}_{12}/A^{de}_{33}, A^{de}_{21}/A^{de}_{33}	[−0.2, 0.2]
m^{dl}_{ii}, $i=1,2,3$	[100, 7000] GeV
m^{dl}_{23}/m^{dl}_{33}	[0.5, 1.0]
m^{dl}_{13}/m^{dl}_{33}	[0.0, 0.5]
m^{dl}_{12}/m^{dl}_{33}	[0.3, 0.7]
m^{ue}_{ii}, $i=1,2,3$	[100, 7000] GeV

Table 7.2: Ranges of the input SUSY parameters in our *final* scan for the GFV_{123} scenario. The parameters that are not explicitly listed in the table (namely A^{u}_{11}, A^{u}_{ij} and m^{ue}_{ij} for $i \neq j$, $A^{de}_{23/32}$, $A^{de}_{13/31}$) have been set to zero.

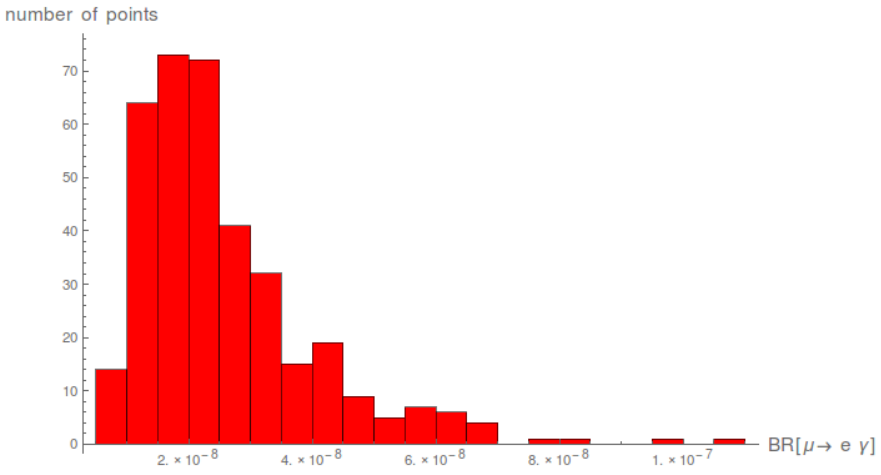

Figure 7.4: Histogram showing $\mathcal{B}(\mu^+ \to e^+\gamma)$ calculated for points satisfying other phenomenological constraints in GFV_{123} scenario. It exceeds the experimental upper bound by five orders of magnitude. They were found by the scan specified by the ranges presented in Table 7.2.

listed in Table 6.1. The dashed lines indicate upper limits on the allowed size of the off-diagonal trilinear terms. One can see that the CCB stability bounds are violated by around an order of magnitude. The situation is even worse in the case of the UFB bounds where the size of the elements A^{e}_{ij} are around four orders of magnitude larger than it is allowed by the stability constraint. It results from the fact that the UFB limit on A^{e}_{ij} is of the order of the muon mass. Therefore, we conclude that the EW MSSM vacuum is not stable in the

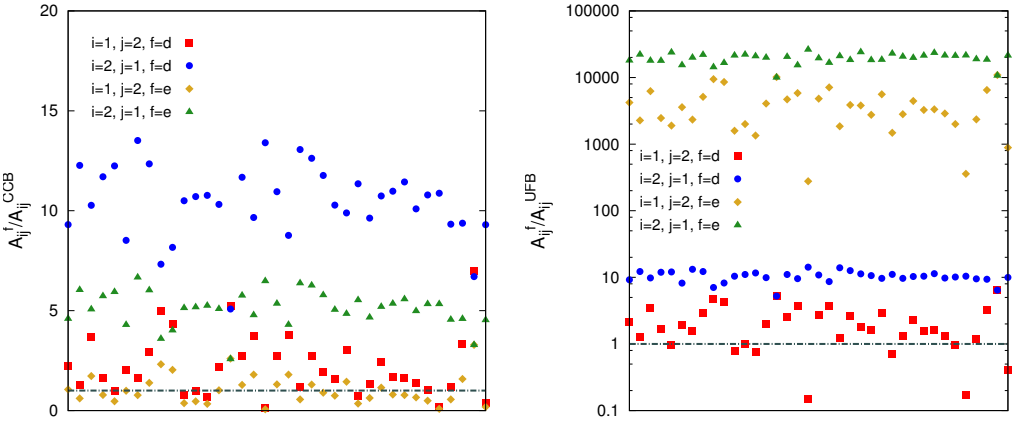

(a) (b)

Figure 7.5: EW vacuum CCB (a) and UFB (b) stability bounds on the elements $A^d_{12/21}$ and $A^e_{12/21}$. Dashed line indicates the upper limit on the allowed size of the off-diagonal trilinear terms.

GFV_{123} Yukawa unification scenario.

On the other hand, even if a CCB minimum appears, it does not imply that a considered model is not valid, as long as the standard EW vacuum lives longer than the age of the universe. Moreover, in such a case, the UFB bound becomes irrelevant because the probability of a tunnelling process along the CCB direction is much higher [133]. To derive metastability bounds, the bounce action for a given scalar potential should be calculated numerically, which is beyond the scope of our present work. To evaluate the impact of metastability on the validity of the unification scenario, we will use instead the results of the analysis performed in Ref. [133]. The derived metastability bounds do not depend on the Yukawa couplings, and therefore are in general much less stringent than the CCB ones. The effect is the strongest for the $A_{12/21}$ elements, in which case the CCB limit can be weakened by three to four orders of magnitude, depending on a particular choice of the model parameters. We can therefore conclude that the GFV_{123} scenario leads to an unstable, but a long-lived vacuum.

It should be stressed, though, that the tension between the Yukawa unification condition and the EW vacuum stability is less severe in GFV_{123} scenario than in the case of Yukawa unification through large diagonal A-terms where the CCB bounds were violated by two orders of magnitude Sec. 5.3. On the other hand, theoretical calculations of the stability conditions are still marred with many uncertainties. This leaves a possibility that future improvements might further reduce (or even eliminate) the tension between the vacuum stability and the Yukawa unification.

CHAPTER 8

Conclusions

8.1 Summary

This work provided evidence in support of the following statement:

There exist regions in the R-parity conserving MSSM parameter space for which the unification of the down-type quark and lepton Yukawa matrices takes place, while the predicted values of flavour, electroweak and other collider observables are consistent with experimental constraints.

We pointed out three distinct MSSM scenarios that encompass points consistent with the bottom-tau and strange-muon Yukawa unification, and for which all the investigated experimental constraints are satisfied. These constraints include the mass and decay rates of the lightest Higgs boson, EW precision tests, flavour observables, limits on the spin-independent proton-neutralino scattering cross-section, as well as the 8 TeV LHC exclusion bounds from the direct SUSY searches. Our MSSM scenarios are not exclusive, and should be viewed as complementary strategies of tuning the MSSM threshold corrections to the Yukawa couplings. At $M_{\rm GUT}$, they can be characterised by the following parameters expressed in the super-CKM basis:

1. large diagonal entries of the trilinear soft terms A^{de}_{22} and A^{de}_{33};
2. large and negative μ, low value of the ratio m^{dl}_{22}/m^{dl}_{33}, moderate or high $\tan\beta$;
3. non-zero off-diagonal soft mass element m^{dl}_{23}.

The second of the above options was analysed as a special case of our GFV_{23} scenario that allows a non-zero m^{dl}_{23} element. Both the second and the third approach assume diagonal A-terms that are limited in magnitude by the corresponding Yukawa couplings. We provided evidence that the relic density of the neutralino dark matter can be reproduced within the second and third scenario. Points found for both of them are characterised by a large magnitude of the μ term, which increases the well-known fine-tuning problem of the MSSM.

In the first scenario with large A-terms, the MSSM scalar potential possesses a charge- and colour-breaking (CCB) global minimum. However, the decay time of the standard electroweak vacuum in this case is longer than the age of the Universe, so this scenario is not

phenomenologically excluded. In the GFV_{23} scenario, we assumed that $\frac{|A^f_{ii}|}{|A^f_{33}|} < \frac{Y^f_{ii}}{Y^f_{33}}$ to avoid this problem.

We showed that the electron-(down quark) Yukawa unification can take place for any of the following types of parameter configurations in the super-CKM basis:

(i) a large diagonal trilinear term A^{de}_{11};

(ii) non-zero off-diagonal soft terms m^{dl}_{13}, m^{dl}_{12}, A^{de}_{12}, A^{de}_{21}, A^{de}_{13}, A^{de}_{31}.

The latter scenario, however, is excluded by the LFV observables, as all the points consistent with the electron-(down quark) unification that were found by our scan predict values of $\mathcal{B}(\mu^+ \to e^+\gamma)$ that exceed the experimental 90% C.L. upper limit by at least five orders of magnitude. On the other hand, in the case *(i)*, the large A^{de}_{11} makes the MSSM vacuum metastable but long-lived, similarly to the case of large A^{de}_{22} in the second generation case.

8.2 Open questions and discussion

In our analysis, we have assumed validity of the MSSM up to the GUT scale, i.e. we ignored the likely fact that the right-handed neutrinos do not decouple at $M_{\rm GUT}$ but rather at an intermediate scale. Given the existing bounds on the neutrino masses, the size of this scale is correlated with assumed values of the Yukawa couplings in the matrix $\mathbf{Y}^\nu$ that is responsible for generating the dimension-five operator in Eq.(1.10). In the $SU(5)$ context (contrary to the $SO(10)$ one), the size of $\mathbf{Y}^\nu$ is unrelated to $\mathbf{Y^u}$ and $\mathbf{Y^{de}}$. If the elements of $\mathbf{Y}^\nu$ are numerically small, the intermediate scale is much lower than $M_{\rm GUT}$, but the RG-evolution of all the other MSSM parameters is hardly affected due to the very smallness of $\mathbf{Y}^\nu$. In such a situation our approach is valid to a very good approximation. On the other hand, if some of the couplings in $\mathbf{Y}^\nu$ are large, a new analysis would be necessary. In fact, potential effects of $\mathbf{Y}^\nu$ on the Yukawa unification have been already discussed in the literature – see, e.g., Ref. [134].

If the MSSM were to provide an explanation for the exact $SU(5)$ Yukawa matrix unification at $M_{\rm GUT}$, the case of the heavier two families could be resolved by any of the strategies 1-3 mentioned in the previous section. The electron-(down quark) Yukawa unification was shown to be consistent with experiment only in the large A-term case. Nevertheless, the GFV_{123} scenario could be modified, so that the LFV bounds are not violated. One possibility would be to raise the superpartner masses. Another option is to abandon the $SU(5)$ condition of equality of the squark and slepton soft terms, which might be possible if the soft terms are affected by the $SU(5)$-breaking scalar fields. This way, the off-diagonal elements of m^d_{ij} could still be used to adjust the light SM fermion mass ratios, while the off-diagonal m^l_{ij} might remain low enough to satisfy the LFV constraints.

Another natural question is whether it might be possible to unify the down-quark and electron Yukawa couplings in a scenario where neither large diagonal A-terms nor flavour violation in the soft terms are allowed. In such a case, the only source of possible SUSY-scale threshold corrections are the $(\tan\beta)$-enhanced contributions proportional to the μ parameter (2.11). In this case, however, the threshold corrections to the down and strange quark

Yukawa couplings would have the same sign, while opposite signs are phenomenologically required. Therefore, it is unlikely that one could unify both of them in such a setup.

The observed DM relic density was correctly reproduced in the GFV scenarios, showing that the $SU(5)$ Yukawa matrix unification is not at tension with Ωh^2. Although the DM constraint was not taken into account in our large A-term scenario [3], we do not expect it could change our qualitative conclusions. A possible price to pay might be abandoning our assumption of the scalar soft mass universality at the GUT scale.

One might wonder whether including higher-order corrections to our analysis could affect the conclusions. We used one-loop formulae for the threshold corrections, which was consistent with employing the two-loop MSSM RGEs. However, in the case of high $\tan\beta$, some of the two-loop threshold corrections might get enhanced [135]. Although including such corrections would require an extended numerical analysis, we do not expect our final qualitative conclusions could be affected.

The vacuum metastability issue was investigated at tree level. A one-loop calculation might be a valid supplement to the analysis. In fact, there exists public software which could be employed for such a calculation [136]. In any case, again, our qualitative conclusions are unlikely to be modified.

Some issues related to the $SU(5)$ GUT, like the proton lifetime, have remained unaddressed in this work. On the other hand, several ways of saving the proton from decaying too fast in the $SU(5)$ framework have been proposed in the literature, for example by employing higher-dimensional operators [42].

In the present study we aimed at checking whether large GUT-scale threshold corrections or departures from the minimal $SU(5)$ boundary conditions to the Yukawa couplings can be avoided in the R-parity conserving MSSM. We did not aspire, however, to construct a full and self-consistent model valid above the GUT-scale. In reality, the Yukawa unification problem, in the absence of the Georgi-Jarlskog mechanism, might receive a combined solution from both the SUSY-scale and GUT-scale threshold effects. Our study should be viewed as a qualitative test to what extent the GUT-scale corrections are absolutely necessary. We hope that it contributes in a constructive manner to the long-lasting search for a simple GUT model that works.

List of acronyms

The following acronyms are used throughout the text:

CCB = Charge- and Colour-Breaking

CKM = Cabibbo-Kobayashi-Maskawa

CMB = Cosmic Microwave Background

DM = Dark Matter

EW = electroweak

EWSB = Electroweak Symmetry Breaking

GFV = General Flavour Violating

GIM = Glashow-Iliopoulos-Maiani

GUT = Grand Unified Theory

LHC = Large Hadron Collider

LSP = Lightest Supersymmetric Particle

MCMC = Markov Chain Monte Carlo

MET = Missing Transverse Energy

MFV = Minimal Flavour Violating

MSSM = Minimal Supersymmetric Standard Model

NLSP = Next-to-Lightest Supersymmetric Particle

QFT = Quantum Field Theory

RGE = Renormalisation Group Equations

SM = Standard Model

SMS = Simplified Model Scenarios

SUSY = supersymmetry

UFB = Unbounded From Below

VEV = Vacuum Expectation Value

WIMP = Weakly Interacting Massive Particle

soft terms/couplings = soft supersymmetry breaking terms/couplings

A-terms = trilinear soft Higgs-squark-squark couplings (matrices in the flavour space)

Bibliography

[1] S. Dimopoulos and H. Georgi, Nucl. Phys. B **193** (1981) 150.

[2] T.Enkhbat, arXiv:0909.5597 [hep-ph].

[3] M. Iskrzyński, Eur. Phys. J. C **75** (2015) 2, 51 [arXiv:1408.2165 [hep-ph]].

[4] M. Iskrzyński and K. Kowalska, JHEP **1504** (2015) 120 [arXiv:1412.8651 [hep-ph]].

[5] A. Zee, "Quantum field theory in a nutshell", Princeton, N.J: Princeton University Press, 2010.

[6] S. Pokorski, "Gauge field theories", Cambridge New York: Cambridge University Press, 2000.

[7] C. Itzykson and J. B. Zuber, "Quantum field theory", Mineola, N.Y: Dover Publications, 2005

[8] L. H. Ryder, "Quantum field theory", Cambridge New York: Cambridge University Press, 1996.

[9] S.L. Glashow, "Partial-symmetries of weak interactions", Nuclear Physics 22 (4): 579588 (1961)

[10] S. Weinberg, "A Model of Leptons", Physical Review Letters 19 (21): 12641266 (1967), A. Salam, N. Svartholm, ed. "Elementary Particle Physics: Relativistic Groups and Analyticity" (1968), eighth Nobel Symposium, Stockholm: Almquvist and Wiksell. p. 367.

[11] F. Englert, R. Brout, "Broken symmetry and the mass of gauge vector mesons", Phys. Rev. Lett. 13: 321-3. (1964)

[12] P.W. Higgs, "Broken symmetries, massless particles and gauge fields", Phys. Lett. 12: 132-3. (1964)

[13] P.W. Higgs, "Broken symmetries and the masses of gauge bosons", Phys. Rev. Lett. 13: 508-9. (1964)

[14] G.S. Guralnik, C.R. Hagen, T.W.B. Kibble, "Global conservation laws and massless particles", Phys. Rev. Lett. 13: 585-7 (1964)

[15] S. Weinberg, Phys. Rev. Lett. **43** (1979) 1566.

[16] N. Cabibbo, "Unitary Symmetry and Leptonic Decays". Physical Review Letters 10 (12)

[17] M. Kobayashi, T. Maskawa, "CP-Violation in the Renormalizable Theory of Weak Interaction", Progress of Theoretical Physics 49 (2)

[18] H. Georgi and S. L. Glashow, Phys. Rev. Lett. **32** (1974) 438.

[19] K. A. Olive *et al.* [Particle Data Group], Chin. Phys. C **38** (2014) 090001.

[20] A. J. Buras, J. R. Ellis, M. K. Gaillard and D. V. Nanopoulos, Nucl. Phys. B **135** (1978) 66.

[21] A. Arbey, G. Cacciapaglia, H. Cai, A. Deandrea, S. L. Corre and F. Sannino, arXiv:1502.04718 [hep-ph].

[22] D. Barducci, A. Belyaev, M. S. Brown, S. De Curtis, S. Moretti and G. M. Pruna, arXiv:1408.4553 [hep-ph].

[23] A. Djouadi, Eur. Phys. J. C **74** (2014) 2704 [arXiv:1311.0720 [hep-ph]].

[24] P. West, "Introduction to supersymmetry and supergravity", World Scientific, 1986, Singapore

[25] S. P. Martin, A Supersymmetry Primer, [arxiv: hep-ph/9709356].

[26] S. Coleman, J. Mandula, Phys. Rev. 159, 1251 (1967).

[27] Y.A. Golfand, E.S. Likhtman, JETP Lett. 13, 323 (1971)

[28] J. Wess, B. Zumino, Nuclear Physics B, Volume 70, Issue 1 (1974)

[29] R. Haag, J.T. Lopuszański, M. Sohnius, Nucl. Phys. B 88, 257-274 (1975)

[30] A. Salam and J. Strathdee, Phys. Rev. D 11, 1521 (1975); M.T. Grisaru, W. Siegel and M. Rocek, Nucl. Phys. B 159, 429 (1979).

[31] G. 't Hooft, NATO Sci. Ser. B **59** (1980) 135.

[32] J. Rosiek, Phys. Rev. D **41** (1990) 3464 [hep-ph/9511250 (E)].

[33] I. Jack and D. R. T. Jones, Phys. Rev. D **61** (2000) 095002 [hep-ph/9909570].

[34] M. A. Cakir, S. Mutlu and L. Solmaz, Phys. Rev. D **71** (2005) 115005 [hep-ph/0501286].

[35] B. C. Allanach *et al.*, Comput. Phys. Commun. **180** (2009) 8 [arXiv:0801.0045 [hep-ph]].

[36] Z. Berezhiani, M. Chianese, G. Miele and S. Morisi, arXiv:1505.04950 [hep-ph].

[37] H. P. Nilles, Phys. Rept. **110** (1984) 1.

[38] S. P. Martin and M. T. Vaughn, Phys. Rev. D **50** (1994) 2282 [Erratum-ibid. D **78** (2008) 039903] [hep-ph/9311340].

[39] H. Georgi and C. Jarlskog, Phys. Lett. B **86** (1979) 297.

[40] S. Antusch and M. Spinrath, Phys. Rev. D **79** (2009) 095004 [arXiv:0902.4644 [hep-ph]].

[41] S. Antusch, S. F. King and M. Spinrath, Phys. Rev. D **89** (2014) 055027 [arXiv:1311.0877 [hep-ph]].

[42] D. Emmanuel-Costa and S. Wiesenfeldt, Nucl. Phys. B **661** (2003) 62 [hep-ph/0302272].

[43] M. Monaco and M. Spinrath, Phys. Rev. D **84** (2011) 055009 [arXiv:1106.6208 [hep-ph]].

[44] W. Buchmuller and D. Wyler, Phys. Lett. B **121** (1983) 321.

[45] L. J. Hall, V. A. Kostelecky and S. Raby, Nucl. Phys. B **267** (1986) 415.

[46] J. L. Diaz-Cruz, H. Murayama and A. Pierce, Phys. Rev. D **65** (2002) 075011 [hep-ph/0012275].

[47] B. Bajc, S. Lavignac and T. Mede, AIP Conf. Proc. **1604** (2014) 297 [arXiv:1310.3093 [hep-ph]].

[48] F. Brummer, S. Kraml and S. Kulkarni, JHEP **1208** (2012) 089 [arXiv:1204.5977 [hep-ph]].

[49] J. Guasch and J. Sola, Nucl. Phys. B **562** (1999) 3 [hep-ph/9906268].

[50] J. J. Cao, G. Eilam, M. Frank, K. Hikasa, G. L. Liu, I. Turan and J. M. Yang, Phys. Rev. D **75** (2007) 075021 [hep-ph/0702264].

[51] S. Fichet, B. Herrmann and Y. Stoll, arXiv:1403.3397 [hep-ph].

[52] B. Herrmann, M. Klasen and Q. Le Boulc'h, Phys. Rev. D **84** (2011) 095007 [arXiv:1106.6229 [hep-ph]].

[53] S. Heinemeyer, W. Hollik, F. Merz and S. Penaranda, Eur. Phys. J. C **37** (2004) 481 [hep-ph/0403228].

[54] J. Cao, G. Eilam, K. i. Hikasa and J. M. Yang, Phys. Rev. D **74** (2006) 031701 [hep-ph/0604163].

[55] M. Arana-Catania, S. Heinemeyer, M. J. Herrero and S. Penaranda, JHEP **1205** (2012) 015 [arXiv:1109.6232 [hep-ph]].

[56] M. Arana-Catania, S. Heinemeyer and M. J. Herrero, Phys. Rev. D **90** (2014) 075003 [arXiv:1405.6960 [hep-ph]].

[57] K. Kowalska, JHEP **1409** (2014) 139 [arXiv:1406.0710 [hep-ph]].

[58] A. Crivellin, L. Hofer and J. Rosiek, JHEP **1107** (2011) 017 [arXiv:1103.4272 [hep-ph]].

[59] B. C. Allanach, Comput. Phys. Commun. **143** (2002) 305 [hep-ph/0104145].

[60] S.L. Glashow, J. Iliopoulos, L. Maiani, (1970) Phys. Rev. D 2: 1285

[61] M. Misiak, S. Pokorski and J. Rosiek, Adv. Ser. Direct. High Energy Phys. **15** (1998) 795 [hep-ph/9703442].

[62] J. H. Christenson, J. W. Cronin, V. L. Fitch, and R. Turlay Phys. Rev. Lett. 13, 138 (1964)

[63] J. A. Bailey *et al.* [SWME Collaboration], arXiv:1503.06613 [hep-lat].

[64] R. Glattauer [for the BELLE Collaboration], talk presented at the EPS-HEP 2015 Converence, Vienna, July 22-29, 2015.

[65] J. Brod and M. Gorbahn, Phys. Rev. Lett. **108** (2012) 121801 [arXiv:1108.2036 [hep-ph]].

[66] A. Crivellin, J. Rosiek, P. H. Chankowski, A. Dedes, S. Jaeger and P. Tanedo, Comput. Phys. Commun. **184** (2013) 1004 [arXiv:1203.5023 [hep-ph]].

[67] http://www.utfit.org/UTfit/ResultsSummer2014PostMoriondNP

[68] S. Aoki *et al.* [Flavor Lattice Averaging Group Collaboration], Eur. Phys. J. C **74** (2014) 2890 [arXiv:1310.8555 [hep-lat]].

[69] Y. Amhis *et al.* [Heavy Flavor Averaging Group Collaboration], arXiv:1412.7515 [hep-ex].

[70] V. M. Abazov *et al.* [D0 Collaboration], Phys. Rev. D **87** (2013) 7, 072006 [arXiv:1301.4507 [hep-ex]].

[71] V. Khachatryan *et al.* [CMS and LHCb Collaborations], Nature **522** (2015) 68 [arXiv:1411.4413 [hep-ex]].

[72] C. Bobeth, M. Gorbahn, T. Hermann, M. Misiak, E. Stamou and M. Steinhauser, Phys. Rev. Lett. **112** (2014) 101801 [arXiv:1311.0903 [hep-ph]].

[73] A. J. Buras and M. Misiak, Acta Phys. Polon. B **33** (2002) 2597 [hep-ph/0207131].

[74] M.S. Alam *et al.* [CLEO Collaboration], Phys. Rev. Lett. 74 , 2885 (1995).

[75] M. Misiak *et al.*, Phys. Rev. Lett. **114** (2015) 22, 221801 [arXiv:1503.01789 [hep-ph]].

[76] R. H. Bernstein and P. S. Cooper, Phys. Rept. **532** (2013) 27 [arXiv:1307.5787 [hep-ex]].

[77] E.P. Hincks and B. Pontecorvo, Phys. Rev. 73 (1948), 257.

[78] J. Adam *et al.* [MEG Collaboration], Phys. Rev. Lett. **110** (2013) 201801 [arXiv:1303.0754 [hep-ex]].

[79] B. Aubert *et al.* [BaBar Collaboration], Phys. Rev. Lett. **104** (2010) 021802 [arXiv:0908.2381 [hep-ex]].

[80] G. Aad *et al.* [ATLAS Collaboration], Phys. Lett. B **716** (2012) 1 [arXiv:1207.7214 [hep-ex]].

[81] S. Chatrchyan *et al.* [CMS Collaboration], Phys. Lett. B **716** (2012) 30 [arXiv:1207.7235 [hep-ex]].

[82] G. Aad *et al.* [ATLAS and CMS Collaborations], Phys. Rev. Lett. **114** (2015) 191803 [arXiv:1503.07589 [hep-ex]].

[83] M. Carena, J. R. Espinosa, M. Quiros and C. E. M. Wagner, Phys. Lett. B **355** (1995) 209 [hep-ph/9504316].

[84] B. C. Allanach, A. Djouadi, J. L. Kneur, W. Porod and P. Slavich, JHEP **0409** (2004) 044 [hep-ph/0406166].

[85] https://twiki.cern.ch/twiki/bin/view/CMSPublic/SUSYSMSSummaryPlots8TeV

[86] https://atlas.web.cern.ch/Atlas/GROUPS/PHYSICS/CombinedSummaryPlots/SUSY/

[87] J. A. Casas, A. Lleyda and C. Muñoz, Nucl. Phys. B **471** (1996) 3 [hep-ph/9507294].

[88] J. Wilford, Jan H. Oort, Dutch Astronomer In Forefront of Field, Dies at 92, 12 November, 1992.

[89] F. Zwicky, F. Brummer, S. Kraml and S. Kulkarni, JHEP **1208** (2012) 089 [arXiv:1204.5977 [hep-ph]]. Helv.Phys.Acta 6 (1933) 110127.

[90] G. Bertone *et al.*, "Particle Dark Matter: Observations, Models and Searches," Cambridge University Press (United Kingdom), 2010, 738 pp.

[91] K. Begeman, A. Broeils, and R. Sanders, Mon.Not.Roy.Astron.Soc. 249 (1991) 523

[92] NASA, ESA, M.J. Jee and H. Ford (Johns Hopkins University), News Release Number: STScI-2007-17 http://hubblesite.org/newscenter/archive/releases/2007/17/image/a/

[93] L. Bergstrom, Nonbaryonic dark matter: Observational evidence and detection methods, Rept.Prog.Phys. 63 (2000) 793, [hep-ph/0002126]

[94] P. A. R. Ade *et al.* [Planck Collaboration], Astron. Astrophys. (2014) [arXiv:1303.5076 [astro-ph.CO]].

[95] P. Cushman, C. Galbiati, D. N. McKinsey, H. Robertson, T. M. P. Tait, D. Bauer, A. Borgland and B. Cabrera *et al.*, arXiv:1310.8327 [hep-ex].

[96] D. S. Akerib *et al.* [LUX Collaboration], Phys. Rev. Lett. **112** (2014) 9, 091303 [arXiv:1310.8214 [astro-ph.CO]].

[97] W. Porod, decays and SUSY particle production at e+ e- colliders," Comput. Phys. Commun. **153** (2003) 275 [hep-ph/0301101].

[98] B. C. Allanach, D. P. George and B. Gripaios, JHEP **1307** (2013) 098 [arXiv:1304.5462 [hep-ph]].

[99] B. C. Allanach, D. P. George and B. Nachman, JHEP **1402** (2014) 031 [arXiv:1311.3960 [hep-ph]].

[100] B. C. Allanach, W. Porod and P. Slavich, private communication, 2012.

[101] J. Beringer *et al.* [Particle Data Group], Phys. Rev. D **86** (2012) 010001.

[102] A. Fowlie, M. Kazana, K. Kowalska, S. Munir, L. Roszkowski, E. M. Sessolo, S. Trojanowski and Y. L. S. Tsai, Phys. Rev. D **86** (2012) 075010 [arXiv:1206.0264 [hep-ph]];

[103] F. Feroz, M. P. Hobson and M. Bridges, Mon. Not. Roy. Astron. Soc. **398** (2009) 1601 [arXiv:0809.3437 [astro-ph]].

[104] W. Porod and F. Staub, Comput. Phys. Commun. **183** (2012) 2458 [arXiv:1104.1573 [hep-ph]].

[105] P. Gondolo, J. Edsjo, P. Ullio, L. Bergstrom, M. Schelke and E. A. Baltz, JCAP **0407** (2004) 008 [astro-ph/0406204].

[106] T. Hahn, S. Heinemeyer, W. Hollik, H. Rzehak and G. Weiglein, Phys. Rev. Lett. **112** (2014) 141801 [arXiv:1312.4937 [hep-ph]].

[107] M. Frank, T. Hahn, S. Heinemeyer, W. Hollik, H. Rzehak and G. Weiglein, JHEP **0702** (2007) 047 [hep-ph/0611326].

[108] G. Degrassi, S. Heinemeyer, W. Hollik, P. Slavich and G. Weiglein, Eur. Phys. J. C **28** (2003) 133 [hep-ph/0212020].

[109] S. Heinemeyer, W. Hollik and G. Weiglein, Comput. Phys. Commun. **124** (2000) 76 [hep-ph/9812320].

[110] P. Bechtle, O. Brein, S. Heinemeyer, G. Weiglein and K. E. Williams, Comput. Phys. Commun. **181** (2010) 138 [arXiv:0811.4169 [hep-ph]].

[111] P. Bechtle, O. Brein, S. Heinemeyer, G. Weiglein and K. E. Williams, Comput. Phys. Commun. **182** (2011) 2605 [arXiv:1102.1898 [hep-ph]].

[112] P. Bechtle, O. Brein, S. Heinemeyer, O. Stål, T. Stefaniak, G. Weiglein and K. E. Williams, Eur. Phys. J. C **74** (2014) 2693 [arXiv:1311.0055 [hep-ph]].

[113] P. Bechtle, S. Heinemeyer, O. Stål, T. Stefaniak and G. Weiglein, Eur. Phys. J. C **74** (2014) 2711 [arXiv:1305.1933 [hep-ph]].

[114] M. Misiak, *et al.*, Phys. Rev. Lett. **98** (2007) 022002 [hep-ph/0609232].

[115] F. Borzumati, G. R. Farrar, N. Polonsky and S. D. Thomas, Nucl. Phys. B **555** (1999) 53 [hep-ph/9902443].

[116] U. Bellgardt *et al.* [SINDRUM Collaboration], Nucl.Phys. B299 (1988) 1.

[117] Belle and Belle II Collaborations, K. Hayasaka, J.Phys.Conf.Ser. 408 (2013) 012069.

[118] K. Kowalska, L. Roszkowski, E. M. Sessolo and S. Trojanowski, JHEP **1404** (2014) 166 [arXiv:1402.1328 [hep-ph]].

[119] [CMS Collaboration], "Combination of standard model Higgs boson searches and measurements of the properties of the new boson with a mass near 125 GeV," CMS-PAS-HIG-13-005.

[120] C. A. Baker, D. D. Doyle, P. Geltenbort, K. Green, M. G. D. van der Grinten, P. G. Harris, P. Iaydjiev and S. N. Ivanov *et al.*, Phys. Rev. Lett. **97** (2006) 131801 [hep-ex/0602020].

[121] CMS Collaboration "Search for direct production of bottom squark pairs", CMS-PAS-SUS-13-018".

[122] G. Aad *et al.* [ATLAS Collaboration], JHEP **1409** (2014) 176 [arXiv:1405.7875 [hep-ex]].

[123] G. Aad *et al.* [ATLAS Collaboration], JHEP **1405** (2014) 071 [arXiv:1403.5294 [hep-ex]].

[124] E. Aprile [XENON1T Collaboration], Springer Proc. Phys. **148**, 93 (2013) [arXiv:1206.6288 [astro-ph.IM]].

[125] M. Arana-Catania, S. Heinemeyer and M. J. Herrero, Phys. Rev. D **88** (2013) 1, 015026 [arXiv:1304.2783 [hep-ph]].

[126] K. Kowalska and E. M. Sessolo, Phys. Rev. D **88**, no. 7, 075001 (2013) [arXiv:1307.5790 [hep-ph]].

[127] CMS Collaboration "Search for direct EWK production of SUSY particles in multilepton modes with 8TeV data", CMS-PAS-SUS-12-022".

[128] J. M. Frere, D. R. T. Jones and S. Raby, Nucl. Phys. B **222** (1983) 11.

[129] L. Alvarez-Gaume, J. Polchinski and M. B. Wise, Nucl. Phys. B **221** (1983) 495.

[130] J. P. Derendinger and C. A. Savoy, Nucl. Phys. B **237** (1984) 307.

[131] C. Kounnas, A. B. Lahanas, D. V. Nanopoulos and M. Quiros, Nucl. Phys. B **236** (1984) 438

[132] J. A. Casas and S. Dimopoulos, Phys. Lett. B **387** (1996) 107 [hep-ph/9606237].

[133] J. h. Park, Phys. Rev. D **83** (2011) 055015 [arXiv:1011.4939 [hep-ph]].

[134] M. E. Gomez, S. Lola, P. Naranjo and J. Rodriguez-Quintero, AIP Conf. Proc. **1115** (2009) 273 [arXiv:0901.4332 [hep-ph]].

[135] A. Crivellin and C. Greub, Phys. Rev. D **87** (2013) 015013 [arXiv:1210.7453 [hep-ph]].

[136] J. E. Camargo-Molina, B. O'Leary, W. Porod and F. Staub, Eur. Phys. J. C **73** (2013) 10, 2588 [arXiv:1307.1477 [hep-ph]].